UNIVERSITY OF CALIFORNIA,
IRVINE

Approaches to promoting mTOR-mediated growth and regeneration in the mature central nervous system

DISSERTATION

submitted in partial satisfaction of the requirements
for the degree of

DOCTOR OF PHILOSOPHY

in Biomedical Sciences

by

Erin Ann Gallent

Dissertation Committee:
Professor Oswald Steward
Professor Christine Gall, Chair
Professor Richard T. Robertson
Professor Leslie Thompson
Associate Professor David Lyon, Vice-Chair
Assistant Professor Yama Akbari

2018

DEDICATION

To

All of the teachers, professors, and mentors
who I've been lucky enough to receive support and training from.

"the result was far more dramatic than the process, even though, for all practical purposes, the result *was* the process"
-Tom Robbins

For

Bradley Dale Gallent

The single most loving, supportive, compassionate, and unapologetically weird/silly human.
Without you I assuredly would have died from malnutrition and been eaten by the cat.
Thank you for always being the best possible friend, partner, and co-parent.
Our small family is *so* lucky to have you.
I love you.

TABLE OF CONTENTS

LIST OF FIGURES

LIST OF TABLES

ACKNOWLEDGMENTS

I would like to express my deepest gratitude to my research mentor and committee chair, Oswald Steward. Os has an unbridled and infectious passion for scientific discovery (no matter how small the discovery), and his approach to science and mentorship made the inevitable rough patches and growing phases of graduate school bearable. With his invaluable help, I have learned how to truly think and for that I will be forever grateful.

I would like to thank my committee members, Professor Christine Gall, Professor Richard T. Robertson, Professor Leslie Thompson, Professor David Lyon, and Professor Yama Akbari whose patience with my many emails was a feat in and of itself. Each of my committee members pushed me to see questions from new angles, and I thank them for continually increasing my breadth as a scientist.

In addition, I'd like to thank our collaborators Dr. Yama Akbari (and his impressive team of undergraduates), Professor S. Thomas Carmichael of the University of California, Los Angeles, and Dr. Mary Teena Joy of the University of California, Los Angeles. With their help I was afforded the opportunity to extend the reach of my work beyond what was possible in our lab alone. Their contributions are noted in this dissertation.

Last, but far from the least, I'd like to thank my family. Their unwavering support and encouragement throughout my education has been vital to my success. I am so lucky to be able to call them my friends and my family. Thank you to my father, for always believing that I was capable of great things. During stressful times, thoughts of your belief in my ability have kept me going (and listening to Bruce Springsteen, our one true Boss). Thank you to my mom, for always intuiting which moments could use a sweet reminder of your love and which moments call for a margarita. Your strength and drive constantly inspire me, and I hope I've inherited even just a tiny portion of those traits myself. Thank you to my brother Steven, one of the most loyal, hard-working, and caring people I know. I am so grateful for the friendship that has formed between us, and that we have each other to rely on throughout this wild ride called life.

Financial support was provided by the University of California, Irvine, Medical Scientist Training Program (MSTP) NIH grant 5T32GM008620 and NIH Grant NS047718.

CURRICULUM VITAE

Erin Ann Gallent
(Formerly Erin Ann Gutilla)

EDUCATION

2011	**B.S.** with Honors in Biochemistry & Molecular Biology, minors in Mathematics and Psychology at Mills College, Oakland, CA
2011-2013, 2017-2019	**M.D.** in Medical Scientist Training Program at University of California, Irvine
2013-2018	**Ph.D**. in Biomedical Sciences; Department of Anatomy & Neurobiology at University of California, Irvine

FIELD OF STUDY

Neurobiology, Anatomy, Genetics, Molecular Biology, Behavior, and Microscopy

RESEARCH EXPERIENCE

2013-2017 **Graduate Student Researcher**
Department of Anatomy & Neurobiology, UC Irvine
Advisor: Oswald Steward, PhD
Thesis: Approaches to promoting mTOR-mediated growth and regeneration in the mature central nervous system

2009-2011 **Analytical and Computational Visual Neuroscience Intern**
Koret Vision Research Center, UC San Francisco
Advisor: Lawrence Sincich, PhD and Jonathan Horton, PhD

2008 **Undergraduate Research Assistant**
Rutgers University
Research Experience for Undergraduates (REU)
Advisor: John Dighton, PhD

TEACHING & MENTORING EXPERIENCE

2013-2017 **Laboratory Mentor**
UC Irvine, Irvine, CA
Research mentor for UC Irvine Biology Undergraduate student, Sara Jahangiri

2012-2016 **Teaching Assistant**
UC Irvine, Irvine, CA
BIO 097 (Genetics), Summer Session 2012, 2013, 2014, 2015

2011 **Teaching Assistant**
Mills College, Oakland, CA
Neurobiology
General Chemistry Laboratory

2010 **Peer Assistant**
Mills College, Oakland, CA
Hellman Summer Science and Mathematics Fellows Program, 2010
- Biology Course Teaching Assistant
- Resident Assistant for incoming freshmen

2010 **Teaching Assistant**
Mills College, Oakland, CA
Genetics
General Chemistry Laboratory

2009 **Teaching Assistant**
Mills College, Oakland, CA
Analytical Methods in Psychology
General Chemistry Laboratory

2008 **Teaching Assistant**
Mills College, Oakland, CA
Calculus I
General Chemistry Laboratory

LEADERSHIP & COMMITTEE MEMBERSHIP

2012-2017 **Undergraduate Mentor**
UC Irvine, Irvine, CA
Trained, directed, and supervised research conducted by Sara Jahangiri (B.A. in Biology in 2016, UCLA School of Dentistry Fall 2017)
Honors: Undergraduate Research Opportunities Program (2015-2016)

Project title: mTOR Specificity of Cortical Stimulation Used to Promote Neural Regeneration After Spinal Cord Injury

2015-2017 **Co-Chair, Distinguished Lecture Series Committee**
UC Irvine Medical Scientist Training Program, Irvine, CA
Elected to serve as co-chair of student-run lecture series, organized by UC Irvine MD/PhD students

2013-2015 **Admissions Committee for UC Irvine Medical Scientist Training Program**
UC Irvine Medical Scientist Training Program, Irvine, CA
Elected student member

2012-2013 **Chair, Retreat Planning Committee**
UC Irvine Medical Scientist Training Program, Irvine, CA
18th Annual UC Irvine Medical Scientist Training Program Retreat

Interview Committee member
UC Irvine Medical Scientist Training Program, Irvine, CA

COMMUNITY OUTREACH

2012-2017 **Meet the Scientist**
UC Irvine, Irvine, CA
Volunteer for the Meet the Scientist event, hosted by the Reeve-Irvine Research Center. This event provides a unique opportunity for patients with spinal cord injury, their family members, community advocates, and scientists to come together and discuss ongoing research in the spinal cord injury field.

2008-2010 **Expanding Your Horizons Network Workshop Leader**
Mills College, Oakland, CA
Spring 2008, Spring 2009, Spring 2010

- Prepared and taught chemistry workshops for middle school-aged girls in order to inspire girls to pursue careers in STEM fields (science, technology, engineering, and mathematics).
- http://www.expandingyourhorizons.org

PUBLICATIONS

Gallent, EA, Steward O. "Neuronal *PTEN* deletion in adult cortical neurons triggers progressive growth of cell bodies, dendrites, and axons" (2018) *Experimental Neurology* 303: 12-28.

Gutilla, EA, Steward, O. "Selective neuronal *PTEN* deletion: can we take the brakes off of growth without losing control?" (2016) *Neural Regeneration Research* 11.8: 1201.

Gutilla, EA, Buyukozturk, M.B., Steward, O. "Long-term consequences of conditional genetic deletion of *PTEN* in the sensorimotor cortex of neonatal mice" (2016) *Experimental Neurology* 279: 27-39.

ABSTRACTS & PRESENTATIONS

1. Abstract & Poster Presentation at Society for Neuroscience Conference **2016**, San Diego, CA.

EA Gutilla; O Steward. "Adult deletion of *PTEN* in cortical motoneurons leads to robust cell body enlargement that is maintained as the steady-state cell size

2. Abstract & Oral Presentation at Cold Spring Harbor Meeting on Axon Guidance, Synapse Formation, & Regeneration **2016**, Cold Spring Harbor, NY.

EA Gutilla; O Steward. "Enhancing neuronal vitality in the mature brain via *PTEN* deletion".

- *Selected by planning committee for an oral presentation*

3. Oral presentation at UC Irvine Department of Anatomy & Neurobiology Student Retreat **2016**, Irvine, CA.

EA Gutilla; O Steward. "Understanding growth in the adult central nervous system: anatomical and functional effects following conditional *PTEN* deletion in adulthood"

- *Awarded 2nd place for Best Oral Presentation, voted by faculty and students*

4. Abstract & Poster Presentation at American Physician Scientists Association Meeting **2016**, Chicago, IL.

EA Gutilla; O Steward. "Adult cortical motoneurons demonstrate robust growth 6 months after conditional *PTEN* deletion".

5. Oral Presentation at UC Irvine's Progress in Neuroscience Meeting, **2016**, Irvine, CA.

EA Gutilla; O Steward. "Robust adult cortical neuron growth following *PTEN* deletion in adulthood".

6. Abstract & Poster Presentation at Society for Neuroscience Conference **2015**, Chicago, IL.

EA Gutilla; O Steward. "AAV-mediated conditional deletion of PTEN in the adult sensorimotor cortex causes robust hypertrophy of cortical motoneurons".

7. Abstract & Poster Presentation at International Symposium for Neural Regeneration **2015**, Asilomar, CA.

EA Gutilla; O Steward. "AAV-mediated conditional deletion of PTEN in the adult sensorimotor cortex causes robust hypertrophy of cortical motoneurons". EA Gutilla; O Steward.

- *Student Travel Award*

8. Oral presentation at UC Irvine Department of Anatomy & Neurobiology Student Retreat **2015**, Newport Beach, CA.

EA Gutilla; O Steward. "Characterization of adult neuronal growth induced by PTEN deletion"

- *Awarded 2nd place for Best Oral Presentation, voted by faculty and students*

9. Oral presentation at UC Irvine Medical Scientist Program Student Symposium **2015**, Irvine, CA

EA Gutilla; O Steward. "The effects of long-term conditional *PTEN* deletion in neonatal mice"

10. Poster presentation at International Symposium for Neural Regeneration conference **2013**, Asilomar, CA

EA Gutilla, MM Buyukozturk ,B. Brandon, O. Steward. "Comparison of long-term effects following conditional genetic deletion of PTEN in neonatal vs. adult mice"

- *Student Travel Award*

11. Poster Presentation at UC Irvine MSTP Retreat **2012**, Lake Arrowhead, CA.

EA Gutilla, K Yee, O Steward. "Phosphorylation of S6 ribosomal protein induced by *in vivo* motor cortex stimulation in rodents"

12. Poster Presentation at UC Irvine MSTP Symposium **2011**, Irvine, CA.

EA Gutilla, TO Sharpee, JC Horton, LC Sincich. "Diversity of interspike interval distributions in macaque retinal ganglion cells and thalamic relay neurons."

13. Senior Thesis Presentation at Mills College in November **2010**, Oakland, CA.

EA Gutilla. "Excitatory amino acid transporters (EAATs) biochemical structure and function in preventing neuronal excitotoxicity"

14. Abstract and Poster Presentation at Society for Neuroscience Conference **2010**, San Diego, CA

EA Gutilla, TO Sharpee, JC Horton, LC Sincich. "Diversity of interspike interval distributions in macaque retinal ganglion cells and thalamic relay neurons".

15. Poster Presentation at Rutgers University, Camden REU Poster Session, **2008**, Camden, New Jersey.

EA Gutilla, J Dighton "Fungal Succession in Decaying Gypsy Moth Frass".

- *Awarded prize for Top Poster Presentation*

PROFESSIONAL AFFILIATIONS

Society for Neuroscience
Student member 2007-present

Graduate Women in Science
Sigma Delta Epsilon chapter
Member 2013-present

HONORS & AWARDS

2016 **1st Place for Best Student Oral Presentation**
UC Irvine Department of Anatomy & Neurobiology
Graduate Student Retreat 2016

2015 **Student Travel Award**
International Symposium on Neural Regeneration
Asilomar, CA

2nd Place for Best Student Oral Presentation
UC Irvine Department of Anatomy & Neurobiology
Graduate Student Retreat 2015

2013 **Student Travel Award**
International Symposium on Neural Regeneration
Asilomar, CA

2011 **Caryl Parker Haskins Prize**
Mills College, Oakland, CA
Established in 1966 in honor of former Trustee Professor Haskins for a student graduating with distinction in the life sciences

2008-2011 **NAIA Academic All-American Athlete**
Mills College, Oakland, CA
Women's Soccer Team

Daktronics NAIA Scholar Athlete
Mills College, Oakland, CA
Women's Soccer Team

2009-2010 **Highest Cumulative GPA**
Mills College, Oakland, CA
Women's Soccer Team

2008 **Top Poster Presentation Prize**
Rutgers, Camden, New Jersey
Research Experience for Undergraduates

2007 **Scheffler Pre-Medical Science Scholarship & Award**
Mills College, Oakland, CA
Recognizes entering undergraduate students based on academic achievement and demonstrated interest in pre-medical science

Hellman Mathematics and Science Scholarship
Mills College, Oakland, CA
Awarded to student participants in the Hellman Summer Science and Math Fellows Program

Presidential Scholarship
Mills College, Oakland, CA
Recognizes entering fall-term first-year students who have demonstrated scholastic achievement

ABSTRACT OF THE DISSERTATION

Approaches to promoting mTOR-mediated growth and regeneration in the mature central nervous system

By

Erin Ann Gallent

Doctor of Philosophy in Biomedical Sciences

University of California, Irvine, 2018

Professor Christine Gall, Chair

Regeneration of the injured adult central nervous system is limited. The phosphatase and tensin homolog on chromosome ten (*PTEN*) gene has been shown to enable axonal regeneration in optic nerve crush and spinal cord injury models following neonatal conditional genetic deletion of *PTEN* (Park et al., 2008; Liu et al., 2010). As a follow-up to these experiments, I assessed the long-term histological and behavioral consequences of neonatal *PTEN* deletion (Gutilla et al., 2016). In this study, I observed massive cell body enlargement of the neurons that give rise to the major descending voluntary motor tract in the spinal cord (called cortical motoneurons, or CMNs).

This discovery led us to hypothesize that deletion of *PTEN* during adulthood would also result in neuronal growth. Using two-photon microscopy and electron microscopy I found that adult *PTEN* deletion in neurons results in significant cell body and axonal growth, and that these enlarged neurons continue to express markers of growth-promoting pathways throughout life.

To gain a better understanding of the morphological consequences of *PTEN* deletion in adult neurons, I imaged thick sections (200μm) containing fluorescently labeled *PTEN* deleted and control neurons in 3D using a modified CLARITY protocol and two-photon microscopy (Chung and Deisseroth, 2013). 3D images were then used to generate 2D projections that were processed using Sholl analysis, or concentric circle analysis (Sholl, 1953). We found that at both 6 and 12 months post-*PTEN* deletion, pyramidal neurons have a significantly higher density of dendrites, and that this increase is significant at the largest number of radii away from the soma at 12 months after deletion. The progressive changes in dendritic morphology were also seen in the number of basal dendrites projecting off of the soma number, maximal dendritic projections, and nodes, with the highest values for all three measurements seen at 12 months, not 6 months, post-deletion. What's more, the radius of maximal intersection for pyramidal neurons is normally between 60-80 μm away from the soma. Only at 12 months post-deletion did pyramidal neurons exhibit a shift in the radius of maximal intersection, indicating that as *PTEN* deletion-induced changes in morphology progress over time, neurons becomes increasingly abnormal compared to controls.

To assess the effect of adult *PTEN* deletion on neuronal function and behavior, I performed behavioral assessments of forelimb motor function at 2 month intervals following induction of adult *PTEN* deletion. Using the rotarod task to measure baseline coordination and motor learning, and the cylinder task to identify asymmetry in spontaneous forelimb exploration, I found significant improvement in baseline coordination and motor learning beginning at 8 months after *PTEN* deletion, and

spared symmetry of forelimb exploration at all assessed time points. Pulling our structural and functional data together, the timing of functional improvement onset correlates with the progressive development of increased dendritic density, implicating a role for *PTEN* deletion-induced dendritic changes in mediating the functional gains.

The regenerative effect of *PTEN* deletion is largely due to increased activity of the mammalian target of rapamycin (mTOR) pathway, and a commonly used biomarker for mTOR is phosphorylated ribosomal S6 (pS6, (Sawyers, 2008). Using a high frequency stimulation paradigm, I found that stimulation of the motor cortex results in marked induction of pS6 and therefore mTOR activation. It remains to be determined whether pathways other than mTOR contribute to stimulation-induced S6 phosphorylation, or if high frequency stimulation of the motor cortex could be used to promote regeneration after spinal cord injury. Altogether, the findings reported here highlight the ability for *PTEN* deletion to induce a robust, life-long mTOR-mediated growth program even in adult neurons, and that *PTEN* loss in the adult motor cortex results in functional improvements.

CHAPTER 1: Introduction

In 2008, Park et al. demonstrated that conditional genetic deletion of *PTEN* enabled axonal regeneration of retinal ganglion cells (RGCs) following optic nerve crush. (Park et al., 2008). The rationale for this experimental approach is rooted in the discovery of intrinsic and extrinsic factors that prevent regeneration of injured axons (Schwab and Bartholdi, 1996; Fitch and Silver, 2008). One theoretical approach to addressing these intrinsic factors focuses on attempting to "recapitulate development", in order to return adult neurons to a more growth permissive state (Filbin, 2006). A collaborative follow-up study to Park et al. involved our lab and demonstrated that conditional *PTEN* deletion in the cortex one day after birth enabled robust regeneration of descending axons in the spinal cord after sustaining spinal cord injuries as adults (Liu et al., 2010). This finding further highlighted the potential use of *PTEN* loss as a pro-regenerative strategy for spinal cord injury (SCI) (Park et al., 2010).

PTEN converts phosphatidylinositol (3,4,5)-triphosphate (PIP3) to inactivate phosphatidylinositol (4,5)-bisphosphate (PIP2). The reverse reaction is catalyzed by phosphoinositide 3-kinase (PI3K), and the balance between these reactions determines the level of activation of AKT and downstream activation of mammalian target of rapamycin (mTOR) (Georgescu, 2010). The mTOR pathway is well known for its ability to regulate cell growth and proliferation (Laplante and Sabatini, 2012). PTEN's upstream and non-redundant negative regulation of the AKT/mTOR pathways makes it a potentially therapeutic target following central nervous system injury (Don et al., 2012).

The regenerative and growth-promoting effects of *PTEN* deletion or PTEN hypofunction is largely due to activation of the mammalian target of rapamycin (mTOR) pathway. Treatment with rapamycin, an mTOR inhibitor, attenuates *PTEN* deletion-induced axonal regeneration and prevents the morphological and functional effects caused by neuron-specific *PTEN* deletion (Kwon et al., 2003; Park et al., 2008; Ljungberg et al., 2009; Zhou et al., 2009; Sunnen et al., 2011). Elevated mTOR activity results in increased phosphorylation of ribosomal protein S6 (pS6), an important biomarker for mTOR pathway activation and regulator of protein translation (Nygard and Nilsson, 1990; Sawyers, 2008). Chapter 6 explores an alternative approach to increasing mTOR activity and pS6 induction without genetic manipulation of *PTEN*.

In the human population, *PTEN* mutations have been associated with macrocephaly, autism, and several cancer syndromes (Ali et al., 1999; Goffin et al., 2001; Zhou et al., 2003; Butler et al., 2005; Varga et al., 2009). In an effort to understand the role of inactivated *PTEN* in the central nervous system (CNS), a substantial amount of research has been done on genetically driven *PTEN* deletion in transgenic mouse models. Since germline *PTEN* deletion is embryonic lethal, researchers have utilized mice with lox-P flanked *PTEN* gene ($Pten^{loxP/loxP}$ mice) and Cre recombinase expression regulated under the control of CNS-specific promoters, including neuron specific enolase (NSE, (Kwon et al., 2006; Ogawa et al., 2007; Takeuchi et al., 2013)), glial fibrillary acid protein (GFAP, (Backman et al., 2001; Kwon et al., 2001; Fraser et al., 2004; Yue et al., 2005; Fraser et al., 2008; Wen et al., 2013; Lugo et al., 2014)), Ca^{2+}/calmodulin-dependent protein kinase II (CamKII, (Sperow et al., 2012)), the dopamine active transporter (DAT, (Diaz-Ruiz et al., 2009)), and the γ-

amino butyric acid$_{\alpha}$6 subunit (GABA$_{\alpha}$6, (Goebbels et al., 2017)) . The effect of *PTEN* loss depends greatly on the cell type or extent of the region affected by the deletion (see Table 1.1 for summary). It is worth noting that the embryonic onset of Cre recombinase expression differs for each promoter (Burgin et al., 1990; Forss-Petter et al., 1990; Brenner et al., 1994; Funfschilling and Reichardt, 2002; Smits and Smidt, 2006), and in the GFAP-Cre models, multiple groups have identified neurons with successful *PTEN* deletion in the cerebellum, hippocampus, and the cerebral cortex (Backman et al., 2001; Kwon et al., 2001; Fraser et al., 2004; Fraser et al., 2008). Pulling together the findings from all of these studies, it is nearly impossible to come up with a singularly agreed upon structural, physiological, or behavioral phenotype following *PTEN* deletion during development. To assess these effects in a model previously shown to promote regeneration after spinal cord injury, we selectively deleted *PTEN* in early postnatal neurons of the sensorimotor cortex and characterized the histological and behavioral consequences one year later, these results are discussed at length in Chapter 2.

To address some of the conflicting morphological and physiological findings from the transgenic mouse strains described in Table 1.1, several groups have begun to use inducible *PTEN* deletion systems that allow for tighter control over the developmental timing of *PTEN* deletion (Luikart et al., 2011; Pun et al., 2012; Williams et al., 2015). By using tamoxifen-induced Cre-recombinase expression in neural progenitor cells (Gli1-expressing cells), Pun et al. selectively deleted *PTEN* in subgranular zone progenitors (which give rise to dentate granule cells) and subventricular zone progenitors (give rise to olfactory neurons) by injecting mice with tamoxifen at 2 weeks of age (Pun et al., 2012). They found that *PTEN* expression was lost in a subset of postnatally derived

granule cells, and these granule cells exhibited hypertrophy, increased dendrite thickness, and increased spine density. Mice with *PTEN* deletion also exhibited spontaneous progressive seizures that worsened in frequency and severity with time. The severity of the seizure phenotype correlated with the percentage of *PTEN* deleted granule cells and was preceded by hypertrophy of *PTEN* deleted granule cell somata.

An alternative approach that allows for spatiotemporal control over the induction of *PTEN* deletion involves short hairpin ribonucleic acid (shRNA)-mediated knockdown of PTEN expression via recombinant vector delivery. Luikart et al. performed intra-hippocampal injections of shPTEN with a fluorescent reporter into postnatal (7 days old) and young adult mice (6-8 weeks old) (Luikart et al., 2011). They found that 2 weeks after postnatal PTEN knockdown, the cross-sectional area of granule cells was significantly larger than controls. Additionally, even at this early time point following PTEN knockdown, they found increased dendrite thickness and increased spine density. These anatomical changes were maintained out to 4 months, their furthest time point following PTEN knockdown.

In the mice that had PTEN expression knocked down as adults, a longer amount of time was required following deletion prior to the onset of significant anatomical changes. Not until 4 months following knockdown did granule cell cross-sectional area or the dendritic spine density differ significantly from controls. Functionally, 4 months after both postnatal and young adult PTEN knockdown, enlarged granule cells had increased cell capacitance and decreased input resistance. By 3 weeks following knockdown in young adults, granule cells had increased spontaneous excitatory

postsynaptic currents (sEPSCs), and this difference was not attributed to an increased likelihood of glutamate release. Inhibitory synaptic activity was unaffected by PTEN knockdown. While this study provides important insight into the single cell synaptic effect of PTEN hypofunction, a major limitation to their findings is that subgranular zone progenitors reside within the dentate of the hippocampus and produce newborn granule cells even in adult mice, thus precluding the ability of the authors to reliably report the age of the granule cells being studied. Importantly, the findings were largely concurrent following postnatal and young adult PTEN knockdown.

To avoid the "birthdating" issue with dentate granule cells, Haws et al. used a similar knockdown approach (with shPTEN-Luciferase) but instead performed their injections into the basolateral amygdala (BLA) in young adult mice (7 weeks old) (Haws et al., 2014). Using Sholl analysis based on 3D reconstructed Z-stacks, they found that roughly three weeks following shPTEN-luciferase injection, that BLA neurons did not differ significantly from controls in dendritic length or number of dendritic nodes. Interestingly, they did observe hypertrophy of BLA neuron cell bodies following PTEN knockdown and the diameter of individual dendrites. Contrary to the findings of multiple previous studies ((Kwon et al., 2006; Zhou et al., 2009; Luikart et al., 2011)), they found a *decrease* in spine density following PTEN knockdown in both the BLA and in dentate granule cells, rather than an increased density. They attribute this contradictory finding to an increase in the proportion and size of mushroom spines, which are likely over-counted/detected by less sensitive visualization techniques that cell-filling. Lastly, at 3 weeks following BLA knockdown, they observed no behavioral phenotype (anxiety, social interaction, open field, startle threshold, or locomotion). Due

to the relatively early time points at which they conducted their analyses, it is possible that dendritic changes (detected by Sholl analysis) and behavioral phenotypes may not appear until later time points post-knockdown.

In 2015, Williams et al. conducted a similar experiment to Luikart et al., but injected retroviruses carry Cre-recombinase to deleted *PTEN* at postnatal day 7 instead of injecting shPTEN to knockdown PTEN at postnatal day 7 (Williams et al., 2015). They found hypertrophy of granule cells (by 7.5 days post injection of Cre), increased membrane capacitance, and decreased input resistance, in line with the findings by Luikart et al. Using perforant path presynaptic stimulation, they also found that *PTEN* deleted granule cells fired more and at lower intensities of perforant path stimulation than did controls, indicating that the increased activity of *PTEN* deleted neurons is due to an increased sensitivity to depolarizing synaptic input. To account for the increased current needed to elicit an action potential and the paradoxical increased responsiveness to presynaptic input, Williams showed that *PTEN* deleted neurons had increased dendrites and dendritic protrusions (increased number of all types of protrusions, not just mushroom). It remains to be seen why Haws and Williams found disparate results in dendritic density and protrusions following *PTEN* deletion, though one explanation may be the time at which deletion was induced (7 weeks old vs. postnatal day 7).

More recently, groups have begun to assess the effects of *PTEN* deletion or PTEN knockdown on regeneration after injury in adult neurons. In 2015, Danilov and Steward showed that deletion of *PTEN* via AAV-Cre injection into $Pten^{loxP/loxP}$ mice immediately

following cervical contusion spinal cord in young mice (5-7 weeks old) resulted in improved grip strength and hanging ability, as well as increased regeneration of descending corticospinal tract axons (Danilov and Steward, 2015). Even more impressively, Du et al. found that deletion of *PTEN* via AAV-Cre injection in $Pten^{loxP/loxP}$ 4 weeks and even one year following thoracic crush spinal cord injury induced robust regeneration of the corticospinal tract (Du et al., 2015).

Silencing PTEN expression using shPTEN injections allows for the examination of the effect of PTEN hypofunction without the use of transgenic mice, providing a more therapeutically relevant model for injury and regeneration. shPTEN knockdown in the sensorimotor cortex of postnatal day 1 (P1) mice resulted in marked regeneration of corticospinal tract axons (descending from motor neurons in which PTEN had been silenced) following thoracic crush spinal cord injuries as young adults (Zukor et al., 2013). Tis study silenced provided an important proof of concept for using PTEN expression to promote axon regeneration after injury, however knockdown began during the growth-permissive period of early postnatal development, which is not therapeutically reasonable. A study by Lewandowski & Steward showed that silencing PTEN in the sensorimotor cortex of adult rats just prior to cervical dorsal hemisection also caused corticospinal tract regeneration and improved voluntary motor function (Lewandowski and Steward, 2014). While neither of these studies demonstrated efficacy of PTEN knockdown *following* spinal cord injury in adult rodents, they do support the notion that gene knockdown holds promise for promoting neuronal regeneration.

In addition to promoting regeneration after injury, *PTEN* deletion also increases neuronal resilience and survival against toxic insults. *PTEN* deletion in dopaminergic neurons of adult mice attenuates the histopathology (spares dopaminergic neurons) and motor impairment in a Parkinson's disease mouse model (Domanskyi et al., 2011). Cultured isolated granule neurons lacking *PTEN* show significant resistance to low potassium-induced cell death compared to controls (Yue et al., 2005). In the seminal paper that discovered *PTEN*'s role in promoting axon regeneration, Park et al. also showed that following *PTEN* deletion in the vitreous humor of adult mice, a significantly increased number of *PTEN* deleted retinal ganglion survived the optic nerve crush injury (Park et al., 2008).

Pulling together the findings from studies involving neonatal *PTEN* deletion/knockdown in intact mice and *PTEN* deletion/knockdown in injury or disease models, *PTEN* hypofunction holds increasing therapeutic promise for modifying neurodegenerative diseases, acute injuries, and aging-related changes. While a great amount of knowledge has been gained through the aforementioned studies, very little is known about the role of *PTEN* loss in intact, adult neurons. The only study that has attempted to address this role involved silencing PTEN using shRNA, and because the cells that were analyzed were dentate granule cells, they could be anywhere from newly born to the age of the mouse itself (and therefore not an ideal examination of PTEN knockdown in *adult* neurons). Furthermore, *PTEN*'s role as a tumor suppressor gene necessitates a thorough examination of the long-term effects of the loss of *PTEN* in the context of promoting axon regeneration following spinal cord injury.

Table 1.1- Summary of Mouse Models of Neonatal *PTEN* Deletion

Strain	Cre Regulation& Onset	Survival	Behavioral Change	Physiological Change	Histological Change	Synaptic or Spine Change	Reference
$Pten^{loxP/loxP}$	- NSE-Cre expression ~E12.5 (Forss-Petter et al., 1990)	- NA (not reported, survived 10 months)	- Spontaneous seizures (EEG) - Impaired social interaction - Hyperactive under stress - Anxiety - Enhanced performance on rotarod in late trials	- EEG-repetitive spike-wave patterns - Continuous spike wave bursting - 0.67 seizures/day - 10 min 50s ave. duration	- Progressive macrocephaly - Granule cell body hypertrophy - Deletion in hippocampus and sensory cortex	- Ectopic granule cell axons - 24.9% increase in dendritic spine density in ML - Dendritic ectopia	Kwon 2006 (Kwon et al., 2006)
$Pten^{loxP/loxP}$	- NSE-Cre expression ~E12.5 (Forss-Petter et al., 1990)	- NA (not reported)	- Initial increases in open field locomotion - Decreased dark phase wheel-running	- Age-related increases in seizure (EEG and EMG) activity - Frequent subclinical epileptiform activity	- Mice with high seizure rates also had increase dentate granule cell dispersion - Neuronal hypertrophy - Macrocephaly	- NA	Ogawa 2007
$Pten^{loxP/loxP}$	- NSE-Cre with LacZ reporter expression ~E12.5 (Forss-Petter et al., 1990)	- Animals survived up to 30 weeks	- NA	- Normal paired pulse ratio (PPR) in young (8-12 wks) and old mice (20-30 wks) - Decreased PPR in middle aged mice (14-19 wks) - Elevated long term potentiation (LTP) in young mice, impaired in older mice - Impaired LTD at all ages	- Enlarged DGCs and mossy fiber axons - Morphological changes apparent after onset of abnormal physiology	- NA	Takeuchi 2013 (Takeuchi et al., 2013)
$Pten^{loxP/loxP}$	- GFAP-Cre expression ~E13.5 (Brenner et al., 1994)	- 0% survival at 29 weeks	- Seizures and ataxia by 9 weeks	- NA	- Cerebellar enlargement and dentate dysplasia - Increased soma size of granule cells by 4 weeks - No changes in proliferation or death	- NA	Backman 2001 (Backman et al., 2001)
$Pten^{loxP/loxP}$	- GFAP-Cre, with LacZ reporter expression ~E13.5 (Brenner et al., 1994)	- Death between 9-48 weeks	- Tonic clonic seizures by 7-10 weeks	- NA	- Cerebellar enlargement - Abnormal cell migration - Granule cell enlargement - No change in proliferation or cell death	- NA	Kwon 2001 (Kwon et al., 2001)

Strain	Cre Regulation& Onset	Survival	Behavioral Change	Physiological Change	Histological Change	Synaptic or Spine Change	Reference
$Pten^{loxP/loxP}$	- GFAP-Cre, with LacZ reporter expression ~E13.5 (Brenner et al., 1994)	- 40% died by 6 weeks of age	- Seizures, developed in 20% of mice by 10 weeks of age	- NA	- Progressive macrocephaly - Neuron and astrocyte hypertrophy - Astrocyte proliferation	- NA	Fraser 2004 (Fraser et al., 2004)
$Pten^{loxP/loxP}$	- GFAP-Cre expression ~E13.5 (Brenner et al., 1994)	- Death by 21 days of age	- NA (none reported)	- NA	- Macrocephaly and cerebellar enlargement - Purkinje and granule layering defect - Enhanced cell survival in potassium induced apoptosis test	- NA	Yue 2005 (Yue et al., 2005)
$Pten^{loxP/loxP}$	- GFAP-Cre expression ~E13.5 (Brenner et al., 1994)	- NA (not reported)	- NA (not reported)	- Impaired field excitatory postsynaptic potentials (fEPSPs) - Normal PPR - Reduced LTP	- Significantly larger layer V pyramidal nucleoli - Increased electron density of soma due to more ribosomes - Increased presynaptic vesicles - Enlarged postsynaptic densities	- Enlarged dendrites - Abnormal dendrite size - Enlarged axons, more myelin (oligo *PTEN* loss)	Fraser 2008 (Fraser et al., 2008)
$Pten^{loxP/loxP}$	- GFAP-Cre expression ~E13.5 (Brenner et al., 1994)	- All animals died between 13 and 20 days of age	- Ataxia - Motor tremor - Muscle spasms	- NA	- Gliosis - Gross brain hypertrophy - Hydrocephalus - Enlarged ventricles - Disrupted hippocampal and cerebellar lamination - Astrocyte and neuronal *PTEN* loss	- NA	Wen 2013 (Wen et al., 2013)
$Pten^{loxP/loxP}$	- GFAP-Cre expression ~E13.5 (Brenner et al., 1994)	- NA (not reported)	- Impaired social interaction - Spared odor discrimination - Decreased marble burying and nose pokes - Open field hyperactivity - Decreased anxiety in elevated plus	- NA	- NA	- Decreased mGluR - Elevated fragile X mental retardation protein (FMRP) and phosph. FMRp - Decreased $K_v4.2$	Lugo 2014 (Lugo et al., 2014)

Strain	Cre Regulation& Onset	Survival	Behavioral Change	Physiological Change	Histological Change	Synaptic or Spine Change	Reference
$Pten^{loxP/loxP}$	- CamKIIα-Cre expression at P4 (Burgin et al., 1990)	- Died by 11 weeks of age NOTE: deletion was not detectable until P14	- Normal spatial learning - Impaired spatial memory	- Normal fEPSP - Normal basal synaptic transmission between CA3-CA1 - Normal PPR - Normal mEPSC - Decreased LTP following HFS at Schaffer collaterals - Decreased LTD	- Normal hippocampal development - No change in soma size of neurons lacking *PTEN* (likely to due the brief time between deletion of PTEN and death)	- Dendritic length and width comparable to controls - Synaptic structure comparable to controls	Sperow 2012 (Sperow et al., 2012)
$Pten^{loxP/loxP}$	- DAT-Cre expression at E15 (Smits and Smidt, 2006)	- NA (not reported)	- NA (not reported)	- NA	- Enlarged and increased # of neurons in the SNc and TVA - Enlarged neurons did not have enhanced TH staining - *PTEN* loss protective against 6OHDA insult	- Increased number of dendritic processes	Diaz Ruiz 2009 (Diaz-Ruiz et al., 2009)
$Pten^{loxP/loxP}$	- $GABA_{\alpha}6$- Cre expression At P5 (Funfschilling and Reichardt, 2002)	- NA (not reported)	- Ataxia and tremor in older mice	- No altered input from granule cells to oligodendrocyte precursor cells (OPCs)or Purkinje cells	- Increased granule cell soma and axon size - Aberrant parallel fiber myelination - OPC proliferation - Cerebellar hypertrophy - White matter atrophy	- Normal synapses present along myelinated parallel fibers emanating from granule cells	Goebbels 2017 (Goebbels et al., 2017)

CHAPTER 2: Long-term consequences of *PTEN* deletion in the sensorimotor cortex of neonatal mice

Previously published in and selected to be featured as the cover in *Experimental Neurology* in 2015 as: Gutilla, Erin A., Melda M. Buyukozturk, and Oswald Steward. "Long-term consequences of conditional genetic deletion of PTEN in the sensorimotor cortex of neonatal mice." *Experimental neurology* 279 (2016): 27-39.

ABSTRACT

Targeted deletion of the phosphatase and tensin homolog on chromosome ten (*PTEN)* gene in the sensorimotor cortex of neonatal mice enables robust regeneration of corticospinal tract (CST) axons following spinal cord injury as adults. Here, we assess the consequences of long-term conditional genetic *PTEN* deletion on cortical structure and neuronal morphology and screen for neuropathology. Mice with a LoxP-flanked exon 5 of the *PTEN* gene (*PTENf/f* mice) received AAV-Cre injections into the sensorimotor cortex at postnatal day 1 (P1) and were allowed to survive for up to 18 months. As adults, mice were assessed for exploratory activity (open field), and motor coordination using the Rotarod®. Some mice received injections of fluorogold into the spinal cord to retrogradely label the cells of origin of the CST. Brains were prepared for neurohistology and immunostained for PTEN and phospho-S6, which is a downstream marker of mammalian target of rapamycin (mTOR) activation. Immunostaining revealed a focal area of *PTEN* deletion affecting neurons in all cortical layers, although in some cases *PTEN* expression was maintained in many small-medium sized neurons

in layers III-IV. Neurons lacking *PTEN* were robustly stained for pS6. Cortical thickness was significantly increased and cortical lamination was disrupted in the area of *PTEN* deletion. *PTEN*-negative layer V neurons that give rise to the CST, identified by retrograde labeling, were larger than neurons with maintained *PTEN* expression, and the relative area occupied by neuropil vs. cell bodies was increased. There was no evidence of tumor formation or other neuropathology. Mice with *PTEN* deletion exhibited open field activity comparable to controls and there was a trend for impaired Rotarod performance (not statistically significant). Our findings indicate that early postnatal genetic deletion of *PTEN* that is sufficient to enable axon regeneration by adult neurons causes neuronal hypertrophy but no other detectable neuropathology.

INTRODUCTION

The phosphatase and tensin homolog (*PTEN*) gene has emerged as a promising target for enhancing axon regeneration in the mature central nervous system (CNS). The initial finding was that deletion of *PTEN* enabled regeneration of axons of retinal ganglion cells following optic nerve crush (Park et al., 2008) and reduced the retrograde degeneration of axotomized RGCs that otherwise occurred. This study used transgenic mice with a floxed *PTEN* gene that was deleted by local injections of AAV-Cre. A subsequent study used the same approach to show that conditional genetic deletion of *PTEN* in the sensorimotor cortex of neonatal mice enabled regeneration of corticospinal (CST) axons following spinal cord injury (SCI) in adulthood. CST regeneration was seen following both dorsal hemisection and complete crush injury (Liu et al., 2010). Follow-up studies using similar approaches reported CST regeneration with conditional genetic deletion of *PTEN* in adult mice at the time of a spinal cord injury (Danilov & Steward, 2015) as well as in the chronic post-injury period (Du et al., 2015). These results, coupled with PTEN's upstream and non-redundant negative regulation of the PI3K/AKT pathway, make it a potentially important therapeutic target following CNS injury (Don et al., 2012).

The *PTEN* gene has been extensively studied for its role as a tumor suppressor and mutations are seen in several human cancers and cancer syndromes (Ali et al., 1999) (Goffin et al., 2001; Shi et al., 2012). Also, the PTEN/mammalian target of rapamycin (mTOR) pathway is well known for its ability to regulate cell growth and proliferation (Laplante and Sabatini, 2012). mTOR is up-regulated by activation of

phosphoinositide 3-kinase (PI3K), which converts phosphatidylinositol (4,5)-bisphosphate (PIP2) to phosphatidylinositol (3,4,5)-triphosphate (PIP3) (Georgescu, 2010). Via its action as a phosphatase, PTEN opposes PI3K activity by converting PIP3 into PIP2, thus damping activation of downstream pathway components, such as phosphorylated ribosomal protein S6 (pS6), limiting cell growth (Park et al., 2010). Deleting *PTEN* activates mTOR, which presumably leads to downstream changes in mRNA translation regulated by mTOR signaling. *PTEN* mutations in humans have been associated with neurological abnormalities, including macrocephaly and autism (Goffin et al., 2001; Waite and Eng, 2002).

Previous studies have explored the consequences of deleting *PTEN* using transgenic promoter-driven Cre expression in *PTEN*$^{f/f}$ mice, including Ca^{2+}/calmodulin-dependent protein kinase II (CamKII), (Sperow et al., 2012), dopamine active transporter (DAT), (Diaz-Ruiz et al., 2009), glial fibrillary acid protein (GFAP), (Backman et al., 2001; Kwon et al., 2001; Fraser et al., 2004; Yue et al., 2005; Fraser et al., 2008; Wen et al., 2013), and neuron specific enolase (NSE), (Kwon et al., 2006; Takeuchi et al., 2013). The expression of each promoter (and therefore Cre recombinase) varies, with the earliest expression beginning at embryonic day 12.5 (E12.5) for NSE (Forss-Petter et al., 1990), E13.5 for GFAP (Brenner et al., 1994), E15 for DAT (Smits and Smidt, 2006), and postnatal day 4 for CamKII (Burgin et al., 1990).

Deletion of *PTEN* in neurons via transgenic promoter-driven Cre expression *in vivo* leads to increased brain mass, cerebellar enlargement, disruption of cortical lamination, and neuronal hypertrophy (Kwon et al., 2001; Marino et al., 2002; Yue et

al., 2005; van Diepen and Eickholt, 2008). In addition to the gross and microscopic anatomical changes following *in vivo PTEN* deletion, neuropathologies including seizures, hydrocephalus, and ataxia were observed (Kwon et al., 2001; Fraser et al., 2004; Pun et al., 2012).

Previous studies involving conditional postnatal *PTEN* deletion in neurons using transgenic promoter-driven Cre expression have limited their analyses primarily to young adult mice (up to 30 weeks old) (Kwon et al., 2006; Luikart et al., 2011; Takeuchi et al., 2013; Williams et al., 2015). The consequences of longer-term *PTEN* deletion have not been assessed. Also, there have not yet been assessments of the consequences of early postnatal AAV-mediated *PTEN* deletion in the sensorimotor cortex, in the way that enables robust regeneration of adult CST axons (Liu et al., 2010).

The goal of the present study was to determine the consequences of long-term *PTEN* deletion in the sensorimotor cortex, focusing on the effects on cortical structure, neuronal size, functional consequences (if any), and whether there is evidence of tumors or other neuropathology. We show that AAV-Cre injections at postnatal day 1 lead to focal deletion of *PTEN* but with selective maintenance of *PTEN* expression in some neuronal types (small-medium sized neurons). There were increases in cortical thickness in the area of *PTEN* deletion, and cortical lamination was altered, with increases in the ratio of neuropil to cell bodies. Cortical motoneurons lacking *PTEN* identified by retrograde labeling were hypertrophied. There was no evidence of tumors, necrosis, inflammation, or other evident neuropathology. Maintained *PTEN* expression

by some neurons may be a result of selective tropism of AAV-Cre for certain neuron types in the neonatal stage of development.

METHODS

PTEN Deletion in the Motor Cortex

All experimental procedures were approved by the Institutional Animal Care and Use Committee at the University of California, Irvine. Transgenic mice with a floxed exon 5 of the *PTEN* gene (*PTENf/f*) were from our local breeding colony that was established from founders obtained from Jackson Laboratories (Strain: C;129S4-$Pten^{tm1Hwu}$/J, Stock number: 004597). The colony was maintained by intercrossing mice homozygous for the floxed allele.

PTENf/f mice were injected on postnatal day 1 with AAV-Cre (n=22) or AAV-GFP (n=12). The vectors were AAV serotype 2, and were obtained from Vector Bio Labs (1 x 10^{13} genome copies/mL, Catalog number 7011). The virus was diluted with sterile-filtered PBS and 5% glycerol for a final concentration of 1 x 10^{12} genome copies/mL. To perform the injections, 1-day-old pups were anesthetized by hypothermia (up to 5 minutes) and placed on a clay body mold attached to the bite bar of a stereotaxic apparatus. Injections were made using a Hamilton microsyringe with a pulled glass micropipette tip. Six mice received injections as in Liu et al. with two unilateral injections of AAV-Cre (0.5 mm lateral, 0.5 mm deep to the cortical surface, and +0.5 and 0.0 mm with respect to bregma) for a total volume of 2 µl (Liu et al., 2010). Twenty-three mice were injected using a procedure developed in Dr. Zhigang He's lab

involving three unilateral injections (0.5 mm lateral, 0.5 mm deep to the cortical surface, and +0.5, 0.00, and -0.5 mm with respect to bregma) for a final total injection volume of 1.5µl of vector (n=11 AAV-Cre and 12 AAV-GFP). After injection, pups were dipped in a few drops of sesame oil and returned to their home cages. After weaning, mice were maintained under standard vivarium conditions for 12-18 months. Table 2.1 summarizes animals and experimental conditions.

Rotarod Assessment of Motor Coordination

Animals with PTEN deletion (n=9) and AAV-GFP injected controls (n=12) were tested for motor coordination when they were 48 to 53 weeks of age (51.6 weeks of age, on average). Mice were placed individually in each of the four chambers on the rod of a Rotarod® (San Diego Instruments) were allowed to acclimate to the stationary rod for 30 seconds before starting every trial. Initial speed of the rotorod was set to 3 RPM and acceleration was set at 1 RPM/second. Mice were allowed to stay on the rod until they fell off or up to a maximum of two minutes, for a total of 7 trials/day. The first two trials were considered training trials, and the next 5 were testing trials. The time at which the mice fell from the rod during the testing trials (if at all) was recorded. PTEN deletion was assessed by immunocytochemistry (see below) and data from 3 mice with PTEN deletion located outside of the motor cortex were excluded from the statistical analysis, leaving a final n=6 for the PTEN deletion group.

Open Field Test

The same mice that were tested using the Rotarod were also tested for general locomotion and spatial learning in the open field (9 animals with PTEN deletion and 12

animals with AAV-GFP). A 24-inch by 24-inch dark plexiglass box was used for the open field test. A 3-inch by 3-inch grid was drawn onto the bottom of the plexiglass box. The grid had four different colored zones, a center square, and the corner squares marked. The four differently colored zones were determined based on their proximity to the center square. The lines that comprised the outer two zones were considered "outer", while the lines of the inner two zones and the center square were considered "inner" lines. Individual mice were placed in the center of the box and allowed to explore freely for 5 minutes. One observer recorded total grid line crossings by forepaws, noting whether the lines crossed were "outer" or "inner" lines. The second observer recorded other events such as defecation, urination, grooming, and rearing. Open field activity was tested once a day for four consecutive days.

Retrograde tracing of the cells of origin of the CST with Fluorogold

At approximately 1 year of age, mice that had received AAV-Cre (n=6) or AAV-GFP (n=2) received bilateral injections of the retrograde tracer Fluorogold (FG) into the spinal cord. Mice were anaesthetized with isoflurane and a laminectomy was performed to expose the spinal cord at C5. 0.2µl of 1% FG was injected with a Hamilton syringe bilaterally from the midline (0.5mm lateral, 0.5mm deep) over 1 minute. The syringe was left in place for an additional minute. After completing the injections, the skin was closed with sutures and staples, and mice were kept on a 37°C water circulating heating pad until they recovered from the anesthetic. Mice received subcutaneous injections of buprenorphine, Baytril, and lactated Ringer's solution twice a day for 3 days post surgery, and were allowed to remain in their home cages for 3 (n=7) to 4 (n=1) days before tissue collection.

Tissue Collection and Immunohistochemistry

At 12-18 months of age, mice received intraperitoneal injections of Euthasol (1mL/300g), and were perfused transcardially with 4% paraformaldehyde (PFA). The brain and spinal cord were dissected and post-fixed in PFA overnight, then placed in 30% sucrose solution in PBS overnight for cryoprotection. Brains were embedded in OCT compound and frozen in a container of methyl butane surrounded by ethanol/dry ice slush. 20μm thick coronal sections were collected at 200μm intervals and stored in PBS with 0.1% sodium azide at 4°C until staining.

Sections were either directly mounted for Fluorogold visualization under fluorescent microscopy, stained for H&E or cresyl violet, or immunostained (see Table I for summary). To visualize GFP signal in the control animals, we examined unstained sections for GFP fluorescence and immunostained sections for GFP.

For immunostaining for cleaved caspase-3, Ki67, pS6, and PTEN, an antigen retrieval protocol was used in which sections were placed in 1.7ml Eppendorf tubes with 1 mL 10mM citrate buffer, pH 8.80. Tubes were then immersed in boiling water for 5 minutes, followed by immediate immersion in an ice bath for 10 minutes. Sections immunostained for GFP were incubated in 1% H_2O_2 for 20 minutes to quench endogenous peroxidase activity. Primary antibodies and dilutions were as follows: PTEN (Cell signaling, 1:250), pS6 (Cell signaling, 1:250, #4858), GABA (1:500), GFAP (Sigma, 1:1000), GFP (Lifetech, 1:1500), Ki-67 (Thermo Scientific, 1:200), Cleaved caspase-3 (BD Biosciences, 1:250), GFP (Lifetech, 1:1000). Antibodies were diluted in Blocking Reagent for cleaved caspase-3, pS6, and PTEN (PerkinElmer), 5% secondary

antibody host serum in PBS with 0.5% Triton (GABA, GFAP, Ki67), or 5% secondary host serum in TBS with 0.1% Triton (GFP).

Sections were incubated in primary antibody dilutions overnight at room temperature, with the exception of GABA, which was incubated for 36-48 hours at 4°C. Secondary antibodies were diluted in the same blocking solution as the respective primary, and applied for two hours at room temperature. For immunofluorescence, Alexa Fluor 488 or Alexa Fluor 594 (ThermoFisher Scientific, both at 1:250 dilution) were used. For sections undergoing DAB detection and fluorescent amplification, a biotinylated IgG secondary antibody was used (Vector Laboratories, 1:250 dilution). Following secondary incubation, sections were washed 3X, incubated for 1 hour with avidin and biotinylated horseradish peroxidase (Vectastain ABC kit, Vector Laboratories) and reacted with DAB (DAB Substrate Kit for Peroxidase, Vector Laboratories) or FITC (made in house, 1:250 in 0.003% H_2O_2 borate buffer).

Layer V Pyramidal Cell Size Measurements

To determine the effect of *PTEN* deletion on pyramidal neurons that give rise to the CST, cortical sections from AAV-Cre injected animals that had received intra-spinal FG injections were analyzed. Immunostaining for PTEN using a DAB reaction quenched FG fluorescence in PTEN-positive CST neurons whereas fluorescence was still prominent in CST neurons lacking PTEN. We then measured the cross sectional area of 50 PTEN-negative/FG positive CST neurons per animal. For control cells we used the nearest neighboring unstained section and visualized FG signal in the contralateral

cortex in unstained sections. This allowed us to specifically measure PTEN-positive layer V pyramidal cells.

Measurement of Cortical Thickness and Assessment of Cortical Lamination

It has previously been reported that promoter-driven *PTEN* deletion in the forebrain results in cortical enlargement. To assess this, we measured the thickness of the cortex (distance from the edge of the corpus callosum to the pial surface) in H&E stained-sections within the area of deletion (n=5 mice). The region of *PTEN* deletion was verified in a nearby section that had been immunostained for PTEN. To examine changes in cortical laminar patterning, we screened H&E-stained sections from animals with *PTEN* deletion and compared the region of deletion to the homotopic contralateral control cortex.

Measurement of Cell Density

To determine whether conditional postnatal *PTEN* deletion results in altered cell density in the motor cortex we performed point-counting analysis. H&E stained sections within the region of *PTEN* deletion were imaged at 20x along with images from the control cortex contralateral to the *PTEN* deletion. These images were then overlaid with a 50μm grid and analyzed in ImageJ for the number of grid crosshairs overlying cells vs. cell-free neuropil (154 maximum). This value was then used to calculate the relative area of neuropil vs. cell bodies.

RESULTS

Pattern of PTEN deletion in the sensorimotor cortex with AAV-Cre injections on postnatal day 1

To define the area of *PTEN* deletion, sections were immunostained for PTEN. On the non-injected control side, neurons in all cortical layers stained positively for PTEN. There was also diffuse staining in the neuropil layers (Figure 2.1B, right cortex). Higher magnification views reveal that large pyramidal neurons in layer V are robustly stained (Figure 2.1C, arrows). PTEN immunostains of sections from mice that received intracortical AAV-GFP injections appeared similar to the contralateral control cortex of AAV-Cre injected mice.

On the side of the AAV-Cre injection, the area of *PTEN* deletion is easily identified by the decrease in PTEN immunostaining (Figure 2.1A, left cortex). Higher magnification views reveal a characteristic immunostaining pattern in which neurons lacking PTEN stood out in negative relief as "ghost cells" (Figure 2.1B, arrows). Although these cells resemble holes in the tissue, visualizing the same section immunostained for PTEN using phase contrast microscopy confirms that the ghost cells are neuronal cell bodies (Figure 2.1E-F).

Ghost cells were especially evident in layer V (the location of the cells of origin of the CST), and large PTEN-negative dendrites could be seen emerging from the apex of the pyramid-shaped cell bodies and extending through more superficial layers of the cortex (Figure 2.2A). The area of deletion was defined as the total region containing

ghost cells. Although neurons lacking PTEN were evident, in some cases there were many PTEN-positive cells throughout the area of deletion. In these cases, PTEN-positive neurons were especially evident in cortical layers II and IV and these layers contained fewer ghost cells than layers III and V (Figure 2.2A). Many of the PTEN-positive medium-sized neurons in the AAV-Cre injected cortex had the morphology typical of cortical interneurons (Figure 2.2A).

To assess whether neurons with preserved PTEN expression were inhibitory interneurons, two nearby sections were immunostained for PTEN or γ-Aminobutyric acid (GABA) (Figure 2.2B and 2.2C). GABA-positive neurons were present in all cortical layers within the area of deletion, but their distribution did not align with the distribution of PTEN-positive neurons within the area of deletion; thus, neurons that are PTEN-positive are not exclusively inhibitory interneurons (Figure 2.2B and 2.2C).

Variations in the size of the region of deletion

All mice injected with AAV-Cre had areas with ghost cells characteristic of successful *PTEN* deletion. The location and size of the area of PTEN deletion varied across cases, however, even when comparing cases that had used identical AAV-Cre titers, injection volumes, number of injections, and injection coordinates. By visual comparison, we found that two injections of 1.0μl of AAV-Cre resulted in more robust *PTEN* deletion than three injections of 0.5μl AAV-Cre. In all 6 mice that received two injections of greater volume, the rostral to caudal spread of the *PTEN* deletion area appeared larger and appeared to contain more ghost cells in PTEN immunostains when compared to the 11 mice that had received three injections of lower volume.

Neurons lacking PTEN have increased phosphorylation of ribosomal protein S6

Deletion of *PTEN* results in the activation of AKT, which in turn activates mTOR. One downstream marker for mTOR activation is phosphorylation of ribosomal protein S6 (Ma and Blenis, 2009). Confirming previous findings (Liu et al., 2010), immunostaining with antibodies specific for S6 phosphorylated at ser235/236 revealed increased S6 phosphorylation in neurons within the area of *PTEN* deletion, even a year after deletion. Fig. 2.3A illustrates a neighboring section to the section immunostained for PTEN in Figure 1A, B, E. In the area of *PTEN* deletion, individual neurons exhibited elevated levels of immunostaining in comparison to the same region on the control side (Figure 2.3A, left vs. right cortex). Pyramidal neurons in layer V with elevated levels of pS6 appeared larger than neurons in the homologous part of the cortex on the contralateral side (compare Fig. 2.3B with 2.3C). There was also increased pS6 immunostaining of ascending apical and basal dendrites of the large layer V pyramidal neurons (Figure 2.3B) in comparison to the contralateral control side (Figure 2.3C). As a technical aside, co-labeling sections for pS6 and PTEN was not attempted because both primary antibodies were generated in rabbit.

In the control cortex and areas where PTEN expression was maintained in the AAV-Cre injected cortex, neurons in all cortical layers stained positively for pS6 with the highest levels of staining exhibited by large pyramidal neurons in layer V (Figure 2.3C). Levels of immunostaining were highest in neuronal cell bodies and proximal dendrites.

An important technical point is that levels of immunostaining for pS6 depend on the animals' experience during the time just before death, varying in a way that is

similar to immediate early gene (IEG) expression. For this reason, it is important to have an internal control, provided here by comparisons of immunostaining in areas with maintained PTEN expression (for example, the side contralateral to the AAV-Cre injection).

No evidence of neuropathology with long-term PTEN deletion

Previous studies have reported neuronal and cortical hypertrophy when *PTEN* is deleted in developing mice using promoter-driven CRE expression (Kwon et al., 2001; Kwon et al., 2003; Fraser et al., 2004; Sperow et al., 2012). To assess whether focal *PTEN* deletion led to detectable changes in the histological appearance of the cortex, 20μm sections taken every 200μm throughout the brain were stained with hematoxylin and eosin (H&E). Areas of *PTEN* deletion were evident in several respects. First, in most mice, the cortex was noticeably thicker, and in some mice, there was actually a bulge in the cortex corresponding to the area of *PTEN* deletion (Figure 2.3D, left vs. right cortex). Second, cortical cytoarchitecture was somewhat different in that cortical layers were less distinct and cell-packing density appeared lower with increased spacing between neuronal cell bodies (particularly in layer V, compare Figure 2.3E and 2.3F). There was no evident neuropathology, such as accumulations of basophilic (basic) immune cells. Note that the tear in the tissue in Figure 2.3D is a result of tissue processing damage and not damage due to the injection, as was seen in some mice (see below).

In AAV-GFP injected controls native GFP fluorescence was not detectable one year following injection. Immunostaining for GFP revealed scattered GFP positive

astrocytes and a few neurons in the area of the injection (Figure 2.4A and 2.4B). In contrast to the situation with AAV-Cre-mediated *PTEN* deletion, cortical cytoarchitecture appeared essentially normal in cases injected with AAV-GFP (Figure 2.4C). As expected, PTEN immunostaining was intact in this region (Figure 2.4D) and there were no increases in immunostaining for pS6 in comparison to the contralateral, non-injected side (Figure 2.4E and 2.4F).

PTEN is a tumor suppressor, so it was important to screen for any evidence of tumors. No unusual cell clusters were evident in H&E stained sections. For five cases, 20μm sections taken every 200μm were immunostained with GFAP in order to detect areas of astrogliosis indicative of neurodegeneration or any astroglial tumors. GFAP stained sections within the *PTEN* deletion region had GFAP-positive astrocytes in the glia limitans and in white matter tracts, similar to what we found in the contralateral control cortex (Figure 2.5A and 2.5B). No abnormal accumulations of GFAP-positive cells were identified in the area of *PTEN* deletion.

We noticed that one animal that received AAV-Cre injections and two animals that received AAV-GFP injections had cortical defects in the region of the injection. Sections through the defect were immunostained for GFAP (Figure 2.5C and 2.5D); examination of these revealed that the defects were lined with GFAP positive stellate astrocytes. The defects are probably areas of cortical injury produced at the time of the P1 injection, although other explanations cannot be excluded.

To screen for ongoing abnormal cell proliferation in areas of *PTEN* deletion, sections were immunostained for Ki-67. As a positive control, Ki-67 positive cells were evident in the subventricular zone (SVZ) lining the lateral ventricles. There were no Ki-67 positive cells in the area of *PTEN* deletion (Figure 2.6B and 2.6C). Note that small fluorescent particles evident in Figure 2.5C were also present in the contralateral *PTEN* intact cortex immunostained for Ki-67 (Figure 2.6D). These particles have a different appearance than the Ki-67-positive cells in the SVZ (Figure 2.6E), and thus are likely immunostaining artifacts. To assess whether the decreased ratios of cell bodies relative to neuropil following *PTEN* deletion might be due to apoptotic cell death, we immunostained sections for cleaved caspase-3 since cleavage of caspase-3 reflects activation of pro-apoptotic pathways. We did not find any cells within the *PTEN* deleted or control motor cortex that were positive for cleaved caspase-3 (Figure 2.6F).

Changes in the cell density and lamination within the region of deletion

Previous studies have reported alterations in cortical lamination and cell packing following promoter-driven *PTEN* deletion during early development (Yue et al., 2005; Wen et al., 2013). Similar though less severe effects were qualitatively evident in the area of *PTEN* deletion. In H&E stained sections, the hexilaminar patterning of the cortex appeared disorganized (Figure 2.7A vs. 2.7B). To quantify cell-packing density in the region of *PTEN* deletion, we used a point-counting method to determine the relative area occupied by cell bodies vs. neuropil in the *PTEN*-deleted area of the motor cortex vs. the contralateral non-injected cortex. The percentage of neuropil in the control motor cortex was 71.76%±3.47% vs. 79.52%±2.73% in the area of *PTEN* deletion (paired

t-test 12.70, $p<0.0002$, see Figure 2.7C). The percentage of neuropil is the inverse of cell-packing density.

Increased cortical thickness following long-term PTEN deletion

Previous studies have also reported cortical hypertrophy following neonatal *PTEN* deletion (Fraser et al., 2004; Kwon et al., 2006). Since AAV-CRE injections were unilateral, we compared cortical thickness in the area of maximal *PTEN* deletion vs. the contralateral control. In the area of deletion, cortical thickness ranged from 1171.1 μm to 1527.9 μm (1332.7 μm average, ±139.6), vs. 980.2 μm to 1290.9 μm (1177.6 μm average, ±123.1) on the contralateral un-injected side (two-way ANOVA: $F=12.69$ for vector type, $p<0.002$, Figure 2.8). In mice that received injections of AAV-GFP, the injected region of the cortex was somewhat thinner than the contralateral cortex. In the area of AAV-GFP injection, cortical thickness ranged from 913.4 μm to 1242.2 μm (1087.5 μm average, ±105.9), vs. 967.2 μm to 1160.1 μm (1104.6 μm average, ±67.1) on the contralateral un-injected side (two-way ANOVA: $F=0.6280$, $p=0.4413$).

Hypertrophy of retrogradely-labeled PTEN-negative cortical motoneurons

To identify PTEN-negative cells of origin of the CST, 6 mice that had received unilateral injections of AAV-Cre at P1 received bilateral injections of Fluorogold (FG) at C5 as adults. In 5 mice with sufficient FG labeling, FG-positive neurons were evident bilaterally in layer V of the sensorimotor cortex (Figure 2.9A and 2.9B). FG-positive dendrites could be seen extending from the labeled cell bodies, and in some cases their dendritic processes and axonal projections were also labeled with FG.

FG-labeled neurons in layer V within the region of *PTEN* deletion (Figure 2.9A) appeared larger than FG-labeled layer V neurons in the homologous part of the contralateral cortex (Figure 2.9B). To identify retrogradely-labeled neurons lacking *PTEN*, sections from mice that had received FG injections were immunostained for PTEN using DAB for detection. The DAB reaction quenched the FG signal in any neurons that stained positively for PTEN, leaving FG fluorescence intact in neurons that did not stain for PTEN (Figure 2.9C). For comparison, retrogradely-labeled neurons in the cortex contralateral to the *PTEN* deletion were identified in near-adjacent sections that were not immunostained for PTEN. The cross-sectional areas of *PTEN* negative vs. *PTEN* positive cell bodies were measured in NIH ImageJ. Figure 2.9E-I illustrate the cell body size distributions in 5 mice; values of t-tests for cell size data in each individual animal are illustrated in each graph; two way AVOVA of data of individual cell sizes from all 5 cases: $F=178.9$, $p<0.0001$, $df=392$. In Figure 2.9J, data points are the average size of neurons in the 5 individual animals. The overall average cross-sectional area for FG-positive, *PTEN* negative neurons was 484.0 ±125.7μm² vs. 291.3 ±35.1μm² for FG-positive neurons in the contralateral cortex (paired t-test=5.47, n=5 pairs, $p=0.005$).

We also prepared tissue from 2 mice that had received vector control injections of AAV-GFP and intra-spinal Fluorogold injections. Examination of GFP immunostained sections from these two cases revealed only a few GFP labeled neurons consistent with the findings above, which precluded meaningful cell size measurements. Thus, we were not able to compare the size of neurons that had been transfected with AAV-GFP with controls.

Mice with PTEN deletion do not differ significantly from controls in the Rotorod or open field tasks

Casual observation revealed no noticeable behavioral differences between mice with *PTEN* deletion in the cortex vs. control mice. Mice grew to normal size, appeared as healthy as controls even up to 18 months of age, were active, seizures were not observed, and there was no premature death.

To screen for major deficits in overall motor function of mice with *PTEN* deletion, motor coordination was assessed by Rotorod on 4 non-consecutive days in mice that had received AAV-Cre vs. AAV-GFP (Figure 2.10A). Behavioral testing was carried out when the mice were 48 to 53 weeks old. For both groups, the average amount of time spent on the rod increased over the testing period, reflecting motor learning. Mice with *PTEN* deletion did not achieve the same level of performance as controls, but the difference was not statistically significant ($p=0.3764$, $df= 16$, repeated measures two way ANOVA).

Activity in an open field is considered to be a measure of overall locomotor activity, exploratory activity, spatial memory, and anxiety. Decreases in exploration with repeated exposure is considered to be a measure of familiarity with the open field (and thus spatial memory). During the initial exposure to a novel environment, mice typically remain close to the walls of the enclosure (thigmotaxis) (Simon et al., 1994) and with repeated exposure, tend to increase time spent in the center of the open field. To examine these behaviors in our mice, we tested them over four consecutive days.

Open field performance was measured in the same mice used for Rotorod assessment, and was carried out when the mice were around 51.6 weeks of age.

Over the testing period the overall activity of both groups declined (measured as a decrease in total number of lines crossed during the testing period) (Figure 2.10B). Both groups also demonstrated a preference for the perimeter of the arena throughout the testing period (determined by perimeter line crossings), and a progressive decline in the total number of perimeter lines crossed over the four days of testing (Figure 2.10D). For both *PTEN* deleted and AAV-GFP injected controls, the change in total lines crossed/day, inner lines crossed/day, and outer lines crossed/day were only significant between day 1 and day 2 (repeated measures two way ANOVA, p=0.0007, df=16 for total lines, p=0.0006, df=16 for inner lines, p=0.0001, df=16 for outer lines). From day 2 to day 4 both *PTEN* deleted and control animals crossed a stable number of inner lines, illustrating an increase in exploratory behavior across testing sessions (Figure 2.10C). Comparing the *PTEN* deleted and AAV-GFP injected controls, there were no significant differences on any of the measures (repeated measured two way ANOVA, p=0.7380, df=16 for total lines crossed/day over four days, p=0.8455, df=16 for perimeter lines crossed/day over four days, p=0.8569, df=16 for inner lines crossed/day over four days).

DISCUSSION

The present study was undertaken to define the long-term consequences of postnatal deletion of *PTEN* in the sensorimotor cortex, which previous studies have shown enables cortical motoneurons to regenerate their axons after an adult spinal cord

injury (Liu et al., 2010; Zukor et al., 2013; Lewandowski and Steward, 2014; Danilov and Steward, 2015). These findings, together with previous findings in other systems, establish *PTEN* deletion as an effective way to enable axon regeneration following injury (Park et al., 2008). We show here that conditional deletion of *PTEN* in the motor cortex of early postnatal mice results in robust hypertrophy of layer V cortical motoneurons and of the cortex itself, decreased cell density in the motor cortex, and maintained mTOR pathway activation a year after *PTEN* deletion. There was no evident neuropathology, and behavioral assessment revealed normal open field activity and somewhat impaired motor coordination on the Rotarod task that was not statistically significant.

Our results extend previous studies reporting structural and functional phenotypes resulting from promoter-driven genetic deletion of *PTEN* in early development. Other groups have observed a variety of neuropathologies following the loss of *PTEN* in multiple brain regions during development including macrocephaly, alterations in cortical lamination, hydrocephalus, seizures, premature death, and autism phenotypes (Backman et al., 2001; Kwon et al., 2001; Fraser et al., 2004; Yue et al., 2005; Kwon et al., 2006; Fraser et al., 2008; Sperow et al., 2012; Wen et al., 2013). Most of these previous studies examined the effects of *PTEN* deletion after only a few months. Indeed, morbidity and premature death would have precluded longer-term analyses. It is noteworthy that we did not observe any of the major neuropathologies, perhaps because *PTEN* deletion was postnatal and focal.

Cell-type specificity of PTEN deletion

Immunostaining for PTEN in mice that received AAV-Cre intracortical injections confirmed *PTEN* deletion in neurons in layer V that give rise to the CST as well as neurons in other cortical layers. *PTEN* expression was maintained in some neurons in layers II and IV that had the morphological features of cortical interneurons. Immunostaining for GABA revealed that GABAergic neurons did not account for the *PTEN* positive neurons within the deletion region.

It is noteworthy that intracortical injections of AAV-PTEN shRNA (shPTEN) in adult rats create a focal region in which there is a complete loss of PTEN immunostaining in all cell types (Lewandowski and Steward, 2014). The same is true of AAV-Cre injections into the cerebral cortex of adult *PTEN*$^{f/f}$ mice (Danilov et al., 2015). Thus, selective preservation of expression in some neuron types following injections at P1 is likely to be due to the stage of development and not differential promoter-driven expression of the AAV in different neuron types.

Selective preservation of *PTEN* expression in some neurons of mice with neonatal deletion of *PTEN* may be due to neuron type selectivity of AAV transfection at the age of deletion or a developmentally time sensitive expression of the necessary receptors and co-receptors for AAV transfection. AAV-2 is known to use heparan sulfate proteoglycan, αVβ5 integrin, and the laminin receptor as receptors for transfection (Summerford and Samulski, 1998; Summerford et al., 1999; Akache et al., 2006). Onset of expression of these necessary receptors may vary by cell type so that a subpopulation of neurons are preferentially transfected by AAV-Cre in neonatal mice.

In control mice that received AAV-GFP injections, we did not detect native GFP fluorescence in animals one year after viral injection, but immunostaining for GFP revealed GFP-positive astrocytes and a few neurons. Preferential preservation of expression in astrocytes up to 1 year is noteworthy; previous studies have reported maintained AAV-GFP mediated GFP fluorescence up to 3 months following injection (Chamberlin et al., 1998), but to our knowledge this is the first time that AAV-GFP expression has been found up to 12 months after injection,

Variability in the size of the region of deletion

While *PTEN* deletion was successfully achieved in all experimental animals, the size of the deletion region varied between animals. The inconsistency in size may have implications for SCI research projects that utilize conditional *PTEN* deletion as a therapeutic intervention. If the number of layer V upper motor neurons that have *PTEN* deleted varies between animals, the regenerative capacity of injured CST axons will vary similarly and appear less robust when averaging data across multiple animals. It may be useful in future experiments to determine the relationship between the area of *PTEN* deletion and functional recovery measures.

Increased mTOR activity following PTEN deletion

Phosphorylation of ribosomal protein S6 (pS6) is a biomarker of mTOR activation, and immunostains for pS6 following *PTEN* deletion in adult neurons show increased S6 phosphorylation even a year following deletion. The regenerative effect of *PTEN* deletion is thought to be due to increased activity of mTOR, and specifically rapamycin-sensitive mTOR complex 1 (mTORC1) (Park et al., 2008). mTORC1

regulates the translation of a subset of mRNAs that contain either a long unstructured 5' un-translated region (5'UTR), or a 5'UTR with a specific structure (Ma and Blenis, 2009). mTOR regulates the transcription of these transcripts by phosphorylating three downstream targets- the S6 kinases, the inhibitory eIF4E- binding proteins (4E-BPs), and eIF4G initiation factors (Thoreen et al., 2012). It is not yet established how *PTEN* deletion and activation of s6 phosphorylation actually affects mRNA translation in neurons.

No evidence of neuropathology

Histological assessment revealed no necrosis, abnormal growths, or tumor formation in areas of *PTEN* deletion. There was evidence of cortical injury in some mice, with GFAP positive astrocytes bordering the lesion, but this is most likely a result of damage caused at the time of the injections. Since astrocytes are responsible for repairing damage in the central nervous system, this finding is not surprising.

Cortical hypertrophy and lamination

Focal increases in cortical thickness could be related to the increased cell body size of *PTEN* deleted neurons. Other groups have found marked cortical hypertrophy in mice with *PTEN* deletion (Kwon et al., 2001; Kwon et al., 2006; Fraser et al., 2008), and in some of our cases, cortical hypertrophy was evident. The laminar disruptions that we observed were more qualitative in nature, in that it was difficult to identify the 6 cortical layers in H&E stains in the *PTEN* deletion region.

Neuronal hypertrophy and decreased cell density

Layer V cells of CST origin with *PTEN* deletion exhibited considerable cell body hypertrophy. Promoter regulated *PTEN* deletion has been associated with cell body enlargement of dentate and cerebellar granule cells, dopaminergic cells in the substantia nigra, and cortical neurons (Kwon et al., 2001; Fraser et al., 2008; Diaz-Ruiz et al., 2009). Assessment of the size of *PTEN* deleted layer V output neurons in the motor cortex had not been previously assessed, and here we demonstrate that layer V neurons are capable of robust growth. Within the motor cortex we found a statistically significant decrease in cell density (the ratio of neuropil to cell bodies) following *PTEN* deletion. It remains to be determined how neuronal hypertrophy and decreased cortical cell density affect the signaling properties of these neurons or the motor cortex.

Lack of obvious functional consequences

Despite the presence of markedly hypertrophied layer V pyramidal cells, and in some cases hypertrophy of the cortex itself, we did not observe any adverse behavioral effects of AAV-Cre injection into the sensorimotor cortex of *PTEN*f/f mice. Casual observations and our limited testing of exploratory activity did not reveal obvious behavioral differences in mice with *PTEN* deletion, although time spent on the Rotarod was shorter than for AAV-GFP-injected controls. Previous studies of mice in which *PTEN* deletion was regulated by neuron specific enolase-Cre (NSE-Cre) revealed no difference in initial Rotarod performance and an eventual increase in time spent on the rod later in testing compared to controls (Kwon et al., 2006). The lack of major behavioral consequences seen here may be due to the localized deletion of *PTEN* in the

motor cortex rather than deletion in widespread brain regions that occurs with promoter-driven Cre expression.

Although we did not monitor animals for seizure activity, the animals were handled throughout the duration of the experiment and never exhibited visible signs of motor seizures. Due to previous findings of seizure activity in animals with conditional transgenic promoter-driver *PTEN* deletion (Backman et al., 2001; Kwon et al., 2001; Ogawa et al., 2007; Pun et al., 2012), the possibility of sub-clinical seizures cannot be excluded without additional studies with electrophysiological monitoring.

The results of the present study provide provisional insights into the potential risks of complete and long-term deletion of *PTEN* in a subpopulation of neurons, as might occur with a therapeutic intervention to enable axon regeneration. We focused our analyses on the long-term effects of *PTEN* deletion induced early in postnatal life in order to closely mimic the method used to promote axon regeneration after injury (Park et al., 2008; Liu et al., 2010). The lack of major negative consequences is noteworthy, although it remains possible that some negative consequences were not detected.

It remains to be determined if *PTEN* deletion performed similarly in adult animals, which has also been shown to enhance axon regeneration and recovery following SCI, will be as benign histologically and behaviorally (Danilov and Steward, 2015; Du et al., 2015). It will also be of interest to explore interactions between the alterations in cortical morphology seen here and responses to axotomy due to spinal cord injury.

TABLE 2.1- Summary of Experimental Groups

Vector	# of Injections	Volume/ Injection	# of Mice	Age (ave)	Fluorogold	Behavior	Histology
AAV-Cre	2	1µl	6	415 days	n=1	-	H&E, n=6 pS6, n=6 PTEN, n=6
AAV-Cre	3	0.5µl	11	406 days	n=5	Rotarod, Open Field, n=9	Cleaved caspase-3, n=2 Cresyl Violet, n=2 GABA, n= 3 GFAP, n=6 H&E, n=11 Cell density and cortical thickness analysis in H&E, n=5 Ki-67, n=3 pS6, n=12 PTEN, n=12
AAV-GFP	3	0.5µl	12	388 days	n=2	Rotarod, Open Field, n=12	Cleaved caspase-3, n=1 Cresyl Violet, n=2 GABA GFAP, n=2 GFP, n=12 H&E, n=12 Ki-67, n=2 pS6, n=12 PTEN, n=12

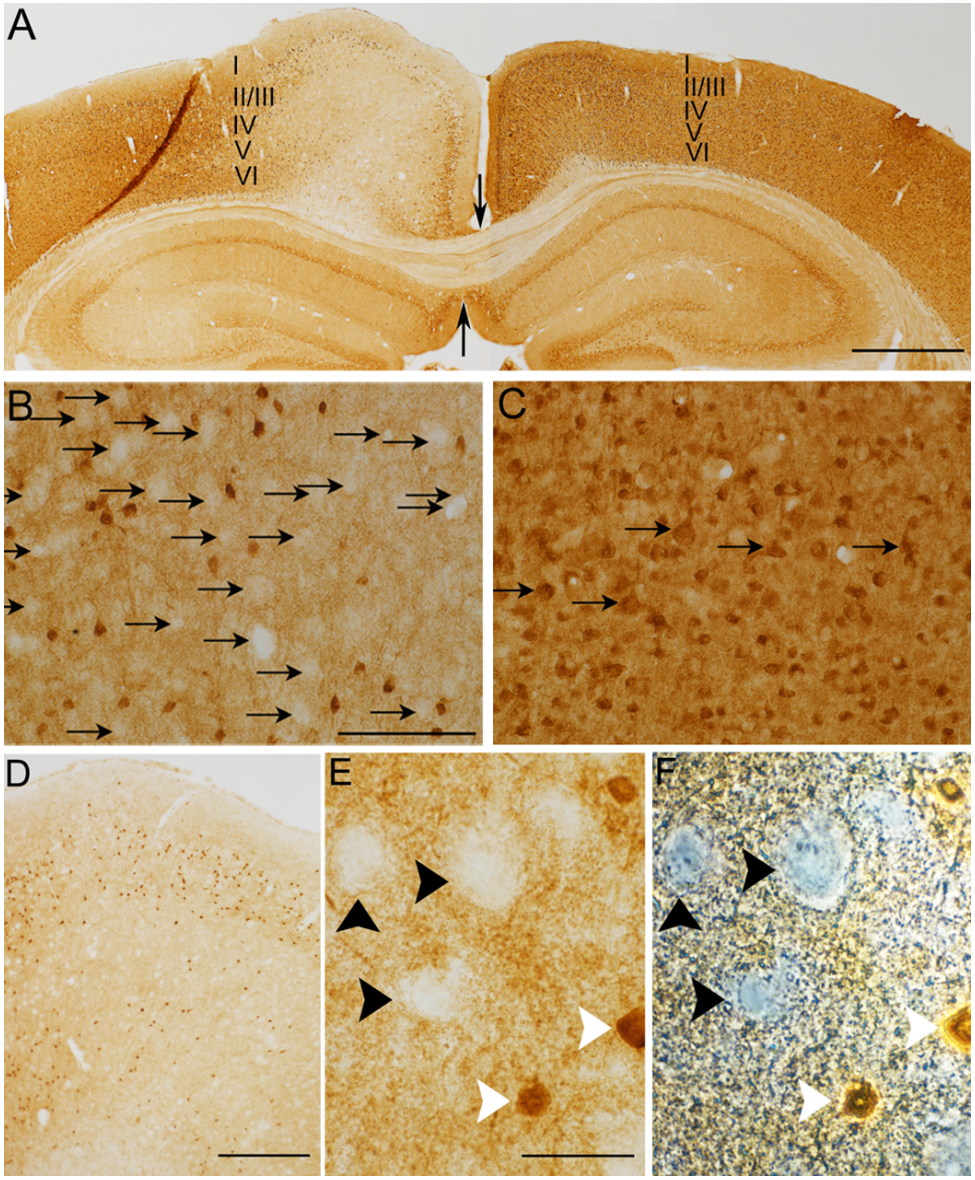

FIGURE 2.1 Area of *PTEN* deletion in the sensorimotor cortex following AAV-Cre at postnatal day 1. A. PTEN immunostain of AAV-Cre injected cortex (left side) and contralateral cortex. Roman numerals indicate cortical layers. **B.** Higher mag view of PTEN-negative neurons in left cortex of **A. C.** Higher mag view of control cortex in **A** (right) showing neurons positive for PTEN. **D.)**A second case with *PTEN* deletion, showing preserved PTEN expression in neurons in layers II and IV. **E.** High mag view of PTEN negative ghost cells (black arrowheads) and nearby PTEN-positive neurons (white arrowheads) centered over layer V. **F.** Same microscopic field as in panel E viewed with phase microscopy to verify that PTEN-negative areas are neurons. Scale bar in A=800 μm, in B and C=80 μm, in D=300 μm, in E and F=20 μm.

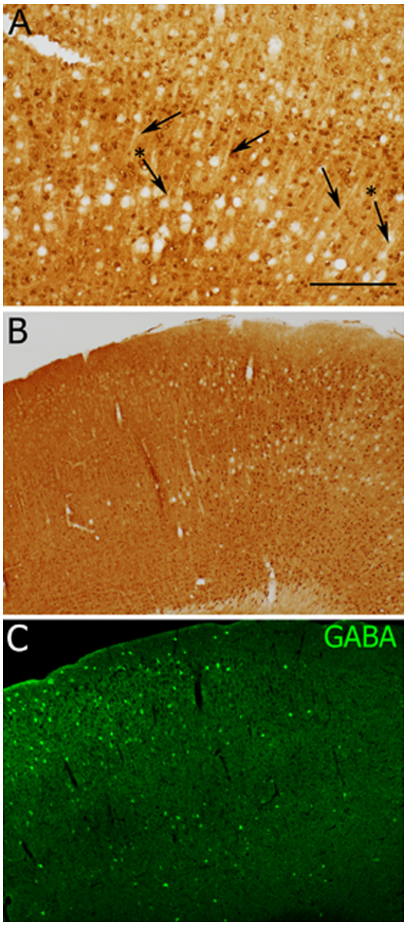

FIGURE 2.2 *PTEN* expression is preserved in small-medium sized neurons within the deletion region. A. PTEN immunostain illustrating preservation of PTEN expression in neurons in layers IV and VI. Note PTEN-negative dendrites (arrows), some of which can be seen emanating from PTEN deleted ghost cells in layer V (arrows with asterisks) **B.** PTEN immunostain from mouse with maintained PTEN expression in multiple cortical layers, especially layers IV and VI. **C.** GABA immunostain of nearby section to section in panel **B**, note that GABA positive cells in panel **C** do not account for the pattern of maintained PTEN expression in **B.** Scale bar in A, B, and C= 300μm.

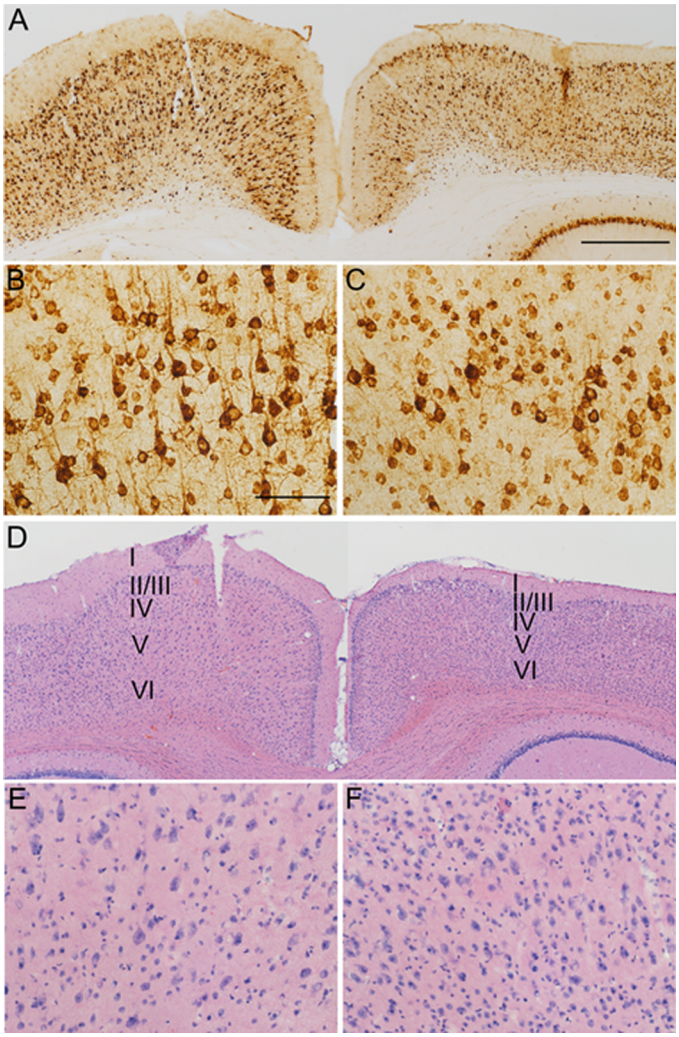

FIGURE 2.3 Activation of phosphorylation of ribosomal protein S6 and overall cytology in area of *PTEN* deletion. A. Immunostain for phosphorylated ribosomal protein S6 (pS6, Ser234/235) on the side of the *PTEN* deletion cortex (left) and contralateral control cortex (right). This section is nearby the one illustrated in Figure 1A. **B.** Higher mag view of pS6 immunostain in the *PTEN* deletion region in **A** (left cortex). Note the highly stained apical and basal dendrites. **C.** Higher mag view of pS6 immunostain of control cortex in **A** (right cortex). **D.** H&E stain of a nearby neighboring section to the section in **A**, *PTEN* deletion region in the left motor cortex and the homotopic control cortex on the right. **E.** Higher mag view of layer V in the left cortex in **D**, note the decrease in cell packing compared to **F. F.** Higher mag view of layer V in the right motor cortex in **D** (control). Scale Bar in A and D=600 μm, in B, C, E, and F=100 μm.

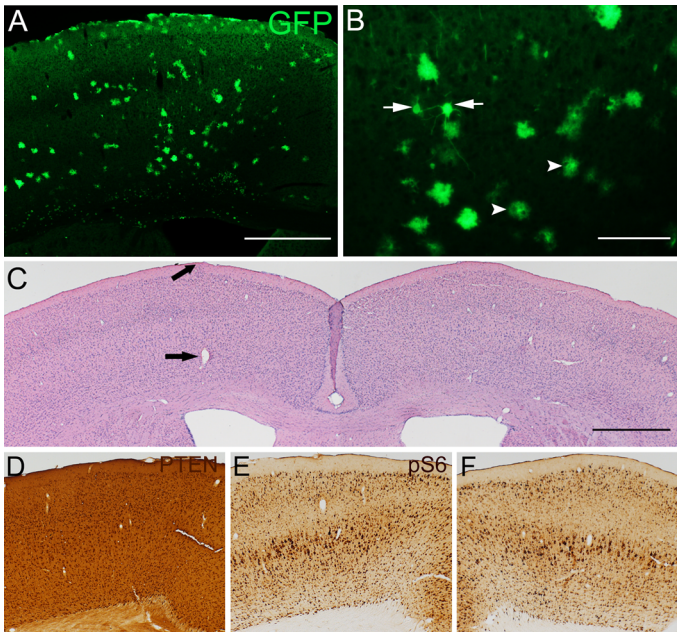

FIGURE 2.4 No obvious alterations in cortical morphology in AAV-GFP injected controls. A. GFP immunostained section from a mouse injected with AAV-GFP. GFP labeling is present in scattered astrocytes and a few neurons . **B.** High mag view of region in **A**, Arrows point to neurons; arrowheads point to astrocytes. **C.** A nearby section to **A-B** stained for H&E. AAV-GFP was injected into the left cortex, and the right cortex was un-injected. Arrows indicate tissue defects that are likely needle tracts from the injections. **D.** PTEN immunostain of a nearby section to **A-C**. No PTEN negative neurons were seen in the region of AAV-GFP injection. **E.** pS6 immunstain of the cortex ipsilateral to AAV-GFP injection in a nearby section to **A-D**. **F.** pS6 immunostain of the contralateral uninjected cortex from the same section in **E.** Scale bar in A, B, C, and D= 600 μm, in B= 150 μm.

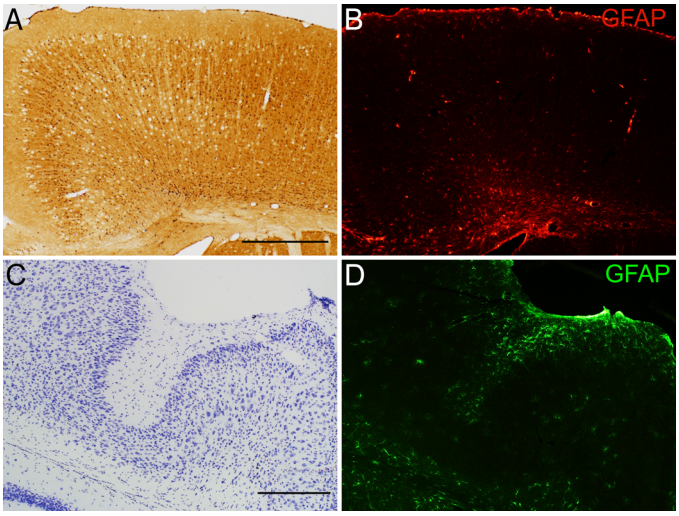

FIGURE 2.5 Immunostaining for GFAP in the area of *PTEN* deletion. A. Representative PTEN immunostain from one of the five mice used to assess the distribution of GFAP positive cells following *PTEN* deletion. **B.** GFAP immunostained of a neighboring section to the section in panel **A.** No qualitative increase in GFAP positive cells or clusters of GFAP cells were found in the *PTEN* deleted motor cortex or in any other brain regions. **C.** Cresyl violet stain of section from an animal with a cortical lesion caused by intracortical injections. **D.** GFAP immunostain of a nearby neighboring section to **C**, Astrocytes surrounding the cortical defect shown in **C**. Scale bar in A and B=300 μm, C and D=600 μm.

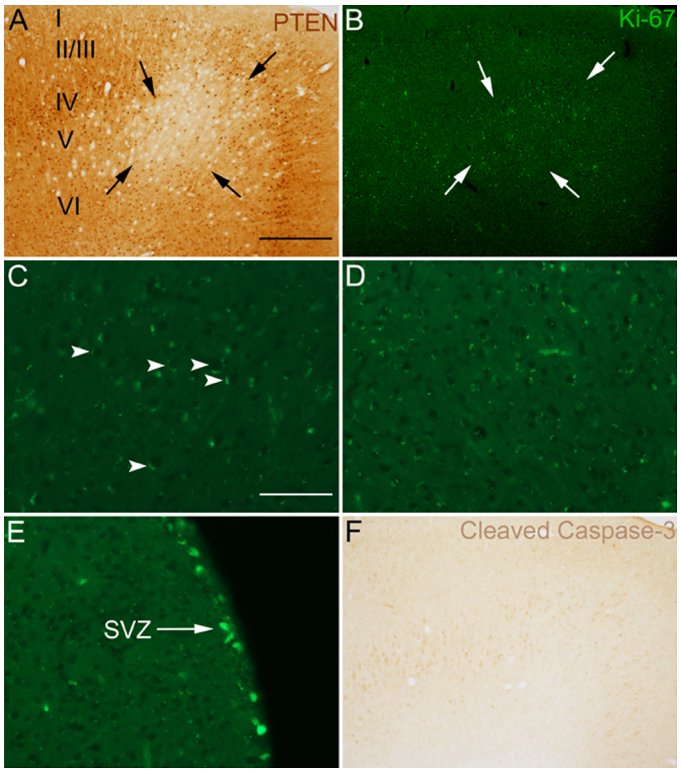

FIGURE 2.6 No ongoing cell division or apoptotic cell death in the region of *PTEN* deletion. A. PTEN immunostain of a nearby section to panels **B- F**. Arrows indicate boundaries of the region of *PTEN* deletion. Cortical layers are labeled. **B.** Low mag view of Ki-67 immunostain in the region of *PTEN* deletion (region indicated by arrows). **C.** High mag view of the section in **B**. Arrowheads point to large layer V neurons in the region of *PTEN* deletion (likely *PTEN* negative ghost cells). **D.** Ki-67 immunostain of contralateral control cortex from the same section as **B**. Fluorescent particles in **B** and **D** have a different appearance than bona fide Ki-67 positive cells in the subventricular zone (SVZ, **E**). **E.** Ki-67 positive cells in the subventricular zone of the same section as **B- D. F.** Cleaved caspase-3 immunostain from a nearby section to **B- E** in the *PTEN* deletion region contains no apoptotic (cleaved caspase-3) cells. Scale bar in A, B, and F= 300μm, in C, D, and E= 150μm.

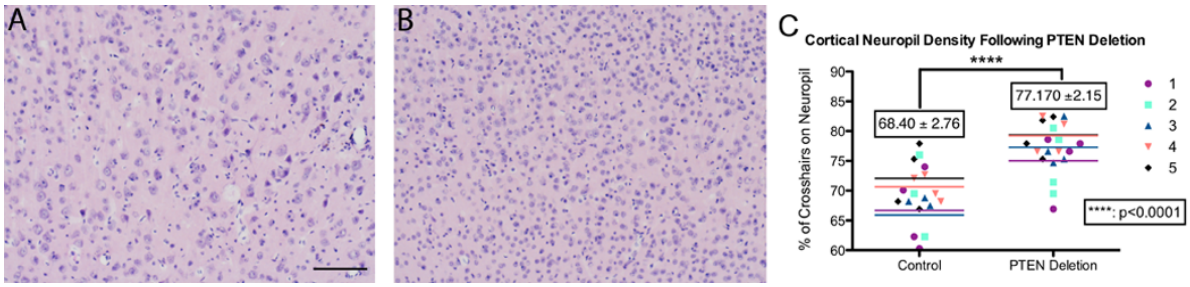

FIGURE 2.7 Decreased cell density the area of *PTEN* deletion. **A.** H&E stained section of motor cortex in the area of *PTEN* deletion. **B.** H&E stained section of control motor cortex contralateral to panel **A.** **C.** Data from 5 animals used for measurement of cell density. The percentage of crosshairs overlying cell bodies vs. neuropil is represented in the graph (paired t-test=12.70, p=0.0002). Scale bar in A=100 μm.

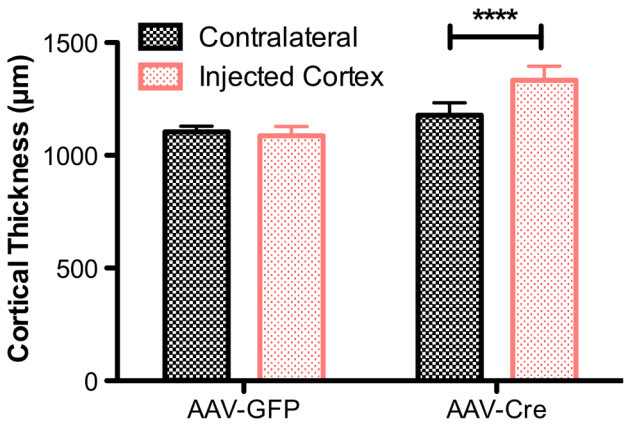

FIGURE 2.8 Increased cortical thickness in the area of *PTEN* deletion. Data from 5 animals were used to measure cortical thickness. The thickness of the *PTEN* deleted and contralateral control motor cortex were measured by drawing a line from the corpus callosum to the pial surface in ImageJ. The first pair of bars illustrate data from mice injected with AAV-GFP; the second pair of bars illustrate data from mice injected with AAV-Cre. Gray bars indicate average thickness of the uninjected cortex contralateral to the AAV injections; red bars are data from the injected side. Asterisks indicate p=0.002 (repeated measures two way ANOVA, F=12.69 for vector type).

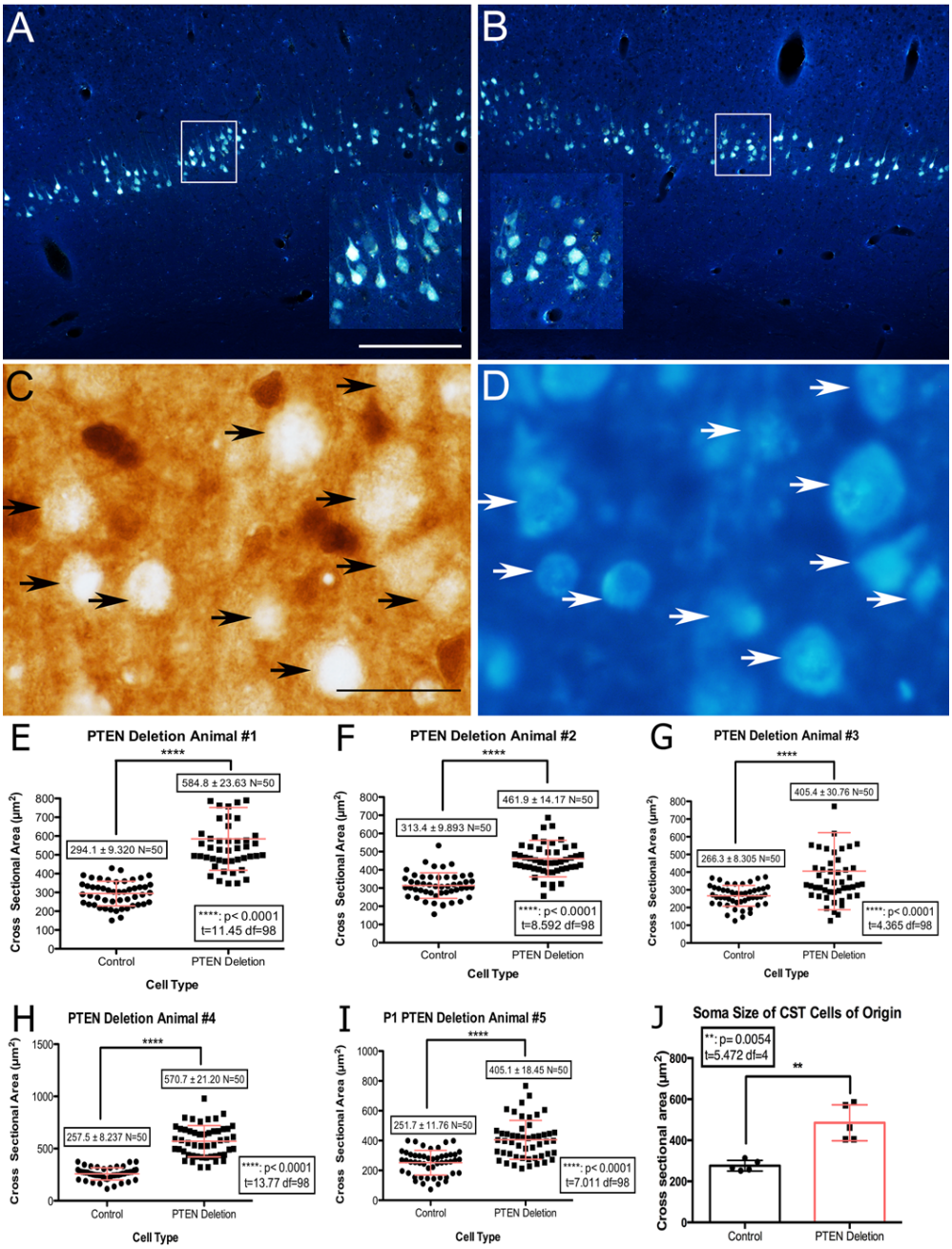

Figure 2.9 Hypertrophy of CST neurons following *PTEN* deletion. A. Fluorogold (FG)-labeled CST neurons in the area of *PTEN* deletion. Inset is a high magnification view of the area indicated by the rectangle. **B.** FG signal in contralateral control cortex **C.** *PTEN* deletion region immunostained for PTEN, bright field microscopy. **D.** Same field as in panel C, UV microscopy **E-I.** Distribution of cell body cross sectional area from 5 cases. **J.** Data points indicate the average size of PTEN-negative vs. PTEN-positive CST neurons in the 5 individual cases (paired t-test=5.47, n=5 pairs, p=0.005). Scale bar in A= 300 μm, in C=30 μm.

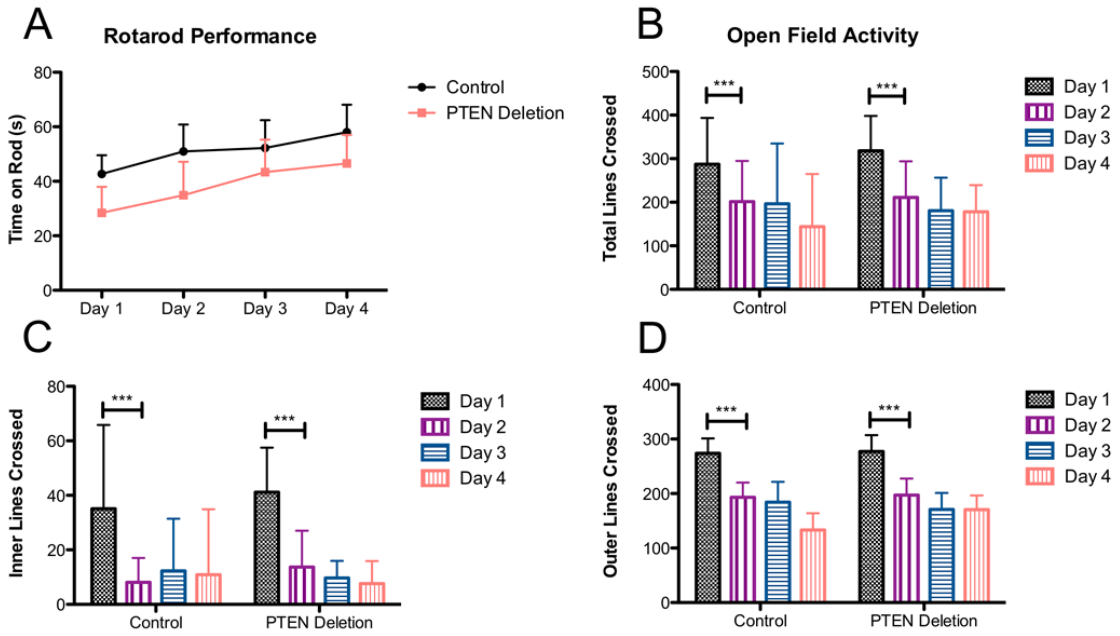

Figure 2.10 Functional assessments of mice with unilateral postnatal *PTEN* deletion in the motor cortex. **A.** Average time spent on accelerating Rotarod over four testing days. Data are from mice in which *PTEN* deletion was verified by immunohistochemistry (n=6) vs. AAV-GFP-injected controls (n=12). Difference in time spent on the rod was not significantly different between *PTEN* deleted and control mice (repeated measures two way ANOVA, p=0.3764, df=16, F=0.8279). **B.** Open field activity of *PTEN* deleted and control mice over four testing days as measured by total lines crossed/day (repeated measures two way ANOVA for total lines cross/day p=0.7380, df=16, F=0.1159). **C.** Open field inner lines crossed/day over four days (repeated measures two way ANOVA for inner lines crossed/day p=0.8455, df=16, F=0.03922). **D.** Open field outer lines crossed/day over four days (repeated measures two way ANOVA for outer lines crossed/day p=0.8659, df=16, F=0.03358).

CHAPTER 3: *PTEN* deletion in the adult sensorimotor cortex triggers robust mature neuronal growth and improved motor learning

Previously published in *Experimental Neurology* in 2018 as: Gallent, Erin A., Steward, Oswald. "Neuronal *PTEN* deletion in adult cortical neurons triggers progressive growth of cell bodies, dendrites, and axons." *Experimental neurology* 303 (2018): 12-28.

ABSTRACT

Deletion of the phosphatase and tensin (*PTEN*) gene in neonatal mice leads to enlargement of the cell bodies of cortical motoneurons (CMNs) in adulthood (Gutilla et al., 2016). Here, we assessed whether *PTEN* deletion in adult mice would trigger growth of mature neurons. *PTEN* was deleted by injecting AAV-Cre into the sensorimotor cortex of adult transgenic mice with a lox-P flanked exon 5 of the *PTEN* gene and Cre-dependent reporter gene tdTomato. *PTEN*-deleted CMN's identified by tdT expression and retrograde labeling with fluorogold (FG) were significantly enlarged four months following *PTEN* deletion, and continued to increase in size through the latest time intervals examined (12–15 months post-deletion). Sholl analyses of tdT-positive pyramidal neurons revealed increases in dendritic branches at 6 months following adult *PTEN* deletion, and greater increases at 12 months. 12 months after adult *PTEN* deletion, axons in the medullary pyramids were significantly larger and G-ratios were higher. Mice with *PTEN* deletion exhibited no overt neurological symptoms and no seizures. Assessment of motor function on the rotarod and cylinder test revealed slight impairment of coordination with unilateral deletion; however, mice with bilateral *PTEN*

deletion in the motor cortex performed better than controls on the rotarod at 8 and 10 months post-deletion. Our findings demonstrate that robust neuronal growth can be induced in fully mature cortical neurons long after the developmental period has ended and that this continuous growth occurs without obvious functional impairments.

INTRODUCTION

Neurons in the adult central nervous system have a low intrinsic ability to regenerate, accounting for limited recovery following trauma, damage due to stroke, or neurodegenerative processes. Experimental attempts to increase the regenerative potential of injured adult axons have identified the phosphatase and tensin gene (*PTEN*) as an important negative regulator of axon regeneration. In optic nerve crush and spinal cord injury models, injured axons that originate from *PTEN* deleted neurons exhibit robust regeneration (Park et al., 2008; Liu et al., 2010). In these studies, AAV-Cre was injected into the eye or cortex of *PTEN* floxed mice to delete *PTEN* in retinal ganglion cells in the optic nerve crush injury, or neurons of the motor cortex in the spinal cord injury model respectively. Subsequent studies revealed regenerative growth of corticospinal (CST) axons following *PTEN* deletion in mature mice and after AAV-shRNA-mediated knockdown in mature rats, which was accompanied by recovery of motor function (Zukor et al., 2013; Lewandowski and Steward, 2014; Danilov and Steward, 2015; Du et al., 2015).

The above studies highlight the potential of therapeutic applications targeting *PTEN* to enhance regeneration; however, the long-term consequences of interventions targeting *PTEN* in a therapeutically-relevant way (in adult animals) are unknown. *PTEN* is a phosphatase that catalyzes the conversion of PIP3 to PIP2, countering the action of phosphatidylinositol-3-kinase (PI3K). Accordingly, *PTEN* deletion leads to increases in PIP3, resulting in increased activation of Akt and mammalian target of rapamycin

(mTOR). mTOR is an important regulator of neuronal growth, including axon growth and guidance and dendritic outgrowth (Jaworski and Sheng, 2006).

Several studies have assessed the consequences of *PTEN* deletion during embryonic or early postnatal development. For example, promoter-driven deletion of *PTEN* in neurons expressing neuron specific enolase (NSE) or Ca2+/calmodulin-dependent protein kinase II (CAMKII) leads to striking neuronal hypertrophy and macrocephaly. Physiological studies reveal impaired long-term potentiation (LTP) and spontaneous seizures have been detected by electroencephalography (EEG) (Kwon et al., 2006; Sperow et al., 2012; Takeuchi et al., 2013). Knockdown of *PTEN* in postnatally derived dentate granule cells via injection of short hairpin RNA or injections of retroviruses expressing Cre recombinase into *PTEN* floxed mice leads to increased excitatory drive of dentate granule cells, and increases in total dendrites, dendritic spines, and synapses (Luikart et al., 2011; Williams et al., 2015).

We recently assessed the long-term consequences of deleting *PTEN* in the sensorimotor cortex at postnatal day 1, using the approach that enables regeneration of CST axons following spinal cord injury in adults (Liu et al., 2010; Gutilla et al., 2016). Following unilateral AAV-Cre injections into the sensorimotor cortex of *PTEN* floxed mice at P1, we found substantial hypertrophy of cortical motoneuron cell bodies in mice that had survived for 1 year. We did not assess different time points after AAV-Cre injection so an unresolved question is whether this cellular growth occurs only during development or continues throughout life. Of even greater interest is whether *PTEN*

deletion in mature neurons would initiate a new phase of cellular growth after neurons have ceased growing in adulthood.

The goals of the present study were to determine whether *PTEN* deletion in adult cortical motoneurons also triggered neuronal growth and if so, whether growth was transient or continuous. To address these questions, we used double transgenic mice in which Cre-mediated recombination deletes *PTEN* and activates expression of tdTomato in the same neurons. We show that *PTEN* deletion via intracortical injection of AAV-Cre leads to progressive enlargement of cortical neuronal cell bodies that continues for over 1 year, increases in dendritic arborization as revealed by Sholl analysis, and increases in axonal diameter. Analyses of motor function at different times post-*PTEN* deletion revealed no difference in motor function in comparison to controls at early time points but enhanced motor function in the oldest mice.

METHODS

PTEN deletion in the motor cortex of adult mice

The Institutional Animal Care and Use Committee (IACUC) at the University of California, Irvine approved all experimental procedures. Doubly transgenic mice were generated by breeding mice with lox-P flanked exon 5 of the *PTEN* gene (RRID: IMSR_JAX:004597) to mice with a lox-P flanked STOP cassette in the ROSA locus that prevents expression of tandem dimer tomato (tdTomato) fluorescent protein (RRID: IMSR_JAC:007905). We will refer to these mice as PTEN/tdT mice for brevity.

Transgenic control mice harbor only the lox-P flanked STOP cassette within the ROSA locus that prevents tdTomato expression (referred to hereafter as tdT mice). Table 3.1 summarizes the number of mice used for each assessment

Surgical procedures

For all surgical procedures, mice were anesthetized with Isoflurane (2–3%), their eyes were swabbed with Vaseline, and the skin at the incision site was shaved and cleaned with Betadine. Following completion of the surgery, mice were returned to their home cages on 37 °C water circulating heating pads until they recovered from the anesthetic.

To delete *PTEN* in adult cortical neurons, PTEN/tdT mice (n = 26) received unilateral intracortical injections of AAV-Cre recombinase at 8 or more weeks of age. Transfection by AAV-Cre results in the excision of exon 5 of the *PTEN* gene and the STOP cassette for tdTomato, resulting in deletion of *PTEN* and expression of tdTomato in the same neurons. To control for any effect due to AAV injections, tdT control mice received identical unilateral injections of AAV-Cre. The vectors were AAV serotype 2, and were obtained from Vector Bio Labs (1 × 1013 genome copies/mL, Catalog number 7011). The vector was diluted with sterile-filtered PBS and 5% glycerol for a final concentration of 1 × 1012 genome copies/mL.

For intracranial injections, a midline scalp incision was made. Burr holes were placed in the skull overlying the cortical areas to be injected and 4 unilateral

intracortical injections of AAV-Cre were made into the sensorimotor cortex using a Hamilton syringe with a pulled glass micropipette (1.0 mm lateral and 0.5 mm depth at +0.5 mm, −0.2 mm, −0.5 mm, and −1.0 mm relative to bregma). Each injection was 0.6 μL in volume, for a total injection volume of 2.4 μL. Injections were performed over one minute and the microsyringe was left in place for three minutes.

Retrograde labeling of cortical motoneurons

To definitively identify the cells of origin of corticospinal tract axons (cortical motoneurons), PTEN/tdT (n = 26) and tdT mice (n = 10) mice received bilateral intraspinal injections of the retrograde tracer Fluorogold 3, 4, 5, 6, 7, 9, 12, and 15 months following AAV-Cre injections. Mice were prepared for surgery as above, and a C5 laminectomy was performed to expose the spinal cord. Two injections of 0.2 μL of 1% Fluorogold were made with a Hamilton syringe with a pulled glass micropipette at 0.5 mm lateral to the midline at 0.5 mm depth. Fluorogold was injected over one minute and the syringe was left in place for an additional minute. After completing the injections, the muscles were sutured with 5.0 chromic gut and the skin was closed with staples. Mice received subcutaneous injections of buprenorphine, Baytril and lactated Ringer's twice a day for three days post-operatively and were kept in their home cages for 3–4 days prior to tissue collection.

Tissue Collection and histology

3–4 days after receiving Fluorogold injections, mice received intraperitoneal injections of Fatal-Plus (1 mL/300 g) and were transcardially perfused with 4%

paraformaldehyde (PFA). Brains and spinal cords were dissected and allowed to post-fix for 48 h in 4% PFA before being placed overnight in 30% sucrose/phosphate buffered saline (PBS) for cryoprotection. For Vibratome sectioning, tissue blocks were attached to blocks with cyanoacrylate and sectioned at 200 μm or 40 μm. Sections were collected in serial order in wells containing PBS with 0.1% NaN3. Tissue sectioned on the cryostat was embedded in OCT compound (Tissue-Tek) and frozen by immersion in a container with methyl butane surrounded by crushed dry ice/ethanol slurry. Brains were sectioned in the coronal plane at 20 μm and collected in wells with PBS with 0.1% NaN3.

To visualize neurons co-labeled with tdTomato and Fluorogold, tdTomato fluorescence was visualized directly without immunostaining. To visualize Fluorogold, 20–40 μm sections were incubated overnight at room temperature with rabbit anti-Fluorogold (RRID: AB_2314407) diluted to 1:600 in 5% NDS, 5% BSA, 0.4% triton-X in 50 mM KPBS. Sections were then incubated with an anti-rabbit biotinylated secondary antibody (1:250, RRID: AB_2313606), followed by incubation in avidin and biotinylated horseradish peroxidase (1:100, RRID: AB_2336819), and FITC labeling (made in house, 1:250 dilution in 0.001%H202 borate buffer). Stained sections were slide mounted and cover slipped with Vectashield mounting medium (RRID: AB_2336789).

Sections (one every 200 μm) were stained for H&E or cresyl violet, and/or immunostained for different markers (below). For immunostains other than Fluorogold, an antigen retrieval protocol was used in which sections were placed in 1.7 mL Eppendorf tubes with 1 mL 10 mM citrate buffer, pH 8.80. Tubes were then immersed

in boiling water for 5 min, placed on ice for 5 min, and left at room temperature for 10 min. Primary antibodies and dilutions were as follows: PTEN (1:250, AB_390810), two phospho-specific antibodies for ribosomal protein S6 (1:250 for both, Ser 235/236: RRID: AB_916156, Ser 240/244: RRID: AB_331682), NeuN (1:100, RRID: AB_2298772), and glial fibrillary acid protein (GFAP, 1:2000, RRID: AB_100013482). PTEN and pS6 antibodies were diluted in Blocking Reagent (PerkinElmer), all other antibodies were diluted in 5% secondary antibody host serum in TBS or PBS with 0.3% Triton (GFAP).

Sections were incubated in primary antibody overnight at room temperature, and then in secondary antibodies in the same blocking solution for two hours at room temperature. For immunofluorescence, we used Alexa Fluor 488 (RRID: AB_2535792) or Alexa Fluor 594 (RRID: AB_141637), both at 1:250 dilution. For sections undergoing DAB detection, sections were incubated in a biotinylated IgG secondary antibody (1:250, RRID: AB_2313606), washed 3 times, incubated for 1 h with avidin and biotinylated horseradish peroxidase (1:100, RRID: AB_2336819) and reacted with DAB (RRID: AB_2336382).

Cortical motoneuron cell size measurements

To measure the cell body size of CMNs over time following *PTEN* deletion in adulthood, we used the data from a previously conducted pilot experiment in a power/sample size calculation to determine the minimum number of mice that could be used for each time point. Each time point used for cell body size measurements had a minimum of 3 PTEN/tdT mice (3 months: n = 4, 2 females, 2 males, 4 months: n = 3, 0

females, 3 males, 5 months: n = 4, 2 females, 2 males, 6 months: n = 3, 3 females, 0 males, 7 months: n = 3, 0 females, 3 males, 9 months: n = 3, 0 females, 3 males, 12 months: n = 3, 0 females, 3 males, 15 months: n = 3, 3 females, 0 males). Two tdT control mice were used for cell size measurement at 3, 6, 9, 12, and 15 month time points (3 month: 2 females, 0 males, 6 months: 1 female, 1 male, 9 months: 0 females, 2 males, 12 months: 1 female, 1 male, 15 months: 2 females, 0 males). For the mid-life *PTEN* deletion analyses, 3 PTEN/tdT mice (1 female, 2 males) were assessed at 2 months post-deletion and 5 PTEN/tdT mice (2 females, 2 males) were assessed at 5 months post-deletion. A random number generator was used to determine surgical order and to assign mice to groups.

Cortical motoneurons (CMNs) were identified by retrograde labeling with Fluorogold and *PTEN* deleted neurons were identified by their expression of tdTomato. Neurons co-labeled by both Fluorogold and tdTomato must therefore be *PTEN* deleted CMNs. For cell size measurements, sections that were immunostained for Fluorogold were imaged by 2-photon microscopy for both Fluorogold and tdTomato. The cortical region containing the highest density of neurons co-labeled with tdTomato and Fluorogold was identified, and image stacks were collected (1024 by 1024 μm, depth of 20–40 μm, step distance 0.5 μm). Image stacks of the same size were collected from the homotopic region of the contralateral cortex containing CMNs labeled with FG only. Image stacks were reconstructed in 3D and 2D projections were generated from the 3D image stacks, and analyzed in ImageJ.

We measured the cross-sectional area of 50 *PTEN* deleted, Fluorogold positive CMNs in the area of deletion. Sampling was done by measuring all colabeled cells starting at the lateral aspect of the motor cortex and moving medially, until 50 colabeled cells had been measured. As an intra-animal control, we then measured 50 Fluorogold positive (*PTEN* intact) CMNs in the homotopic cortical region on the contralateral side of the same section using the same lateral-medial sampling strategy. To control for possible effects of transfection by AAV-Cre and tdTomato expression on cell size, we performed identical analyses in tdT mice with intact *PTEN* expression, measuring 50 tdTomato/Fluorogold positive CMNs vs. 50 Fluorogold positive CMNs on the contralateral side. All measurements were done blind to mouse genotype, however the large effect of *PTEN* deletion on cell size made it difficult for the person conducting the analysis to remain blind.

The average values per mouse were then averaged across mice in the time point, in order to calculate the overall mean cross-sectional area for the *PTEN* deletion and control groups at each time point with n = number of mice. Measures of cell body size were analyzed using repeated measures two-way analysis of variance (ANOVA), and comparisons of cell size between time points were done using Sidak's multiple comparisons post hoc analysis. Since there were no significant differences between the intra-animal controls and the AAV injection control mice, statistics are reported using only the intra-animal controls.

Characterization of dendritic arbor

To assess the dendritic arbor of pyramidal neurons following adult *PTEN* deletion, mice that had received AAV-Cre injections were euthanized 6 months (n = 6 PTEN/tdT mice, 4 tdT mice) and 12 months (n = 7 PTEN/tdT mice, 6 tdT mice) post-deletion. These time points were chosen because of the ongoing growth of CMN cell bodies we observed from 6 to 12 months. Mice received injections of Fatal Plus as above, were perfused transcardially with 4% PFA, and brains were post-fixed for 48 h in 4% PFA. The unfrozen brains were adhered to a block with cyanoacrylate and sectioned on a Vibratome into 200 μm sections that were collected in PBS with 0.1% NaN3.

Sections used for 3D imaging were cleared using a passive CLARITY protocol. On day 1, sections were incubated in 4% acrylamide PBS with 0.25% VA-044 thermal initiator at 4 °C for 48 h. The sections were then transferred to a 37 °C oven to allow the acrylamide to polymerize. Once polymerized, the sections were washed in PBS for 30 min to 1 h at room temperature and then were placed in 25 mM borate 500 mM sodium dodecyl sulfate (SDS) overnight at 37 °C. The following day, sections were transferred to fresh borate SDS solution and left at 37 °C overnight, and this was repeated on the next day. After three nights in borate SDS solution, the sections were washed 4 times in PBS over an 8-hour span at room temperature and were then submerged in Sorbitol F overnight at room temperature. Sections were then mounted and cover slipped with Sorbitol F for imaging.

3D imaging and Sholl analysis

Cleared, thick sections were imaged in 3D using a 3i video-rate two-photon laser scanning microscope on the Olympus BX51WIF platform (Olympus America Inc., Center Valley, PA) equipped with a Chameleon Ti:sapphire laser (Coherent, Santa Clara, CA). The laser beam is focused through a 20× water-immersion objective (numerical aperture 0.95) and emitted fluorescence is detected by photomultipliers (Hamamatsu, Middlesex, NJ) to derive a video signal that is captured and analyzed using SlideBook 6.0 (Intelligent Imaging Innovations, Inc., Santa Monica, CA).

tdTomato labeled neurons were selected for imaging based on the following criteria: 1) Neuron had pyramid-shaped soma; 2) Neuron was located near the middle of the section, and not close to a section edge, to avoid asymmetric truncation of dendrites; 3) Neuron was isolated in the field of view, or surrounded by only a few other labeled neurons, such that individual dendritic processes could be unequivocally attributed to the correct neuron. Image stacks were collected (1024 by 1024 μm, scan depth of 150–200 μm, step distance 1.0 μm), and reconstructed in 3D. Stacks were collapsed into 2D images and the dendritic arbor of individual neurons was manually traced.

Traced projections were imported into FIJI, converted to 8-bit binary images, and analyzed using the Sholl Analysis program (Ferreira et al., 2014). Using the center of the soma, concentric circles with an increasing diameter of 10 μm were placed on each traced projection, and the number of intersections at each circle was counted. The cross-sectional area of neurons used for Sholl analysis was measured by manually tracing the cell body of the flattened 2D projection in FIJI. The diameter of the apical

dendrite was measured 30 μm away from the center of the soma in the flattened 2D projection.

For Sholl analysis data, neurons were analyzed based on time post-AAV injection, either 6 or 12 months (Table 3.2). For the 6 month time point, 6 PTEN/tdT mice (3 females, 3 males) and 4 tdT mice (3 females, 1 male) were used. For the 12 month time point 7 PTEN/tdT mice (4 females, 3 males) and 6 tdT mice (4 females, 2 males) were used. Table 3.2 summarizes the number of cells that were analyzed from each mouse. The raw intersection data was analyzed using repeated measures two-way ANOVA, and post hoc comparisons were done using Sidak's multiple comparisons post-test.

Measurement of axon size in the medullary pyramids

To assess the effect of *PTEN* deletion on the size of uninjured corticospinal (CST) tract axons, we examined CST axons in the medullary pyramids. PTEN/tdT (n = 3) and tdT mice (n = 2) mice that had received unilateral AAV-Cre injections were perfused with 2% glutaraldehyde 2% paraformaldehyde. Brains and spinal cords were dissected and allowed to post-fix for 48 h in 2% glutaraldehyde 2% paraformaldehyde. Tissue was then sunk in 30% sucrose PBS overnight before being cut into thick 200 μm sections on a Vibratome. Brainstem sections containing the medullary brainstem were collected and immunostained for tdTomato using an antigen retrieval protocol wherein sections were submerged in centrifuge tubes with ~1 mL 10 mm citrate buffer (pH 8.5–9) and placed in a boiling water bath for 5 min. The tubes were then placed on ice for 5 min and left to sit at room temperature for 10 min. Sections were then incubated with anti-red

fluorescent protein (anti-RFP) primary antibody (1:200, RRID: AB_2209751) diluted in 5% NDS and 0.4% Triton in TBS overnight at room temperature. Sections were then incubated with a horseradish peroxidase conjugated secondary antibody (1:250, RRID: AB_2340590) diluted in the same solution as the primary and were then reacted with DAB (RRID: AB_2336382). Following immunostaining, sections were trimmed to isolate the medullary pyramids, stained with Toluidine blue, and processed for electron microscopy (EM).

Sections were scanned at the EM level at low magnification to identify tdT-labeled axons, and images were taken (185 μm2) of all labeled axons. Images collected by EM were overlaid with a 4 μm grid and analyzed in ImageJ. All tdTomato positive axons were measured (26 axons in 1 female and 18 and 25 axons in 2 male PTEN/tdT mice; 16 and 31 axons in two female tdT mice), along with neighboring unlabeled axons in the field that were intersected by a grid crosshair. The cross-sectional area of the axoplasm, axoplasm plus myelin, and myelin alone were measured. G-ratio was calculated as the ratio of the diameter of the axoplasm/the diameter of the axoplasm plus myelin. Data were compared across groups using repeated measures two-way ANOVA, and Sidak's post-test. Differences in G-ratio were analyzed using student's t-test.

Functional testing following unilateral PTEN deletion

For functional testing, we first tested mice that had received unilateral injections of AAV-Cre at 8 weeks of age (PTEN/tdT; n = 18 and tdT; n = 16). The unilateral injection model allowed separate assessment of limbs controlled by the cortex in which

PTEN had been deleted vs. the contralateral cortex with intact *PTEN* expression. At 6 months post-*PTEN* deletion, motor function was tested using a rotarod and cylinder task.

Rotarod testing was done in a way that allowed assessment of motor learning and performance ability (Rothwell et al., 2014). Overall testing consisted of three trials a day over 4 consecutive days, for a total of 12 trials. All testing was done at night based on performance by age-matched controls in pilot studies. The first two days of testing involved slower rotation speeds and were thus less challenging than the third and fourth days. Briefly, on days 1 and 2 the mice were placed on the rod with an initial speed of 4 RPM with an acceleration of 0.1 RPM/s. On days 3 and 4 the initial speed was increased to 6 RPM with an acceleration of 0.2 RPM/s. Each trial was a maximum of 5 min and ended if a mouse fell off of the rod. Latency to fall was recorded and the maximum attained speed was calculated for each trial.

Performance on the rotarod was compared by taking the latency to fall for each mouse and calculating the speed at which the mouse fell off the rod (latency to fall $*$ acceleration $+$ starting speed) and averaging this value for each trial based on group (control vs. *PTEN* deletion). The average speed for each trial was then compared between groups using two-way ANOVA. Baseline coordination and motor learning were calculated using linear regression analysis (Rothwell et al., 2014).

The same mice were assessed using the cylinder task. Testing for each task was done on non-consecutive days to avoid fatigue. The cylinder task quantifies the preference of forelimb use during spontaneous exploration and was done once at 6 months following unilateral AAV-Cre injection. The cylinder task was conducted in a completely dark room lit by a red lamp. A 1000 mL beaker was placed on a flat surface with the mouth of the beaker open to the environment. A small amount of bedding from the home cage was placed at the bottom of the beaker. A single mouse was then placed in the beaker and videotaped from above for analysis. Forepaw sidedness was recorded each time the mouse reared up and placed one or both forepaws on the walls of the beaker to support body weight. Touches were recorded as R (right forepaw, controlled by the left motor cortex with *PTEN* deletion, L (left forepaw, controlled by the right motor cortex and no *PTEN* deletion), or B (both forepaws simultaneously). A total of 10 weight-bearing touches were recorded per mouse with the requirement that the mouse had to place both forepaws on the bottom of the beaker between successful paw touches. The recorded percentage of forepaw touches executed by each forepaw (or both) was then used to determine forelimb use asymmetry.

Performance in the cylinder task was measured by taking the raw count of forepaw touch sidedness (out of ten total touches), and comparing forepaw touches between groups (control vs. *PTEN* deletion) by repeated measures two-way ANOVA. Sidak's post-test was used to identify asymmetry in forepaw usage (right forepaw vs. left forepaw vs. both forepaws).

Assessment of motor function over time following bilateral PTEN deletion

Based on our behavioral findings following unilateral *PTEN* deletion in neonatal mice (Gutilla et al., 2016) and the bimanual nature of the rotarod task, we assessed performance on the rotarod and in the cylinder task following bilateral *PTEN* deletion in the motor cortex. 10 PTEN/tdT mice and 9 age-matched tdT control mice received bilateral intracortical injections of AAV-Cre at 8 weeks of age as above (total injection volume of 2.4 μL/side).

PTEN/tdT and tdT mice that received bilateral AAV-Cre injections were assessed for motor learning on the rotarod at 2, 4,6, and 8 months following bilateral AAV-Cre injection as described for mice following unilateral *PTEN* deletion. The same person carried out the testing for each session and was blind to the genotype of the mice. At 8 months following AAV-Cre injection, interim statistical analyses were performed to determine whether to continue behavioral testing. Based on rotarod performance trends from 2 to 8 months following injection, we assessed rotarod performance at 10 months following injection in order to evaluate the stability of our observed trend.

The same mice were assessed using the cylinder task at 2, 4, 6, and 8 months following *PTEN* deletion as described for mice following unilateral *PTEN* deletion. Testing for each task was on non-consecutive days to avoid fatigue and was conducted by the same person each time who was blind to genotype. Interim statistical analyses at 8 months following AAV-Cre injection did not reveal a trend, so mice were not tested in the cylinder task at 10 months.

RESULTS

AAV-Cre transfection deletes PTEN and induces concurrent tdTomato expression

To achieve *PTEN* deletion in the motor cortex of adult mice, 8-week-old PTEN/tdT mice and 8 week old tdT control mice received identical intracortical injections of AAV-Cre into the left motor cortex. The region of AAV-Cre injection was readily identifiable as a focal region containing tdTomato-expressing cells and processes (Fig. 3.1A). In both *PTEN* deleted and control cases at all time points, tdTomato labeling extended through all cortical layers.

In our previous study of mice with early postnatal deletion of *PTEN* (Gutilla et al., 2016), we observed hypertrophy of the affected area of the cortex and sometimes there was displacement of the superior sagittal fissure due to cortical enlargement on the side of the *PTEN* deletion. In the present study, we also observed focal enlargement of the motor cortex at the site of AAV-Cre injection (a focal cortical bump, see Fig. 3.), but did not observe displacement of the superior sagittal fissure. “Cortical bumps” were seen in both PTEN/tdT and tdT control mice, so the focal cortical enlargement may be due to decompression of the brain at the cranial defect produced by burr holes drilled for intracranial injections.

At the center of the injection region (where tdTomato expression was maximal), there was dense labeling of cell bodies and neuropil by tdTomato creating a fluorescent sphere roughly 1 mm in diameter (Fig. 1A). Within this sphere it was difficult to identify individual neurons and their respective processes, however neurons located at the

periphery of the core region were identifiable (Fig. 3.1B). Occasionally we also observed tdTomato-positive neurons in the homotopic region of the contralateral motor cortex (not shown). This is likely due to retrograde transport of AAV-Cre by commissural neurons.

Immunostaining sections for PTEN from PTEN/tdT mice revealed focal loss of PTEN expression in the area of tdTomato expression (Fig. 3.1C). Within the area of deletion, the overall level of immunostaining was reduced; (compare the left and right cortices of Fig. 3.1B, which illustrates immunostaining in the homotypic region on the contralateral side). Large cells that were completely negative for PTEN appeared as "ghost cells" (Fig. 3.1D & F). Ghost cells were not evident in the motor cortex contralateral to the region of *PTEN* deletion or in the area of the AAV-Cre injection in tdT mice (Fig. 3.1C & E). Visualizing PTEN immunostained sections using fluorescence microscopy reveals identical overlap of the region of tdTomato expression and the region of *PTEN* deletion seen in bright field (Fig. 3.1F and G). Immunostaining of the same section for NeuN confirms that the tdTomato positive cells lacking PTEN are neurons (Fig. 3.1H).

No evident pathology due to PTEN deletion in adulthood

In H&E-stained sections, there was no evident pathology in the area of *PTEN* deletion except for the minor injury produced by the needle track of the Hamilton syringe, which could be seen in some cases. The area of the injection was identifiable by the "cortical bump" and by differences in cytoarchitecture, including less well-defined lamination and decreased cell packing density (Fig. 3.2A). Even in H&E stains from

PTEN/tdT mice, enlarged neuronal cell bodies were evident in the area of deletion (Fig. 3.2B; C illustrates the homologous region in the contralateral cortex).

In addition to tdTomato-labeled neurons, there were a few tdTomato expressing cells with astrocyte morphology in sections from both PTEN/tdT and tdT mice (Fig. 3.1B). Sections containing the injection site from PTEN/tdT and tdT mice that were immunostained for glial fibrillary acid protein (GFAP) revealed scattered tdTomato positive, GFAP positive cells around the core of the injection (Fig. 3.2E), confirming that some astrocytes had been transfected by AAV-Cre. There were no abnormal collections of GFAP positive cells, except at the core of the injection region along the boundary of the needle track created by the penetration of the micropipette attached to the Hamilton syringe (Fig. 3.2D).

Adult PTEN deletion leads to persistent activation of growth-associated signaling pathways

Early postnatal deletion of *PTEN* in the sensorimotor cortex of mice results in persistent activation of phosphorylation of ribosomal protein S6 in *PTEN*-negative cortical motoneurons (Gutilla et al., 2016). S6 phosphorylation is considered to be a biomarker for mTOR activation and can be documented by immunostaining for pS6 using phospho-specific antibodies. Immunostaining sections in the area of *PTEN* deletion using pS6 specific antibodies revealed elevated S6 phosphorylation in the area of *PTEN* deletion. The area of *PTEN* deletion (Fig. 3.2F, left cortex) is clearly delineated by a distinct border between neurons with high levels of pS6 immunostaining vs. neurons exhibiting immunostaining comparable to neurons on the contralateral side

(Fig. 3.2F, right cortex). Neurons in all cortical layers exhibited higher levels of immunostaining, but layer V pyramidal neurons exhibited the highest levels of pS6 in both the cell bodies and proximal dendrites (Fig. 3.2G). Levels of immunostaining for pS6 remained high at all time points. Indeed, at 15 months following AAV-Cre injection, increased pS6 immunostaining was qualitatively comparable to what is seen 3 months after *PTEN* deletion (Fig. 3.2F). Increases in immunostaining for pS6 were not seen in control mice that received comparable injections of AAV-GFP (data not shown).

Progressive enlargement of PTEN deleted cortical motoneurons

To assess CMN cell bodies following adult *PTEN* deletion, CMNs were definitively identified by labeling with the retrograde tracer Fluorogold (FG) following bilateral intra-spinal injections of FG at cervical level 5 (C5) and the cell body measurements were done based on colabeling by both markers. Sections from FG-injected mice were immunostained for FG to achieve more complete labeling of cell bodies and dendrites. Fig. 3.3A illustrates a section in which the area of *PTEN* deletion is marked by tdTomato expression and CMNs are retrogradely-labeled with FG.

Sections were imaged by 2-photon microscopy and *PTEN*-negative CMNs identified by co-labeling with both FG and tdTomato (Fig. 3.3B & D) were compared with FG-positive CMNs in the homotopic region of the cortex contralateral to the AAV-Cre injection (Fig. 3.3C). 3D image stacks were flattened into 2D projections, and imported into ImageJ and the cross-sectional area of CMNs was manually traced. Identical analyses were done in tdT mice as a control for transfection with AAV-Cre and tdT expression.

Fig. 3.3E–G illustrates the cross-sectional areas of 50 control and 50 *PTEN* deleted CMNs in 3 individual mice at 15 months post-AAV-Cre injection. The average size of *PTEN* deleted and control neurons was calculated for each individual mouse and then the mean across mice was calculated so for statistics, n = number of mice. Fig. 3.3H illustrates the mean cross-sectional area of *PTEN* deleted CMNs in comparison to contralateral control CMNs at different times post-AAV-Cre. Two-way ANOVA revealed an overall difference between groups ($F(1, 37) = 107.3$, $p < .0001$), a significant difference across time ($F(7,37) = 4.911$, $p = .0005$), and a significant interaction ($F(7,37) = 3.821$, $p = .0032$). Sidak's multiple comparisons post-test revealed that there was no significant difference between *PTEN*-negative and control CMNs 3 months following AAV-Cre injection ($p > .9999$, $t = 0.3252$). At all time points 4 or more months following AAV-Cre injection, *PTEN*-negative CMNs were larger than the contralateral control CMNs (see legend of Fig. 3 for values). The magnitude of the difference in cross-sectional area between *PTEN* deleted and control CMNs remained consistent from 4 to 9 months following *PTEN* deletion, but cell size increased further between 12 and 15 months. At 15 months, average CMN cross-sectional area was 310.1 μm2 ± 52.40 μm2 for *PTEN* deleted CMNs vs. 195.8 μm2 ± 1 4.14 μm2 for *PTEN* intact contralateral control CMNs, representing a size difference of 1.6×.

The cross-sectional area of FG-positive CMNs in the contralateral cortex did not differ significantly over time following AAV-injection (Fig. 3.3I, two-way ANOVA, Sidak's post-test $p > .9999$ for all time points). For full statistics, see figure legend. Also,

there was no significant difference in cross-sectional area between the tdT control CMNs and the intra-animal control CMNs in the cortex contralateral to the AAV-Cre injection.

PTEN deletion in mid-life also results in significant growth of cortical motoneurons

The AAV-Cre injections for the above analyses were done at 8 weeks of age, when the mice are young adults. To determine whether *PTEN* deletion-induced neuronal growth is limited to young adults, we performed identical analyses on PTEN/tdT mice that received AAV-Cre injections at 9 months of age. As illustrated in Fig. 3.3J, there was no significant difference in cross-sectional area 2 months following AAV-Cre injection, but by 5 months *PTEN* deleted CMNs were significantly enlarged (two-way ANOVA, $F(1, 6) = 21.36$ $p = .0036$ for *PTEN* deletion, $F(1, 6) = 1.536$, $p = .2615$ for time, $F(1, 6) = 2.002$, $p = .2069$ for interaction). Post hoc analysis revealed that differences were significant at 5 months (two-way ANOVA Sidak's post-test, $p = .0184$) but not at 2 months (two-way ANOVA Sidak's post-test, $p = .4088$).

Although our analysis of soma size focused on CMNs in layer V, *PTEN*-deleted neurons in all cortical layers appeared to be enlarged (Fig. 3.1F). Thus, growth induced by *PTEN* deletion is not restricted to particular neuron types.

Deletion of PTEN in adult cortical pyramidal neurons results in increased dendritic arborization

The Akt-mTOR pathway plays a role in regulating dendritic size and structure (Kumar et al., 2005), and previous studies have documented increases in dendritic size

and arborization with *PTEN* deletion in early development (Kwon et al., 2006; Williams et al., 2015). Accordingly, we assessed whether growth of cell bodies was accompanied by dendritic growth by comparing dendritic arbors of *PTEN* deleted tdTomato positive neurons vs. control neurons expressing tdTomato from tdT mice with intact *PTEN* expression.

For the analysis of dendritic arbors, tdTomato positive pyramidal neurons were imaged in 3D using 2-photon microscopy 6 and 12 months following AAV-Cre injections when mice were 8 and 14 months old. For technical reasons, 3D reconstructions were done on pyramidal neurons in layers II/III rather than CMNs. Although the mice had received FG injections into the spinal cord, FG fluorescence was not consistently discernable by 2-photon microscopy without immunostaining, and immunostaining for FG abrogated tdTomato fluorescence in dendrites. Second, tdT labeling in dendrites extending from layer V neurons faded over the imaging interval. For unknown reasons, this was less of a problem for layer II/III pyramidal neurons. Since our goal was to determine whether *PTEN* deletion in adult neurons triggered growth, the question can be addressed just as well with layer II/III pyramidal neurons as with CMNs. The criteria for inclusion were: 1) pyramid-shaped cell body; 2) location near the center of the section; 3) isolation from other neurons in the field of view to allow accurate identification of dendrites belonging to the selected neuron.

The area containing selected tdT-labeled pyramidal neurons was imaged by 2-photon microscopy, collecting image stacks 1024 by 1024 µm, scan depth of 150–200 µm, step distance 1 µm. Image blocks of this size capture dendritic branches out to

approximately 300 μm in the plane of the thick section, which is oriented along the long axis of the neuron and out to approximately 75–100 μm perpendicular to the plane of the thick section (half the distance of the section thickness). The image stacks were reconstructed in 3D using Imaris. For Sholl analysis, image stacks were collapsed into a 2D projection image, imported into ImageJ and dendrites were traced manually and analyzed using the Sholl Analysis program (Ferreira et al., 2014).

At the 6 month time point, we analyzed the dendritic arbor of 13 pyramidal neurons from 6 PTEN/tdT mice and 11 cells from 4 tdT mice. Fig. 3.4A & B illustrate examples of collapsed 3D images of neurons from control tdT and PTEN/tdT mice respectively. Tracings of these neurons with concentric circles overlaid are illustrated in Fig. 3.4C & E respectively along with heat maps generated by the Sholl analysis program (Fig. 3.4D & F); warmer colors indicate the distances away from the soma at which the maximal number of dendritic intersections occurred and cooler colors indicate the distances at which the fewest dendrites intersected the concentric circles. The graph in Fig. 3.4G plots the average number of intersections at different distances from the soma in control vs. *PTEN* deleted neurons. The total number of intersections summed across distances was significantly higher for *PTEN* deleted neurons by ANOVA (*PTEN* deleted vs. control: $F(1,590) = 65.05$, $p < .0001$, distance: $F(26,590) = 69.56$, $p < .0001$, interaction: $F(26,590) = 1.73$, $p = .0145$). To assess whether increased branching occurred at a particular distances from the soma, we compared the number of intersections at different distances from the soma by Bonferroni's multiple correction

test; this revealed significant differences in intersections at distances from 90 to 130 μm from the soma (for statistics see figure legend).

At 12 months following *PTEN* deletion, we analyzed 44 cells from 7 PTEN/tdT mice and 23 cells from 6 tdT mice. Fig. 3.5A & B illustrate examples of collapsed 3D images of neurons from control tdT mice and PTEN/tdT mice respectively, along with tracings of these neurons with heat maps in Fig. 3.5C–F. Fig. 5G plots the average number of intersections at different distances from the soma in control vs. *PTEN* deleted neurons. The total number of intersections summed across distances was significantly higher for *PTEN* deleted neurons compared to tdT control neurons (*PTEN* deleted vs. controls: $F(1, 1735) = 552.7$ $p < .0001$, for distance $F(26, 1735) = 172.4$ $p < .0001$, for interaction $F(26, 1735) = 17.02$ $p < .0001$). Comparisons of number of intersections at different distances from the soma by Bonferroni's multiple correction test revealed that differences in the number intersections were significant across a wider range of distances from the soma compared to 6 months. ($p < .05$ for 40 μm to 160 μm at 12 months compared to 90 μm to 130 μm for 6 months, see Figure legend for statistics).

To assess the progression of changes in dendritic parameters in *PTEN*-deleted neurons, we compared data sets at 6 and 12 months post-AAV injection. Comparisons of Sholl data from *PTEN* deleted neurons revealed overall increased dendritic branches at 12 month vs. 6 months post-deletion (Fig. 3.6A, $F(1, 1153) = 4.484$ $p = .0344$) and overall significant differences across distance ($F(26, 1153) = 71.94$ $p < .0001$) with no

significant interaction $F(26, 1153) = 0.9145$ $p = .5886$). Post hoc comparisons by Bonferroni's multiple correction test revealed no significant differences at particular distances away from the soma, however.

We also quantified other parameters: 1) the cross-sectional area of the soma and diameter of the apical dendrite and the ratio between these; 2) the number of primary dendrites emanating from the cell body (separated into the apical and basal dendrites depending on their point of origin from the soma); 3) the total number of dendritic branch points for each neuron.

For the analysis of cell body size and subsequent analyses, we used two way ANOVA with *PTEN* status and time post-deletion. Confirming the findings with FG-labeled CMNs, the cell bodies of *PTEN*-deleted layer II/III neurons were significantly larger than controls (Figs. 3.4H and 3.5H respectively; two-way ANOVA: $F(1, 87) = 114.1$ $p < .0001$), and there were significant differences between the time points $F(1, 87) = 17.80$, $p < .0001$). Post hoc comparisons by Sidak's test revealed that cell body size of *PTEN*-deleted neurons was significantly larger at 12 vs. 6 months post-deletion ($t = 3.72$, $p = .0014$).

Apical dendritic diameter was also larger for P*TEN*-deleted layer II/III neurons vs. control neurons (Figs. 3.4I and 3.5I; two-way ANOVA: ($F(1, 87) = 99.24$ $p < .0001$, Sidak's multiple comparisons post-test for 6 month *PTEN* deletion vs. controls $t = 4.470$ $p < .0001$, for 12 months *PTEN* deletion vs. controls $t = 11.61$ $p < .0001$) and there were

significant differences between the time points $F(1, 87) = 15.20$, $p < .0002$). Post hoc comparisons using the Holm-Sidak method revealed that increases in apical dendrite diameter were greater at 12 vs. 6 months ($t = 4.006$, $p < .0002$). The ratio of dendritic diameter to cross-sectional area of the soma was significantly greater in *PTEN*-deleted vs. controls (Figs. 3.4J and 3.5J, $F(1, 87) = 13.12$, $p < .0001$) but there were no significant differences between time points ($F(1, 87) = 0.82$, $p = .367$). Sidak's post-test revealed no significant difference in the ratio between *PTEN* deleted neurons and controls at 6 months ($t = 1.123$ $p = .8419$), however *PTEN* deleted neurons had significantly greater ratio values compared to control neurons at 12 months ($t = 5.023$ $p < .0001$).

Overall, *PTEN* deleted neurons at both time points had more primary dendrites emanating from the soma than control neurons (Figs. 3.4K and 3.5K, two-way ANOVA, for *PTEN* status $F(1, 87) = 18.36$, $p < .0001$). There was no significant difference between the two time points or significant interaction between time and *PTEN* status (for time $F(1, 87) = 0.2328$ $p = .6306$, for interaction $F(1,87) = 0.9716$ $p = .3270$). Differences in total number of primary dendrites were not significant at 6 months (Sidak's post-test, $t = 1.948$ $p = .2860$) but were significant at 12 months ($t = 4.955$, $p < .0001$). At 12 months, the increase in total number of primary dendrites in *PTEN* deleted neurons was due a larger number of primary basal dendrites compared to controls (Fig. 3.5K: Sidak's post-test, for basal dendrites $t = 3.416$ $p = .0058$), with no significant differences in the number of apical dendrites ($t = 2.433$ $p = .0978$). Differences between *PTEN* deleted neurons at 6 vs. 12 months and control neurons at 6

vs. 12 months were not significant for total primary dendrites, basal primary dendrites, or apical primary dendrites (Fig. 3.6C and 3.G, Sidak's post-test for *PTEN* deletion total primary dendrites 6 vs. 12 months t = 0.3855 p = .9993, *PTEN* deletion basal primary dendrites 6 vs. 12 months t = 0.8116, p = .9616, *PTEN* deletion apical primary dendrites 6 vs. 12 months t = 0.4980 p = .9970, control total primary dendrites 6 vs. 12 months t = 0.9688 p = .9138, control basal primary dendrites 6 vs. 12 months t = 0.5168 p = .9963, control apical primary dendrites 6 vs. 12 months t = 1.837 p = .3512).

The maximal number of intersections indicates the maximal number of dendritic segments intersecting concentric circles at any distance from the cell body. Overall, *PTEN* deleted pyramidal neurons had a larger maximal number of intersections than controls, and post-hoc analyses revealed that differences in intersections were significant at 12 months but not 6 (Figs. 3.4L and 3.5L, for *PTEN* status F(1, 87) = 27.43 p < .0001, for time F(1,87) = 0.1695 p = .6816, for interaction F(1,87) = 7.908 p = .0061, Sidak's post-test comparing *PTEN* deletion and controls at 6 months t = 1.423 p = .6380, for 12 months t = 7.567 p < .0001). Comparisons of the values from *PTEN* deleted pyramidal neurons at 6 vs. 12 months revealed no significant differences (Fig. 3.6C, t = 2.470 p = .0892). Differences between control neurons at 6 and 12 months were also not significant (Fig. 6G, t = 1.584 p = .5256).

PTEN deleted layer II/III pyramidal neurons also had more dendritic branch points than controls (Figs. 3.4M and 3.5M, two-way ANOVA, for *PTEN* status F(1, 87) = 29.71 p < .0001, for time F(1, 87) = 2.952 p = .0893, for interaction F(1,87) = 1.716

p = .1937). For *PTEN* deleted pyramidal neurons, the number of dendritic branch points was significantly increased compared to controls at 12 but not 6 months (Figs. 3.4M and 3.5M, Sidak's post-test, for *PTEN* deletion vs. controls at 6 months t = 2.445 p = .0950, for 12 months t = 6.356 p < .0001). Differences in number of branch points between *PTEN* deleted neurons at 6 and 12 months were not significant (Fig. 3.6D, t = 0.3129 p = .9998), and there was no significant effect of time overall (F(1, 87) = 2.952, p = .0893). Post hoc comparisons revealed that while the number of dendritic branch points of control neurons decreased between 6 and 12 months, the differences were not significant (Fig. 3.6H, t = 1.998, p = .2595).

Control pyramidal neurons with intact PTEN expression exhibit age-related dendritic loss

Comparison of dendritic intersections in *PTEN* deleted pyramidal neurons at 6 and 12 months post-deletion revealed a significant increase in intersections with time (Fig. 3.6A, for time post-deletion F(1,1153) = 4.484 p = .0344, for distance from soma F(26,1153) = 71.94 p < .0001, for interaction F(26, 1153) = 0.9145 p = .5886). To assess the stability of dendritic parameters in control neurons, we compared data sets at 6 and 12 months post-AAV injection. Comparisons of Sholl data (Fig. 3.6E) revealed that the number of dendritic intersections in Sholl analysis was significantly decreased at 12 vs. 6 months for control neurons (time following injection F(1, 582) = 6.215 p = .0129, distance F(23, 582) = 33.83 p < .0001, interaction F(23, 582) = 0.5312 p = .9654). Post hoc comparisons by Bonferroni's multiple correction test revealed no significant differences at particular distances away from the soma, however.

Analysis of other dendritic parameters of control neurons at 12 vs. 6 months revealed no significant differences in the total number of primary dendrites (Fig. 3.6F, $t = 1.708$, $p = .097$), the number of basal dendrites ($t = 0.529$, $p = .6003$). Despite a trend towards fewer maximal intersections and branch points at 12 vs. 6 months, these differences were not significant (Fig. 3.6G and H, Sidak's post-test, maximal intersections $t = 1.584$ $p = .5256$, branch points $t = 1.998$ $p = .2595$).

PTEN deletion leads to enlargement of corticospinal tract axons without altering myelination

To examine the effect of adult *PTEN* deletion on axon size and myelination, we identified *PTEN* deleted axons in the medullary pyramids of three PTEN/tdT mice by tdT immunostaining and compared these to neighboring un-labeled control axons. The same analysis was done for tdT-positive axons in the medullary pyramid of two tdT mice. Brainstem sections were immunostained for tdTomato using DAB. One micrometer thick sections were stained with Toluidine blue, and ultrathin sections were processed for electron microscopy. tdT-positive (*PTEN* deleted) axons were easily identified at the electron microscopic level (Fig. 3.7A & E). These and neighboring tdT-negative control axons were manually traced, and axoplasm cross-sectional area, axoplasm plus myelin cross-sectional area, myelin cross-sectional area, axoplasm diameter, and axoplasm plus myelin diameter were measured. The ratio of the diameter of the axoplasm and the diameter of the axoplasm plus myelin was used to calculate the G-ratio.

Two-way ANOVA revealed significant differences based on *PTEN* status (Fig. 3.7B,: ($F(1, 12) = 15.35$ $p = .0020$), and structure measured ($F(2, 12) = 11.66$ $p = .0015$), with no significant interaction ($F(2, 12) = 2.481$ $p = .1254$). Cross-sectional areas of tdT-labeled axons were significantly larger in PTEN/tdT mice (Fig. 3.7B, Sidak's post-test $p = .0373$). The cross-sectional areas of tdT-positive axons in tdT control mice were very similar to the unlabeled controls in both genotypes (Fig. 3.7B & F). There were no significant differences in cross-sectional area of myelin alone (Fig. 3.7C, Sidak's post-test $p = .9577$), but there were significant differences in the values for axoplasm plus myelin area (Sidak's post-test $p = .0159$).

G-ratios were significantly higher for *PTEN*-deleted axons compared to controls (Fig. 3.7D, students t-test = 87.01, $p = .0005$, $df = 4$). Taken together, the unchanged cross-sectional area of myelin and the increased G-ratio seen in *PTEN* deleted axons one year following adult deletion indicate that *PTEN* deletion-induced increases in axon diameter do not trigger compensatory increases in myelination. Cross-sectional areas of myelin on tdT-labeled axons in tdT mice (*PTEN* intact) did not differ significantly from neighboring controls in any of the measurements (Fig. 3.7F–H, see figure legend for statistics). Also, the cross-sectional areas of myelin on tdT-positive axons in tdT control mice were very similar to that of unlabeled axons in both genotypes (Fig. 3.7B & F).

Unilateral adult PTEN deletion impairs motor coordination but does not affect symmetry of forelimb use during exploration

To examine the functional effects of unilateral *PTEN* deletion in the adult motor cortex, mice were tested on the rotarod and cylinder task. Testing was done 6 months after unilateral AAV-Cre injection in 8-week-old PTEN/tdT mice (n = 18) and age-matched tdT mice with intact *PTEN* expression (n = 16). The rotarod task has been used to assess both motor performance and motor learning (Rothwell et al., 2014). With repeated trials, mice exhibit an improved ability to remain on the accelerating rotating rod. Improvement in performance over time is considered a measure of motor learning, peak performance is considered a measure of motor performance ability, and initial performance is a measure of baseline coordination.

We assessed mice on the rotarod across 4 consecutive days with 3 trials/day (12 total trials). Trials 1–6 on days 1 and 2 of testing entailed less challenging test parameters (slower starting speed, slower acceleration), and trials 7–12 on days 3 and 4 were more challenging (faster starting speed, faster acceleration). This design was utilized to prevent masking of continued performance improvements by a ceiling effect that is typically observed in the absence of a challenge. Latency to fall was measured and used to calculate maximum attained speed for each trial.

Both groups exhibited improved rotarod performance across trials 1–7 (increased latency to fall and higher average maximum speed attained with each successive trial) (Fig. 3.8A). On trials 8–12, both groups exhibited a plateau in performance. Two-way ANOVA revealed that both *PTEN* deletion status and trial number had a significant

effect on maximum terminal speed attained ($F(1, 636) = 38.06$ $p < .0001$ for *PTEN* status; $F(11, 3378) = 18.38$ $p < .0001$ for trial number, $F(11, 25) = 0.1359$ $p = .9996$ for interaction, though the differences at individual trials were not significant.

To determine whether baseline deficits in motor coordination or impaired motor learning was responsible for the reduced performance of mice with unilateral adult *PTEN* deletion, we analyzed the data by linear regression (Rothwell et al., 2014). The slope of the line calculated from maximum terminal speed over successive trials, interpreted as motor learning (dashed lines), did not differ significantly between the two groups (0.7384 ± 0.1058 RPM/trial for controls and 0.7917 ± 0.199 RPM/trial for *PTEN* deletion, student's t-test $p = .7304$, $F(1, 20) = 0.1221$) (Fig. 3.8A). The calculated y-intercept, interpreted as baseline motor coordination (horizontal dashed lines), was significantly lower for mice with *PTEN* deletion compared to controls (7.263 ± 0.7787 RPM for controls and 4.415 ± 0.8089 RPM for *PTEN* deletion, student's t-test $F(1, 21) = 23.5419$, $p < .0001$).

Since the rotarod data were obtained using two paradigms of the same task, we also performed segmental linear regression analysis, analyzing trials 1–6 (pre-challenge) and 7–12 (challenge) separately. The y-intercept (baseline coordination) for controls was 5.689 and 1.173 RPM for *PTEN* deletion cases, again indicating that unilateral adult *PTEN* deletion impairs baseline coordination. The pre-challenge rate of learning (slope) for trials 1–6 was 1.202 RPM/trial for controls and 1.173 RPM/trial for *PTEN* deletion cases, representing a slight impairment in motor learning during the easier trials.

Following the challenge of increased starting speed and increased acceleration in trials 7–12, the rate of learning for controls was 0.3781 RPM/trial and 0.4958 RPM/trial for mice with *PTEN* deletion. Taken together the data suggest that the *PTEN* deletion group has slightly impaired motor learning under easier circumstances, and improved learning level under challenging circumstances. Ultimately, the *PTEN* deletion group failed to achieve a maximum terminal speed equal to that of the control group (15.0375 RPM in trial 9 for controls and 12.844 RPM in trial 7 for *PTEN* deletion).

The same mice were also tested in the cylinder task to determine if unilateral *PTEN* deletion during adulthood causes asymmetry in forelimb use. Plotting the percentage of total touches for each forepaw or both forepaws together, the *PTEN* deletion group had a slight, though insignificant increase in the percentage of right forepaw touches compared to controls. There was no significant difference in sidedness of spontaneous forepaw exploration for the *PTEN* deletion group compared to controls (two-way ANOVA, $F(1, 0.004) = 0.0008059$ $p = .9774$ for PTEN deletion, $F(2, 25) = 2.887$ $p = .0607$ for paw sidedness, $F(2, 22.9) = 2.628$ $p = .0775$ for interaction) (Fig. 3.8B & C).

Mice with bilateral PTEN deletion exhibit improved motor learning 8 or more months post-deletion

Because mice with unilateral deletion of *PTEN* exhibited some impairment in rotarod performance, we wondered whether bilateral *PTEN* deletion would abrogate this impairment. To assess this, 10 PTEN/tdT mice and 9 tdT mice received bilateral

AAV-Cre injections into the somatosensory cortex at 8 weeks of age and were tested on the rotarod every 2 months from 2 to 8 months post-injection (Fig. 3.8D–I).

At 2, 4, and 6 months following injection (when the mice were 4, 6, and 8 months old), mice with bilateral *PTEN* deletion performed comparably to controls over all 12 rotarod trials (Fig. 3.8E–I), see Figure legend for statistics). Surprisingly, at 8 months, mice with bilateral adult *PTEN* deletion demonstrated significantly better rotarod performance in comparison to controls, though differences at individual trials were not significant (Fig. 3.8H, two-way ANOVA, $F(1, 101) = 4.181$ $p = .0422$ for *PTEN* deletion, $F(11, 891) = 3.357$ $p = .0003$ for trial number, $F(11, 142) = 0.5344$ $p = .8785$ for interaction). Linear regression analysis revealed significantly improved motor learning in *PTEN* deletion mice (0.7012 RPM/trial for *PTEN* deletion versus 0.3113 RPM/trial for controls, $F(1, 20) = 9.88212$ $p = .005113$), though differences in baseline coordination were not significant (7.1 for *PTEN* deletion, 8.3 RPM for controls).

Based on the interim statistical analysis, we tested the mice on the rotarod again at 10 months following injection); again, mice with *PTEN* deletion continued to demonstrate significantly improved rotarod performance than controls (Fig. 3.8I, two-way ANOVA, $F(1, 267) = 15.27$ $p < .0001$ for *PTEN* status, $F(11, 63) = 3.605$ $p < .0001$ for trial number, $F(11, 53.5) = 0.2783$ $p = .9893$ for interaction). Linear regression analysis showed that the slopes (rate of motor learning) of the *PTEN* deletion and control performance curves were not significantly different (for *PTEN* deletion slope = 0.5534 RPM/trial, control slope = 0.4162/trial, $F(1, 20) = 2.63073$ $p = .1205$),

though baseline coordination was significantly improved in the *PTEN* deletion group (for *PTEN* deletion y-intercept = 7.705 RPM, control intercept = 6.430 RPM, $F(1, 21) = 51.1406$ $p < .0001$). Mice with bilateral *PTEN* deletion also attained higher average maximum speeds compared to controls. At 6 months post-injection, The highest average maximum attained speed for controls was 14.98 RPM vs. 16.63 RPM for *PTEN* deleted mice at 8 months post-deletion.

Testing in the cylinder task at 2, 4, 6, and 8 months post-deletion revealed no differences in forelimb use between mice with *PTEN* deletion vs. controls (Fig. 3.8J–M).

DISCUSSION

We show here that deleting *PTEN* in the sensorimotor cortex of adult mice leads to progressive growth of cell bodies, dendrites, and axons of cortical neurons that continues for at least 12 months post-deletion. Although there were increases in the number of primary dendrites and extent of dendritic branching, the basic pyramidal phenotype of cortical neurons was preserved (no ectopic apical dendrites, more basal than apical primary dendrites, and similar patterns of dendritic branching).

Progressive enlargement of CMN cell bodies with adult PTEN deletion

In our previous study of the consequences of *PTEN* deletion at postnatal day 1 (Gutilla et al., 2016), cell bodies of CMNs were 1.7× larger than control CMNs at 12 months of age. We did not assess the time course of growth, however. Here we show

that CMNs are about 1.5× larger than control CMNs at 12 months following *PTEN* deletion in early adulthood, and increase further to about 1.6× larger than control CMNs by 15 months. These results indicate that adult neurons can mount a continuous growth response, but the growth may be slower than what occurs with *PTEN* deletion during development. Interestingly, the largest percent increase occurs between 12–15 months post-deletion, suggesting that growth accelerates with increased time following deletion. This finding was unexpected, and further studies will be required to fully explore this late phase of growth.

In our previous study of mice with deletion of *PTEN* at P1, we also observed overall hypertrophy of the motor cortex and sometimes cortical expansion on the side of the *PTEN* deletion led to displacement of the superior sagittal fissure (Gutilla et al., 2016). With *PTEN* deletion in adult mice, we did not observe displacement of the superior sagittal fissure. There was focal cortical enlargement (a bump) in both PTEN/tdT and tdT mice, which was likely a response to surgical burr holes rather than *PTEN* deletion or AAV injections since control mice in our previous study did not have cortical enlargement following neonatal AAV injection.

Progressive increase in dendritic size and number following adult PTEN deletion

For technical reasons, quantitative analyses of dendritic parameters were done on pyramidal neurons in layers II–III. These actually provide an advantage over CMNs because the dendritic arbors of layer II/III pyramidal neurons are less elaborate than CMNs. Our results reveal increases in the number of primary dendrites extending from the soma (specifically basal primary dendrites), number of dendritic branch points, and

number of intersections in concentric circle analysis from *PTEN* deleted pyramidal neurons. For most measures, the *PTEN* deletion-induced morphological phenotype is more pronounced at 12 than 6 months following deletion. In contrast, comparison of control neurons from tdT mice at 6 vs. 12 months revealed decreases in dendritic arborization over time, consistent with age-related dendritic atrophy. Hence, in addition to inducing growth, *PTEN* deletion may prevent age-related dendritic atrophy.

One caveat is that the reconstructions don't capture the complete dendritic arbors. The 3D image stacks are oriented to capture the long axis of the pyramidal neuron, but dendrites extending laterally are captured only out to about 75–100 μm, so distal branches are not visualized. In addition, distal apical dendritic arbors of most neurons were not captured within the area of the scan. Distal apical dendrites may be an additional site of structural modification following adult PTEN deletion, especially because of the known plasticity of these dendrites in the adult brain (Greenough et al., 1979).

One unanswered question is whether the new dendrites receive synaptic connections, and if so, whether synapse numbers are comparable to control neurons. We were not able to visualize spines in our 2-photon reconstructions, even at high resolution. A previous study of the consequences of shRNA-mediated knockdown of *PTEN* in dentate granule cells of adult mice revealed thicker dendrites and an overall increase in dendritic spines at 4 months post-injection (Luikart et al., 2011). A complication with interpreting these findings is that dentate granule cells are one of the

few neuron types that exhibit adult neurogenesis, so the generalizability of the findings to other neuronal populations is unclear. An ideal way to address this question would be to identify newly-grown dendrites via sequential imaging in living animals and assess synapse number on newly-grown vs. previously existing dendrites.

PTEN deletion-induced increases in axon caliber without compensatory increases in myelination

Corticospinal tract axons emanating from *PTEN*-deleted CMNs were larger in diameter, without proportional increases in myelin, resulting in increased G-ratios. It is noteworthy that a recent study reported that selective promoter-driven deletion of *PTEN* in developing cerebellar granule cells led to enlargement of granule cell somata and increases in axon diameter that were accompanied by aberrant myelination of normally unmyelinated parallel fibers (Goebbels et al., 2017). The fact that myelin thickness did not increase in *PTEN*-deleted CST axons may indicate that adjustments in myelin due to *PTEN* deletion-induced axon enlargement differ depending on whether the axon is normally myelinated, or on the developmental timing of the deletion. It remains to be seen whether changes in G-ratio in enlarged CST axons affect action potential propagation.

Persistent mTOR activation following PTEN deletion in adulthood

PTEN is a negative regulator of AKT/mTOR, so the expected result of *PTEN* deletion is persistent activation of mTOR. Strong evidence in support of this conclusion is the sustained activation of S6 phosphorylation in CMNs. Given mTOR's known role in promoting neuronal growth and dendritic outgrowth (Kumar et al., 2005; Urbanska et

al., 2012), persistent mTOR activation due to *PTEN* deletion is a plausible mechanism for the growth that we describe here. The fact that growth can be initiated in mid-life supports the surprising conclusion that mature uninjured neurons retain the ability to reinitiate a robust growth response after they have reached their steady-state size. This finding supports the possibility of using *PTEN* modifying interventions to ameliorate neuronal atrophy following axon injury (Barron et al., 1988; Schwab and Bartholdi, 1996; Kobayashi et al., 1997).

Phosphorylation of ribosomal protein S6 is a downstream marker of mTOR activation, and may alter mRNA translation, but persistent activation of S6 phosphorylation is not likely to be the primary cause of neuronal growth. Activation of AKT and mTOR also leads to a host of other processes including signaling to the nucleus, which likely has multiple effects on gene expression. Understanding the mechanisms that actually contribute to growth is of great importance, especially in terms of potential clinical applications. The differential roles of the multiple processes triggered by persistent AKT/mTOR activation remain to be defined.

Functional consequences of adult PTEN deletion

Our initial analysis of functional consequences of *PTEN* deletion in the motor cortex revealed mixed effects on motor function as assessed by the rotarod and cylinder tasks. Mice with unilateral *PTEN* deletion exhibited slight rotarod impairment but maintained symmetry in spontaneous forelimb exploration. Mice with bilateral *PTEN* performed comparably to controls until 8 months post-deletion and exhibited improved rotarod performance to controls at later intervals.

Motor impairment with unilateral deletion involved impaired baseline performance that persisted over multiple trials (implying impaired coordination), lower maximum attained speed, but no difference in the rate of performance improvement (interpreted as motor learning). These performance trends are similar to that of mice one year following unilateral *PTEN* deletion during early postnatal development (Gutilla et al., 2016). A possible explanation for the impaired motor coordination and performance is that *PTEN* deletion is unilateral whereas the rotarod assesses overall motor function involving bilateral coordination.

Improved rotarod performance of mice with bilateral adult *PTEN* deletion manifested as improved baseline performance (motor coordination), a faster rate of performance improvement (motor learning), and higher maximum attained speeds. The fact that enhanced performance occurs in parallel with neuron growth invites the speculation that there is a causal relationship. In contrast to mice with *PTEN* deletion, control mice exhibited diminished rotarod performance at older ages. Again, diminished performance occurs in parallel with age-related decreases in dendrites suggesting a relationship. Our motor function analyses only assessed gross aspects of motor function following *PTEN* deletion in adult mice, and it will be of interest in future studies to test more sophisticated, fine motor functions. Unfortunately we did not assess motor function following bilateral *PTEN* deletion in neonatal mice, so we are unable to compare our present findings in the adult with the developing system.

PTEN deletion in non-neuronal cells

Expression of tdTomato following AAV-Cre transfection revealed tdT-positive cells with astrocyte morphology; these were confirmed to be astrocytes by co-immunolabeling with GFAP. Different AAV serotypes exhibit differential tropisms (Burger et al., 2004; Taymans et al., 2007; Aschauer et al., 2013), and the AAV-2 serotype used here has been shown to be relatively neuron-specific (Bartlett et al., 1998). Positive identification of tdT-positive astrocytes highlights the utility of fluorescent reporter genes in identifying cell types that are transfected in low abundance. It remains to be seen whether *PTEN* deletion in non-neuronal cell types contributes to the anatomical and behavioral phenotypes reported here.

Implications of adult neuronal growth for neurodegenerative diseases and neurological injury

Neuronal and axonal atrophy are hallmarks of injury, many neurodegenerative diseases, and normal aging (Barron et al., 1989; McBride et al., 1989; Finch, 1993; Bronfman et al., 2000). Reducing such atrophy might be a promising way to attenuate the cognitive and functional declines associated with aging and neurodegenerative disease. Bringing together *PTEN*'s negative regulation of neuronal and axonal regeneration, neuronal survival, and neuronal growth, PTEN inhibition may be a promising way to abrogate injury and age-related atrophy as well as attenuate the negative pathophysiological consequences.

Table 3.1- Mice used for cell body size measurements and unilateral behavior assessment.

Months post-AAV-Cre	# PTEN/tdT mice	# tdT mice	# injected with fluorogold	# Used in behavior at 6 months post-deletion
3	n=6	n=2	n=8	n=0
4	n=5	n=0	n=5	n=0
5	n=5	n=0	n=5	n=0
6	n=3	n=2	n=5	n=0
7	n=4	n=0	n=4	n=4 PTEN/tdT
8	n=3	n=0	n=3	n=3 PTEN/tdT
9	n=6	n=0	n=8	n=4 PTEN/tdT
12	n=5	n=2	n=6	n=4 PTEN/tdT
15	n=3	n=2	n=5	n=3 PTEN/tdT

Table 3.2- Summary of mice used for Sholl analysis

Mouse	Time point	Age	Group	Genotype	Sex	# of cells	Total cells
1	6 months	8 months	*PTEN* deletion	PTEN/tdT	M	1	
2	6 months	8 months	*PTEN* deletion	PTEN/tdT	M	5	
3	6 months	8 months	*PTEN* deletion	PTEN/tdT	M	1	
4	6 months	8 months	*PTEN* deletion	PTEN/tdT	F	3	
5	6 months	8 months	*PTEN* deletion	PTEN/tdT	F	1	
6	6 months	8 months	*PTEN* deletion	PTEN/tdT	F	1	n= 12
1	6 months	8 months	Control	tdT	M	4	
2	6 months	8 months	Control	tdT	F	1	
3	6 months	8 months	Control	tdT	F	3	
4	6 months	8 months	Control	tdT	F	3	n= 11
1	12 months	14 months	*PTEN* deletion	PTEN/tdT	M	7	
2	12 months	14 months	*PTEN* deletion	PTEN/tdT	M	5	
3	12 months	14 months	*PTEN* deletion	PTEN/tdT	M	4	
4	12 months	14 months	*PTEN* deletion	PTEN/tdT	F	4	
5	12 months	14 months	*PTEN* deletion	PTEN/tdT	F	4	
6	12 months	14 months	*PTEN* deletion	PTEN/tdT	F	6	
7	12 months	14 months	*PTEN* deletion	PTEN/tdT	F	11	n= 41
1	12 months	14 months	Control	tdT	F	1	
2	12 months	14 months	Control	tdT	F	6	
3	12 months	14 months	Control	tdT	F	2	
4	12 months	14 months	Control	tdT	F	4	
5	12 months	14 months	Control	tdT	M	5	
6	12 months	14 months	Control	tdT	M	5	n= 23

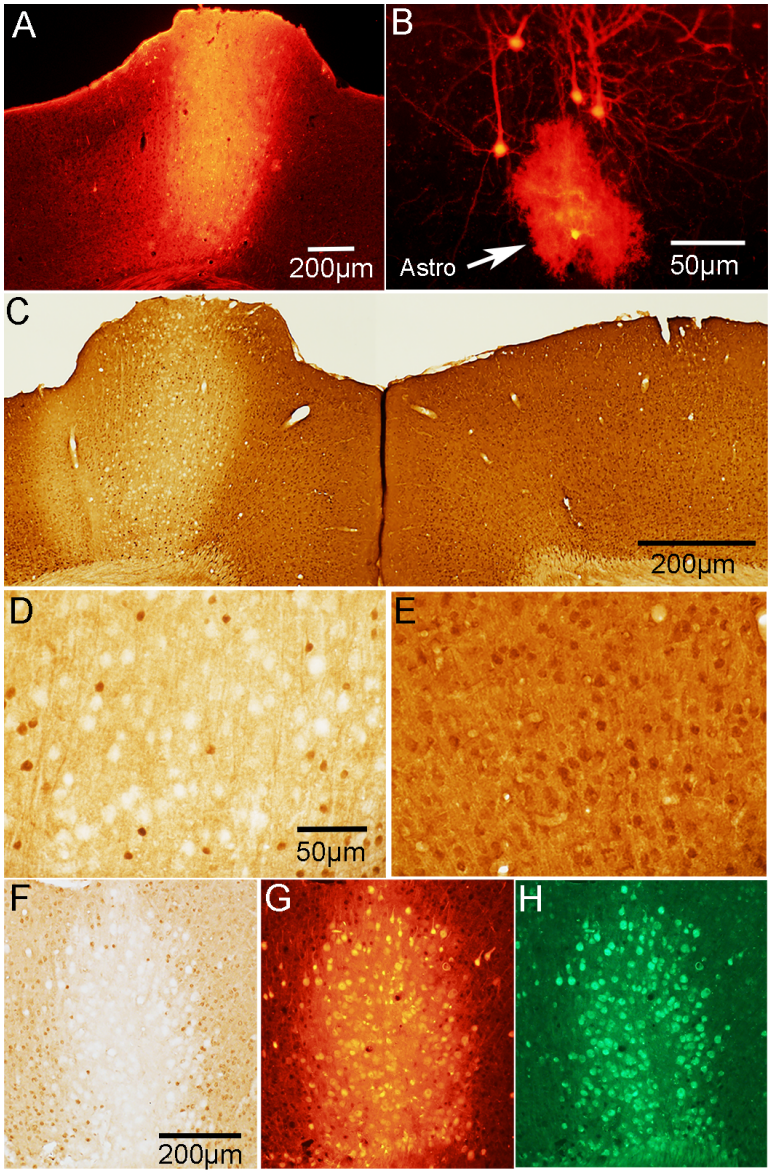

Figure 3.1- Expression of tdTomato and concurrent *PTEN* deletion in PTEN/tdT mice following AAV-Cre injection in adult mice. A. tdTomato expression in the area of AAV-Cre injection into the left sensorimotor cortex. **B.** tdT-labeled pyramidal neurons and one astrocyte in the penumbra of the injection (arrowhead indicates astrocyte). **C.** PTEN immunostain of left and right motor cortex; area of deletion (about 1 mm diameter) corresponds to the area of tdT expression in panel **A**. **D.** Higher magnification of layer V in the area of *PTEN* deletion; note PTEN-negative "ghost cells". **E.** Layer V in the homotypic region of the contralateral cortex in the same section as D. **F.** PTEN immunostain section viewed in bright field. **G.** The same section as F viewed with fluorescence microscopy to visualize tdTomato-positive cells. **H.** The same section as F&G immunostained for NeuN reveals that cells that are PTEN negative and tdT-positive are neurons.

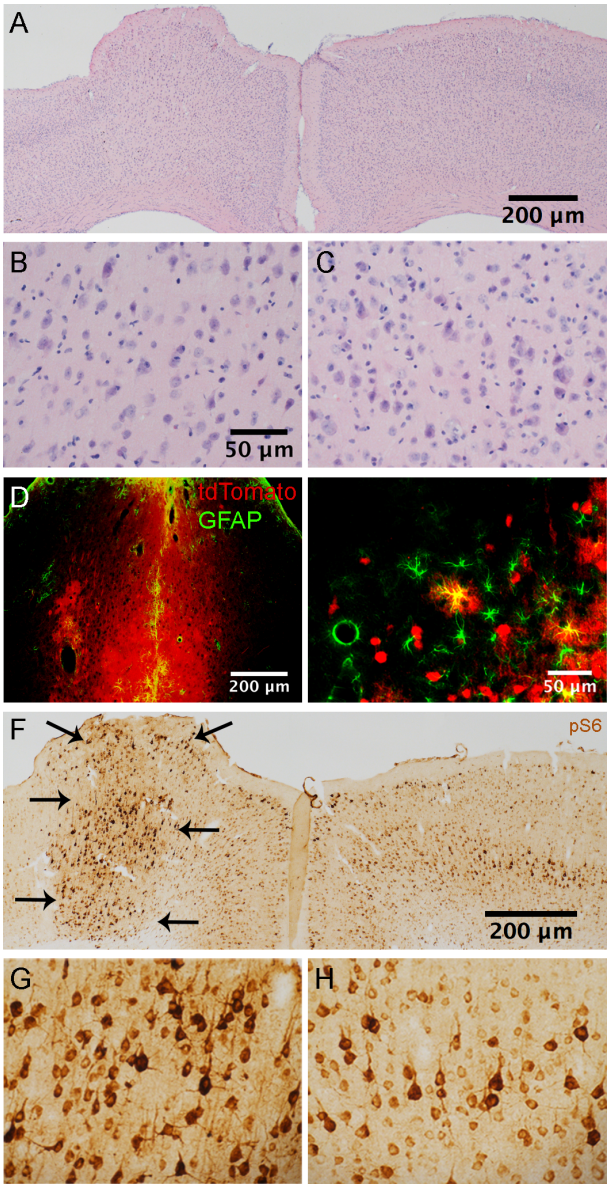

Figure 3.2- Histology following *PTEN* deletion in adult mice. A. H & E stained section illustrating cortical architecture ipsi and contralateral to the AAV-Cre injection at 12 months post-AAV. Arrows indicate the area of the injection. **B.** High magnification view of layer V in the area of *PTEN* deletion from the section in **A**. **C.** Layer V of the contralateral cortex from the section in **A**. **D.** Section at the site of needle track from the intracortical injection immunostained for GFAP. **E.** Nearby area outside the core of the injection from the section in D. Note that some astrocytes are co-labeled for GFAP and tdT (arrowheads). **F.** Immunostaining for pS6 (antibody against p-Ser 235/236) in the area of deletion and contralateral cortex (same mouse shown in panel A). Note distinct boundary (arrows) between area with elevated pS6 immunostaining and surrounding regions **G.** Higher magnification view of pS6-positive neurons in the region of *PTEN* deletion shown in **F**.**H.** pS6 immunostaining in the homologous region of the contralateral control motor cortex.

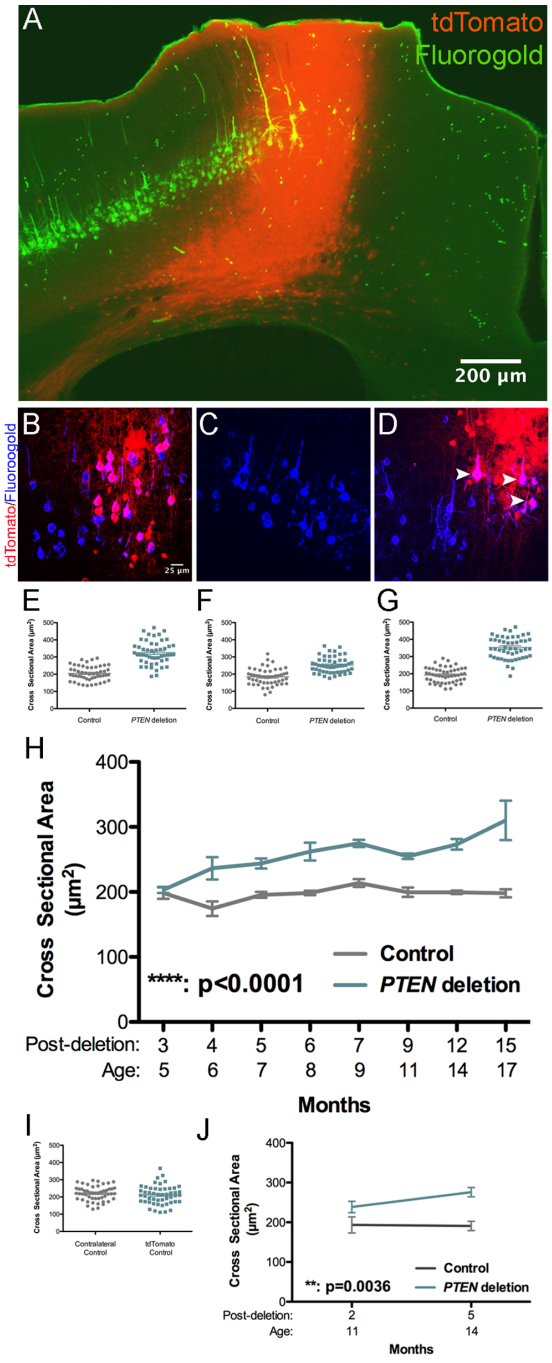

Figure 3.3- Age-dependent neuronal growth following *PTEN* deletion in adulthood. **A.** Section from a PTEN/tdT mouse that had received Fluorogold into the cervical spinal cord; section is immunostained for FG and tdT is visualized by native fluorescence. Two images of the same field were taken with NB and NG illumination on an Olympus AX80 microscope. Paired images were converted to 8-bit, imported into ImageJ and FG fluorescence in NB was assigned to the green channel and tdT fluorescence in NG was assigned to the red channel. **B.** 2D projection of a 3D reconstruction illustrating cortical motoneurons (CMNs) from a tdT mouse, 4 months following AAV-Cre injection retrogradely labeled with FG (blue) some of which express tdT (red). Co-labeled cells are magenta (white arrowheads). **C.** 2D projection of a 3D

multiphoton reconstruction from the homologous area of the motor cortex contralateral to the area shown in **A**; note all CMNs are labeled by Fluorogold only. **D.** 2D projection of a 3D reconstruction illustrating CMNs retrogradely labeled by Fluorogold and tdTomato from a PTEN/tdT mouse (arrowheads). **E.–G.** Scatter plots of CMN cell body sizes from 3 PTEN/tdT mice 15 months following PTEN deletion. **H.** Average cell body size of *PTEN* deleted and control CMNs at different times post-AAV-Cre injection. Sidak's post-test of differences at particular time points: 3 months: NSD ($p > .9999$). 4 months: $p = .0006$. 5 months: $p = .0181$, 6 months: $p = .0023$, 7 months: $p = .0445$, 9 months: $p = .0308$, 12 months: $p = .0008$, 15 months, $p < .0001$). **I.** Scatter plot of cell size from a control tdT mouse, 12 months after AAV-Cre injection. **J.** Average cell body size of *PTEN* deleted and control CMNs after *PTEN* deletion at 9 months of age. (For interpretation of the references to colour in this figure legend, the reader is referred to the web version of this article.)

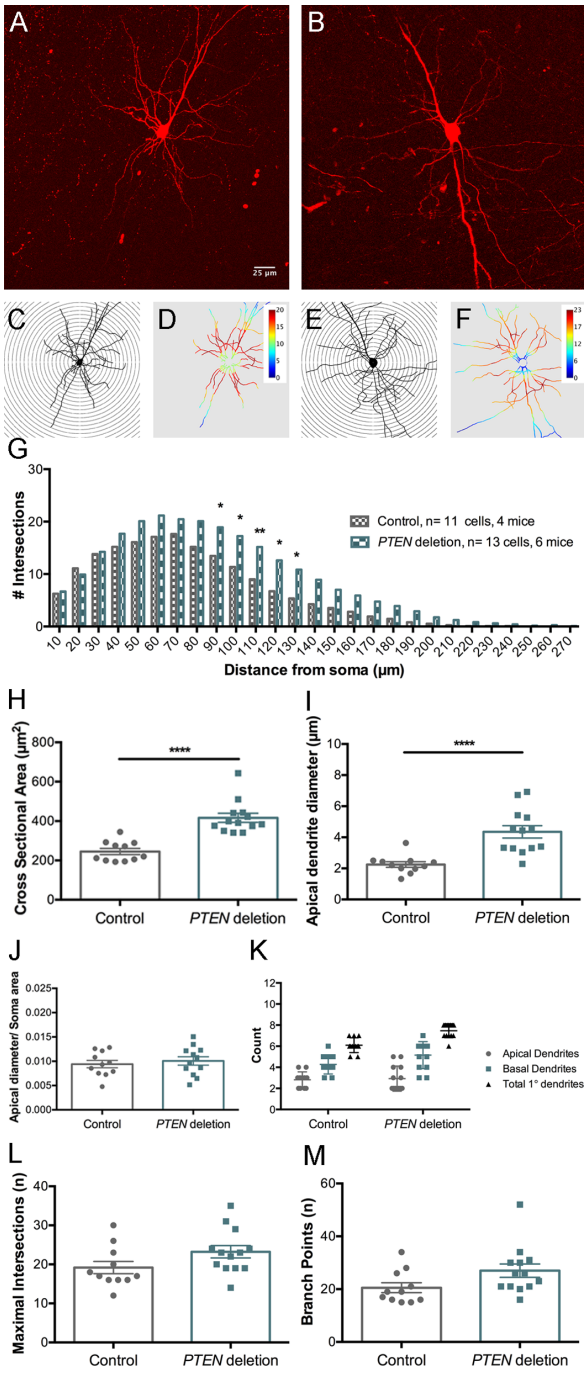

Figure 3.4- Sholl analysis of dendritic number and arborization of cortical pyramidal neurons 6 months following *PTEN* deletion. A. Flattened projection of a 3D reconstruction of tdTomato-labeled control pyramidal neuron from a cleared thick section. **B.** Flattened projection of a tdTomato-labeled *PTEN* deleted pyramidal neuron. **C.** Traced projection of neuron in A overlaid with concentric circles for Sholl analysis. **D.** Heat map of **C** generated by ImageJ Sholl Analysis Program, warmer colors represent a greater number of dendritic intersections, cooler colors represent fewer dendritic intersections. **E.** Traced projection of **B** overlaid with concentric circles. **F.** Heat map of **E** generated by Sholl Analysis

Program. **G.** Average Sholl concentric circle analysis data from 11 control and 13 *PTEN* deleted pyramidal neurons. Asterisks indicate distances at which differences were significant at $p < .05$ by Sidak's post-test (for 90 μm $p = .0281$, 100 μm $p = .0118$, 110 μm $p = .0062$, 120 μm $p = .0113$, 130 μm $p = .0273$). **H.** Cross-sectional area of soma of *PTEN* deleted pyramidal neurons vs. controls. **I.** Diameter of the large apical dendrite (30 μm away from the center of the soma). **J.** Ratio of the diameter of the apical dendrite to the cross-sectional area of the soma. **K.** Number of basal and apical primary dendrites in *PTEN* deleted pyramidal neurons vs. controls. **L.** Maximal number of intersections at any distance from the soma (concentric circle with highest number of crossings). **M.** Total number of branch points in *PTEN* deleted vs. control neurons.

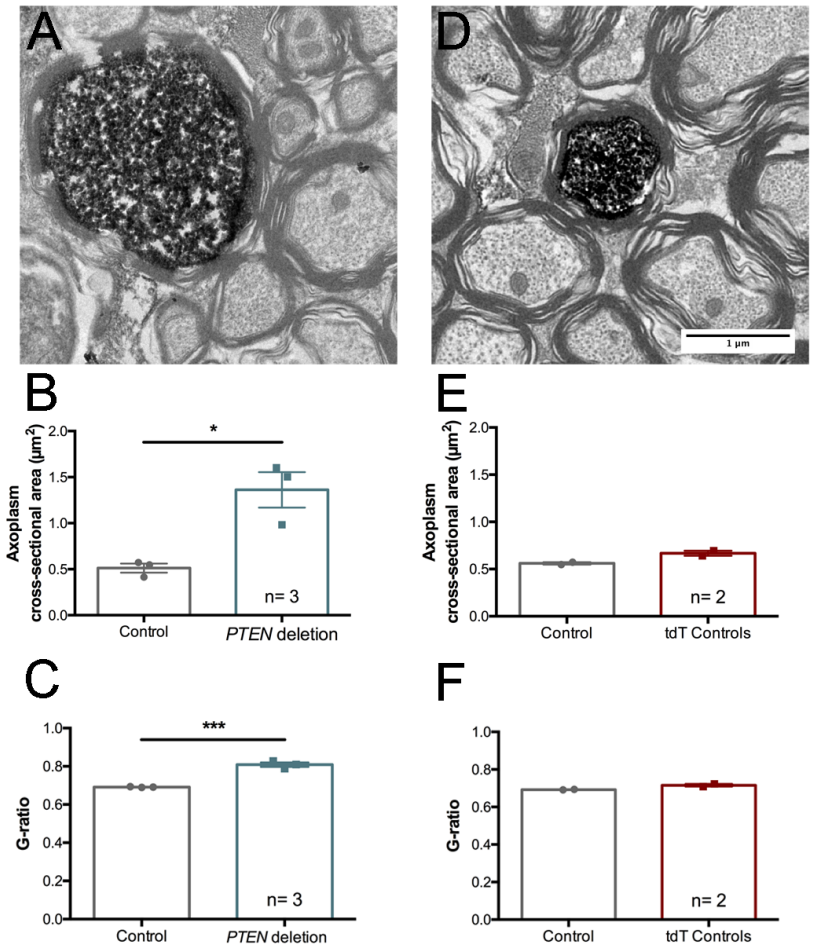

Figure 3.5- Sholl analysis of dendritic number and arborization 12 months following *PTEN* deletion. A. Flattened projection of a 3D reconstruction of tdTomato-labeled control neuron from a cleared thick section. **B.** Flattened projection of a tdTomato-labeled *PTEN* deleted neuron. **C.** Traced projection of **A** overlaid with concentric circles for Sholl analysis. **D.** Heat map of C generated by Sholl Program. **E.** Traced projection of **B** overlaid with concentric circles. **F.** Heat map of **E** generated by Sholl Program. **G.** Average intersections for the Sholl concentric circle analysis data from 23 control and 44 *PTEN* deleted pyramidal neurons. Asterisks indicate distances at which differences were significant at $p < .05$ by Sidak's post-test (for 40 µm–150 µm $p < .0001$, 160 µm $p = .0102$). **H.** Cross-sectional area of soma. **I.** Diameter of the large apical dendrite (30 µm away from the center of the soma). **J.** Ratio of dendrite diameter to cross-sectional area of the soma. **K.** Number of basal and apical primary dendrites. **L.** Maximal number of intersections at any distance from the soma (concentric circle with highest number of crossings). **M.** total number of branch points in *PTEN* deleted vs. control neurons.

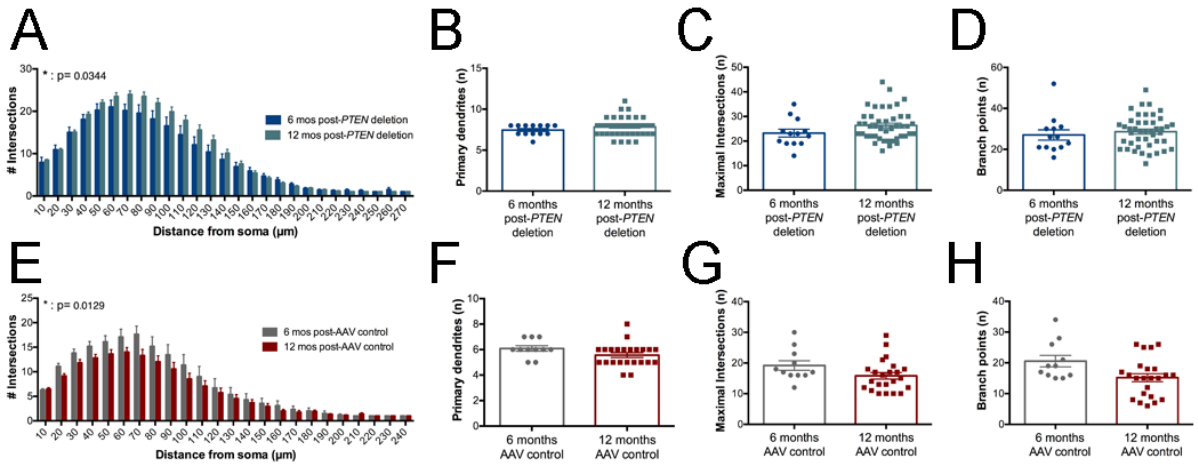

Figure 3.6- *PTEN* deleted neurons exhibit age-related gains in dendritic arborization; control neurons exhibit age-related losses. A. Age-based comparisons of Sholl data from *PTEN* deletion pyramidal neurons at 6 vs. 12 months post-deletion. **B.** Number of primary dendrites of *PTEN*-deleted neurons at 6 vs. 12 months post-injection (8 and 14 months of age). **C.** Maximal intersections of *PTEN* deleted neurons at 6 vs. 12 months post-deletion. **D.** Number of branch points in *PTEN* deleted neurons at 6 vs. 12 months post-deletion. **E.** Age-based comparisons of Sholl data from control pyramidal neurons at 6 vs.12 months post-AAV injection. **F.** Number of primary dendrites of control neurons at 6 vs. 12 months post-injection. **G.** Maximal intersections at 6 vs.12 months post-injection. **H.** Number of branch points at 6 vs. 12 months post-injection.

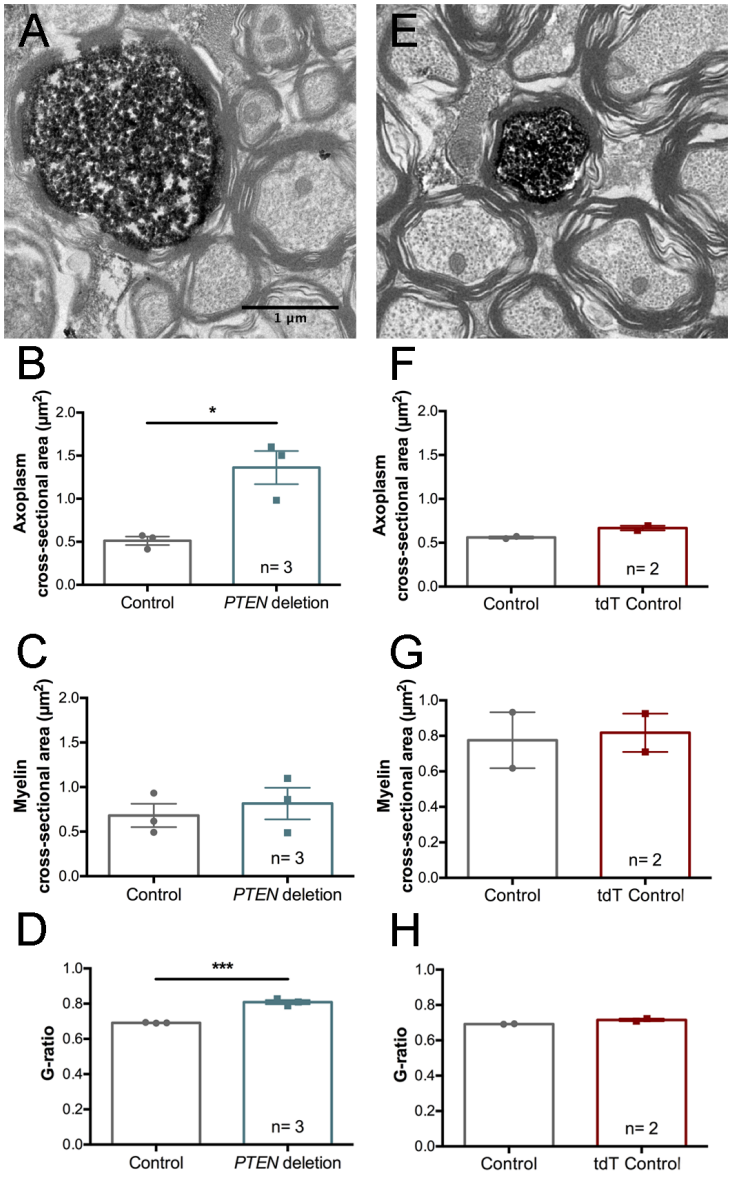

Figure 3.7- Increases in CST axon diameter and decreases in G-ratio following adult *PTEN* deletion. A. Electron microscopic images of tdT-positive (*PTEN* deleted) and nearby unlabeled CST axons from PTEN/tdT mice 12 months post-AAV-Cre. **B.** Points in bar graphs are the average cross-sectional area of the axoplasm of *PTEN* deleted vs. nearby unlabeled control axons in each mouse. **C.** Points in bar graphs are the average cross-sectional area of the myelin sheath of *PTEN* deleted vs. nearby unlabeled control axons in each mouse. **D.** Points in bar graphs are the average G-ratio for *PTEN* deleted vs. nearby unlabeled control axons in each mouse. **E.** tdTomato-positive brainstem axons in tdT control mice one year following AAV-Cre injection. **F, G & H.** Graphs are for the same values as **B,C &D** for tdT control mice (two-way ANOVA, for control type $F(1, 6) = 2.040$ $p = .2031$, for structure measured $F(2, 6) = 32$ $p = .0006$, for interaction $F(2, 6) = 0.3980$ $p = .6881$, Sidak's post-test for axoplasm area: $p > .9999$, for myelin area: $p > .9999$). G-ratio: (student's t-test, $p = .0840$).

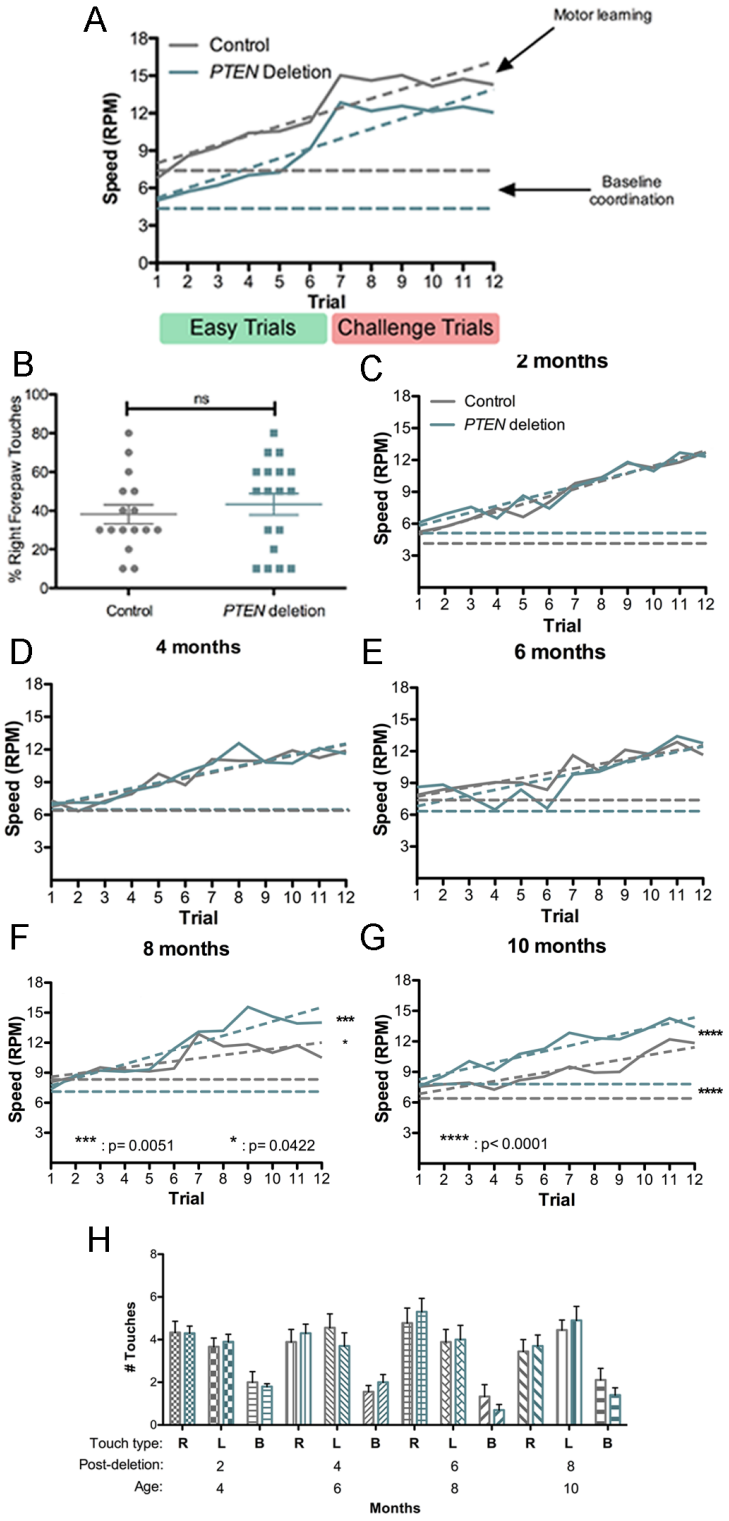

Figure 3.8- Motor learning and forelimb exploration following adult unilateral or bilateral *PTEN* deletion. A. Plot of rotarod performance (maximal speed attained) over trials of mice with unilateral *PTEN* deletion vs. controls. Easier trials 1–6: starting speed of the rod

was 4 rotations per minute (RPM) and the acceleration 0.1 RPM/s (RPM/s). Challenge trials 7–12: starting speed of the rod was increased to 6 RPM with an acceleration of 0.2 RPM/s. **B.** Percent right forepaw touches by mice with unilateral *PTEN* deletion in the left motor cortex in comparison to controls. **C.** Plot of rotarod performance (maximal speed attained) over trials of mice with bilateral *PTEN* deletion vs. controls at 2 months post-AAV. **D.** Rotarod performance at 4 months post-AAV. **E.** Rotarod performance at 6 months post-AAV. **F.** Rotarod performance at 8 months post-AAV injection. **G.** Rotarod performance at 10 months post-AAV. **H.** Assessment of spontaneous forelimb exploration in the cylinder task at 2–8 months post-injection. Two-way ANOVA revealed no significant differences at any time point.

CHAPTER 4: SELECTIVE NEURONAL *PTEN* DELETION: CAN WE TAKE THE BRAKES OFF OF GROWTH WITHOUT LOSING CONTROL?

Previously published in the journal of Neural Regeneration Research in 2016 as: Gutilla, Erin A., and Steward, Oswald. "Selective neuronal PTEN deletion: can we take the brakes off of growth without losing control?" *Neural Regeneration Research* 11.8 (2016): 1201.

ABSTRACT

The limited ability for injured adult axons to regenerate is a major cause for limited functional recovery after injury to the nervous system, motivating numerous efforts to uncover mechanisms capable of enhancing regeneration potential. One promising strategy involves deletion or knockdown of the phosphatase and tensin (*PTEN*) gene. Conditional genetic deletion of *PTEN* before, immediately following, or several months after spinal cord injury enables neurons of the corticospinal tract (CST) to regenerate their axons across the lesion, which is accompanied by enhanced recovery of skilled voluntary motor functions mediated by the CST. Although conditional genetic deletion or knockdown of *PTEN* in neurons enables axon regeneration, *PTEN* is a well-known tumor suppressor and mutations of the *PTEN* gene disrupt normal brain development leading to neurological abnormalities including macrocephaly, seizures, and early mortality. The long-term consequences of manipulating *PTEN* in the adult nervous system, as would be done for therapeutic intervention after injury, are only now being explored. Here, we summarize evidence indicating that long-term deletion of *PTEN* in mature neurons does not cause evident pathology. Studies to date provide only a first look at the potential negative consequences of *PTEN* deletion or knockdown, but

the absence of any detectable neuropathology supports guarded optimism that interventions to enable axon regeneration after injury are achievable.

KEYWORDS

PTEN; mTOR; spinal cord injury; corticospinal tract; motor system; axon regeneration; recovery of function.

INTRODUCTION

Regeneration of injured or unhealthy axons holds great therapeutic promise for neurological disorders including acute trauma to the brain or spinal cord, stroke, and neurodegenerative diseases. The phosphatase and tensin homolog (*PTEN*) gene has emerged as an important regulator of axon regeneration, and recent findings by multiple groups support the potential of using PTEN as a therapeutic target. Our recent paper reports that long-term deletion of *PTEN*, a tumor suppressor gene, does not result in any major detectable pathology and may also enhance neuronal vitality. By selectively deleting *PTEN* in the motor cortex of young mice, we specifically assessed the effects of *PTEN* loss using the same approach that has been used to promote regeneration of the corticospinal tract after spinal cord injury.

PTEN's impact on axon regeneration was discovered in a seminal experiment in which conditional genetic deletion of *PTEN* promoted robust axonal regeneration of retinal ganglion cells (RGCs) following optic nerve crush (Park et al., 2008). The rationale for this experimental approach is rooted in the discovery of inhibitory intrinsic and extrinsic factors that prevent regeneration of injured axons (Schwab and Bartholdi, 1996; Fitch and Silver, 2008). One approach to overcoming the intrinsic inhibitory factors focuses on attempting to "recapitulate development", in order to return adult neurons to a more growth permissive state (Filbin, 2006). Growth cessation after the completion of development is thought to occur in part due to the onset of growth inhibiting genes being expressed.

In their landmark study, Park et al. tested whether axon regeneration could be enhanced if genes that normally repress cell growth were eliminated prior to axon injury. They specifically examined several known tumor suppressor genes including *PTEN*, *p53, retinoblastoma, Smad4, Dicer, or LKB*. The effect of each individual gene was studied using multiple strains of "floxed" mice, with each strain having only one of the aforementioned genes flanked by lox-P sites. The specific gene was deleted in the retina be injecting AAV-Cre into the vitreous humor of the eye prior to performing an optic nerve crush. Only deletion of the *PTEN* gene enabled axotomized RGCs to regenerate, though deletion of both *PTEN* and *p53* reduced retrograde degeneration of RGCs that otherwise occurred. The latter finding, not emphasized at the time, could mean that deleting *PTEN* enhanced RGC vitality such that the neurons could survive traumatic injuries that would normally cause cell death.

PTEN deletion and corticospinal tract (CST) axon regeneration

Following the initial finding that linked *PTEN* deletion to enhanced neural regeneration, a follow up study tested whether neuronal *PTEN* deletion could also enhance regeneration after spinal cord injury. This study focused on regeneration of the corticospinal tract (CST), which mediates voluntary motor function. Damage to CST axons due to spinal cord injury is the cause of paralysis, and enabling regeneration of the CST is the best hope for restoring motor function after injury. Similar to Park et al., this study use floxed *PTEN* mice, and *PTEN* was deleted in the motor cortex of mice one day after birth by injecting AAV-Cre into the sensorimotor cortex. Then, as young adults, mice received spinal cord injuries. Tract tracing of CST axons revealed robust and unprecedented regeneration beyond the injury site (Liu et al., 2010).

Subsequent studies have confirmed and extended findings from these two papers. Genetic deletion of *PTEN* soon after spinal cord injury in adult mice, or knockdown of PTEN expression using short hairpin RNA (shRNA) against PTEN in adult rats a few days before injury was found to enhance the regenerative growth of the adult CST and recovery of skilled motor functions (Zukor et al., 2013; Lewandowski and Steward, 2014; Danilov and Steward, 2015). Remarkably, *PTEN* deletion also induced robust CST regeneration in the chronic injury setting one year following injury (Du et al., 2015). These discoveries further highlight the potential of using *PTEN* interference as a pro-regenerative strategy for treating adult spinal cord injury (Ramon-Cueto et al., 2000).

PTEN's role in regulating normal neuronal development and function

The *PTEN* gene is thought to exert its growth inhibiting effects through the PTEN protein's negative regulation of phosphoinositide 3-kinase (PI3K). As a phosphatase, PTEN converts active phosphatidylinositol (3,4,5)-triphosphate (PIP3) to inactive phosphatidylinositol (4,5)-bisphosphate (PIP2), resulting in diminished AKT and downstream mammalian target of rapamycin (mTOR) activation. Thus, deletion of *PTEN* leads to enhanced levels of PIP3, activation of AKT, and activation of mTOR. The mTOR pathway is well known for its ability to regulate cell growth and proliferation and PTEN's upstream and non-redundant negative regulation of the mTOR pathway make it a promising pro-regenerative therapeutic target (Don et al., 2012).

It's here that we come to the theme of our review; is it possible to take the brakes off of such a powerful growth-promoting pathway without losing control? The logic behind testing *PTEN* was that it had been identified as a tumor suppressor gene. *PTEN* mutations are common in several cancers, and have been associated with developmental disorders including macrocephaly and autism spectrum disorders (Goffin et al., 2001; Hollander et al., 2011). Experimental studies in which *PTEN* was deleted during early development in particular cell types revealed neuronal over-growth, brain enlargement, seizures and premature death. These studies used mice with a lox-P flanked *PTEN* gene paired with Cre recombinase expression regulated under the control of promoters including neuron specific enolase (NSE,(Kwon et al., 2006)), glial fibrillary acid protein (GFAP, (Backman et al., 2001; Kwon et al., 2001; Fraser et al., 2004; Yue et al., 2005; Fraser et al., 2008; Wen et al., 2013)), Ca^{2+}/calmodulin-dependent protein kinase II (CamKII, (Sperow et al., 2012)), and the dopamine active transporter (DAT, (Diaz-Ruiz et al., 2009). In studies using NSE, GFAP, and CamKII promoter driven Cre expression, mice with *PTEN* deletion exhibit significantly higher postnatal mortality and premature death (~11 weeks of age for CamKII-Cre, (Sperow et al., 2012)). In the GFAP-Cre models, multiple groups have identified neurons with successful *PTEN* deletion in the cerebellum, hippocampus, and the cerebral cortex (Backman et al., 2001; Kwon et al., 2001; Fraser et al., 2004; Fraser et al., 2008).

The negative consequences following widespread neuronal *PTEN* loss during development necessitated an in-depth examination of the long-term consequences of deleting *PTEN* in the way that promotes axon regeneration. As a first step in assessing the potential risk, we employed the same experimental model as in our original report of

CST regeneration following spinal cord injury (Liu et al., 2010). *PTEN* was deleted by injecting AAV-Cre into the sensorimotor cortex of floxed *PTEN* mice on postnatal day 1. Mice were then allowed to survive for at least one year, and motor function was tested in the final months prior to euthanasia(Gutilla et al., 2016).

Over several months of handling and testing, mice did not exhibit any obvious behavioral abnormalities or spontaneous seizures. General motor function was tested by open field activity and rotarod and brains were examined extensively for any evidence of tumors or other neuropathology. Mice with *PTEN* deletion exhibited normal exploratory activity in an open field and were slightly, though not significantly, impaired on the rotarod. Most important, we found no evidence of tumors or other neuropathology in the area of *PTEN* deletion. Cortical motoneurons, the cells of origin of CST axons, appeared healthy and exhibited high levels of immunostaining for the phosphorylated form of ribosomal protein S6 (rpS6). rpS6 phosphorylation is considered a bioindiciator of mTOR activation, so high levels of immunostaining for phosphorylated rpS6 indicates continued activated of mTOR more than a year after *PTEN* deletion.

The only histological abnormalities were: 1) cortical motoneurons lacking *PTEN* (identified by retrograde labeling following Fluorogold injections into the spinal cord) were substantially larger than control neurons; 2) there was visible disruption of the normal laminar organization of the cortex in the area of *PTEN* deletion, perhaps as a result of the increase in neuronal size; 3) the ratio of neuropil to cell bodies was higher in the region of *PTEN* deletion. Our speculation is that this is due to cellular

hypertrophy including hypertrophy of dendrites, but we have not yet assessed this quantitatively.

Safety of PTEN interference as a therapeutic strategy and remaining questions

While our study does not qualify as a safety study as would be required for preclinical development of a therapy, the mice survived without any ill effects for up to 18 months after *PTEN* deletion (considered early old age in mice). Other studies involving hundreds of mice and rats with *PTEN* deletion in the sensorimotor cortex report enhanced regeneration and improvements in motor function after spinal cord injury, and there have been no reports of negative effects. Taken together, our findings along with previous reports point to the possibility of targeting *PTEN* therapeutically without triggering untoward effects.

Despite providing an important first look at the long-term consequences of *PTEN* deletion, several questions remain unaddressed. Other groups have reported seizures following deletion of *PTEN* early in development (Backman et al., 2001; Ogawa et al., 2007; Pun et al., 2012) as well as changes in the electrophysiological properties of neurons lacking *PTEN* (Fraser et al., 2008; Sperow et al., 2012; Williams et al., 2015). So far there have been no systematic studies of the physiological consequences of *PTEN* deletion in cortical neurons, but this warrants further investigation. Additionally, since most acute neurological traumas and neurodegenerative diseases occur in adults, it will also be important to assess the consequences of *PTEN* deletion in adults.

The ability to induce a robust growth capability in central nervous system neurons has broad implications even beyond the potential of enabling regeneration of axons after spinal cord injury. Park's original study reported that in addition to promoting axon regeneration, *PTEN* deletion in retinal ganglion cells reduced retrograde cell death following optic nerve crush. It will be of considerable interest to assess whether *PTEN* deletion could prevent or reverse age-related deterioration of neurons such as neuronal atrophy and death that is observed in neurodegenerative diseases including Parkinson's disease, Alzheimer's disease, and amyotrophic lateral sclerosis (ALS). Indeed, there have been reports that show that deleting *PTEN* in the substantia nigra reverses symptoms in an experimental Parkinson's disease model and protects dopaminergic neurons from toxic insults (Diaz-Ruiz et al., 2009; Domanskyi et al., 2011).

The pace of research on *PTEN* related to neural regeneration is clearly accelerating. A PubMed search done on May 21, 2016 using the keywords "PTEN, regeneration, and axon" in "Abstract" yielded a total of 56 papers, with an increasing number being published each year (Figure 4.1). Indeed, 12 papers have been published in the first five months of 2016. This increased effort aimed at understanding *PTEN*'s role in neural regeneration will undoubtedly help to address the questions that still remain.

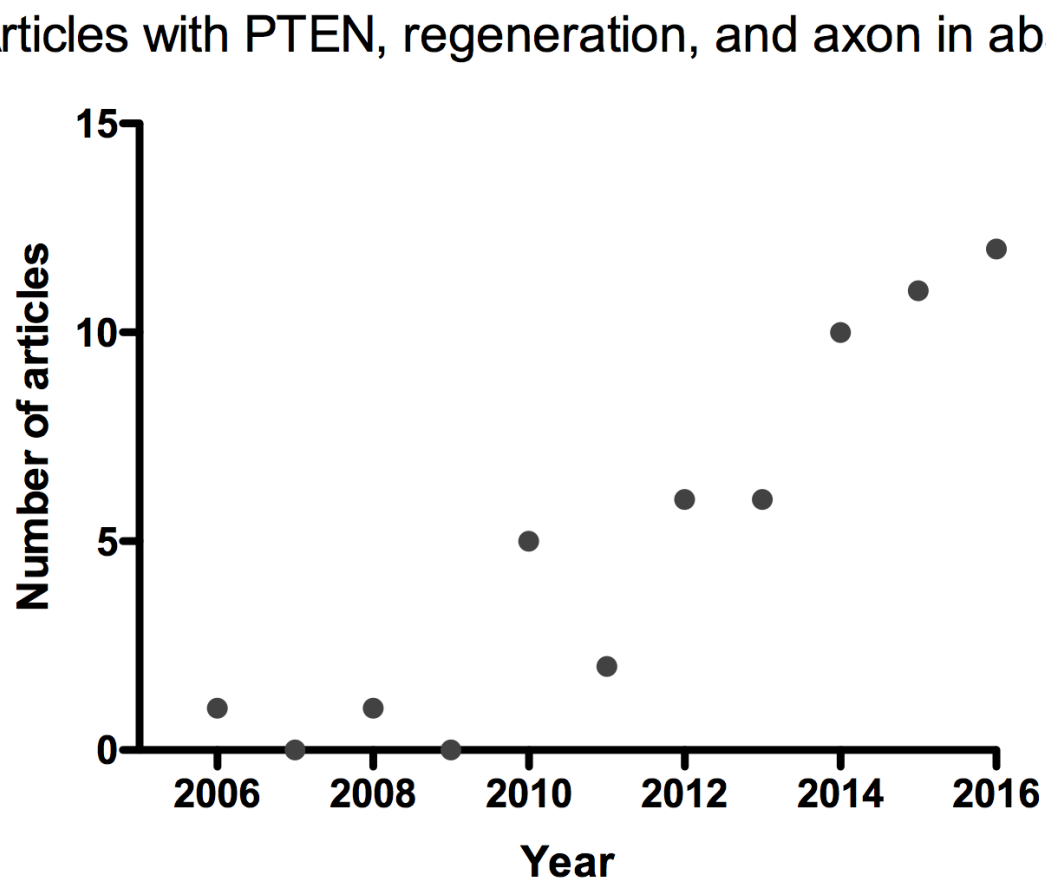

Figure 4.1- Increased number of articles related to *PTEN* and regeneration published per year since 2006. A PubMed search done on May 21, 2016 using the keywords "PTEN, regeneration, and axon" in "Abstract" yielded a total of 56 papers. The graph plots numbers of publications per year.

Chapter 5: Alternative approaches to promote mTOR-mediated regeneration

HIGH FREQUENCY MOTOR CORTEX STIMULATION TO DRIVE mTOR-MEDIATED REGENERATION: A PRELIMINARY STUDY

ABSTRACT

Stimulation of the sensorimotor cortex in rodents is an important contributor to functional recovery following cerebral infarct and pyramidotomy (Teskey et al., 2003; Carmel et al., 2010; Carmel et al., 2013; Carmel et al., 2014). In the clinical setting, deep brain stimulation (DBS) has been used therapeutically since the 1960's for a variety of motor abnormalities, including those associated with Parkinson's disease (Perlmutter and Mink, 2006). Here we have examined the use of motor cortex stimulation as a potential method for optimizing neuronal regeneration following a cervical level spinal cord contusion injury. The rationale for this experiment is rooted in the well-established role of mTOR in promoting growth and regeneration in the adult injured central nervous system. We assessed the ribosomal protein s6 phosphorylation state (p-S6) to infer the regenerative potential of stimulated neurons based on the responsiveness of this biomarker for mammalian target of rapamycin (mTOR) activity. First, we tested various stimulation and post-perfusion parameters in order to identify the optimal stimulation conditions (20 minute stimulation duration, with pS6 induction lasting 1-2 hours post-stimulation). After determining the stimulation paradigm, we tested the effect of stimulation in an injury setting. Female Long Evans rats were implanted with

stimulating electrodes and given C5 contusion spinal cord injuries (SCI). Prior to injury all rats were trained on the Grip Strength Meter (GSM) task, and the axons of the corticospinal tract were traced by performing intracortical injections of AAV-green fluorescent protein (GFP). Beginning one week after SCI, rats were stimulated twice a day, 20 minutes each time, 5 days a week, for 6 weeks. The stimulation consisted of 400 Hz trains, 20 msec in duration, delivered 1/10sec. Rats were tested on GSM once a week for 8 weeks (2 weeks beyond the completion of stimulation). Rats were then perfused and assessed for pS6 induction, behavioral changes on GSM, and axonal regeneration. Our experimental results indicate an enhancement in pS6 induction following stimulation, indicative of enhanced mTOR activation. The relatively minor contusion injury and poor labeling of corticospinal tract (CST) fibers by AAV-GFP precluded us from being able to assess meaningful functional gains or axonal regeneration in stimulated rats. In future experiments, a more severe injury, more sensitive behavioral task, and a more prolific tracer will need to be used in order to more fully understand the impact of cortical stimulation on axonal regeneration and functional recovery after SCI.

INTRODUCTION

Chronic spinal cord injury (SCI) affects the lives of 200,000 people in the US, with an addition of 10,000 new cases/year (Sadowsky, 2001). The ability for axons to grow and regenerate after an injury decreases as the age of the person at the time of injury increases (Bregman et al., 1997). There is no cure for SCI, though progress in our basic research understanding of SCI and regeneration have brought many promising therapies to clinical trial (Silva et al., 2014).

Regeneration of the corticospinal tract (CST) is of particular interest due to its role in mediating voluntary motor control. Increased regeneration of the CST would result in significant gains in quality of life for patients, allowing patients with cervical injuries to regain independence by potentially allowing them to regain the use of their hands or arms. The axons that comprise the CST originate from large layer V cortical motoneurons that reside in the motor cortex.

One of the most promising approaches to increasing CST regeneration after injury involves the conditional deletion of the phosphatase and teinsin homolog (*PTEN*) gene in the cortical motoneurons that give rise to the CST. Using AAV-Cre to conditionally delete *PTEN* in the cortical motoneurons of transgenic mice harboring a lox-P flanked exon 5 of the *PTEN* gene, our lab and others have found that *PTEN*-deficient neurons demonstrate enhanced regenerative ability, neuron survival, and functional recovery after SCI (Liu et al., 2010; Danilov and Steward, 2015; Du et al., 2015).

The PTEN phosphatase is an important upstream, non-redundant inhibitor of the growth-promoting mammalian target of rapamycin (mTOR) pathway. The mTOR pathway regulates a myriad of neuronal functions that are growth permissive, including dendritic outgrowth, dendritic spine development, axon guidance, autophagy, cytoskeletal structure, and protein synthesis (Jaworski et al., 2005; Kumar et al., 2005; Jaworski and Sheng, 2006; Hoeffer and Klann, 2010)

mTOR's role in regulating protein synthesis specifically involves the regulation of a subset of mRNA transcripts called 5' terminal oligopyrimidine (5'TOP) mRNAs (Jefferies et al., 1997; Ma and Blenis, 2009). 5'TOPs mRNAs typically encode components of translational machinery, including ribosomal proteins, initiation factors, and elongation factors. Specifically, ribosomal protein S6 (S6) and eukaryotic initiation factor-1A (eIF-1A) are known to be expressed and translated in an mTOR-dependent fashion (Tsokas et al., 2005).

Increasing mTOR pathway activity and subsequent expression of 5'TOP mRNAs holds great therapeutic promise for treating neuronal injury and disease (Park et al., 2010; Don et al., 2012) (Park et al. 2010, Don et al 2010). Since knocking out a tumor suppressor gene is not a feasible therapeutic approach for patients, we have begun exploring alternative clinically relevant approaches to increase mTOR activity and neural regeneration.

Our lab has found that high-frequency stimulation of a rodent's hippocampus causes an increase in S6 phosphorylation, indicating increased mTOR pathway activation (Pirbhoy et al., 2016). S6 can be phosphorylated at 5 evolutionarily conserved serine residues, Ser 235, Ser 236, Ser 240, Ser 244, and Ser 247 (Wettenhall et al., 1992), and mTOR is known to regulate phosphorylation at all 5 residues. S6 phosphorylation occurs sequentially, beginning with Ser 235 (Ruvinsky and Meyuhas, 2006), and phosphorylation at all five serine residues is at least partially regulated by mTOR via S6 kinase 1 (S6K1) (Biever et al., 2015).

Stimulating the motor cortex of rodents following CST-specific lesions resulted increased axonal regeneration, increased sprouting, and enhanced functional recovery and axon outgrowth (Brus-Ramer et al., 2007; Carmel et al., 2010; Carmel et al., 2013; Carmel and Martin, 2014). Taking the findings from our lab and Carmel et al. together, we have hypothesized that high-frequency stimulation of neurons in the motor cortex will result in increased mTOR activity (indicated by increased S6 phosphorylation), resulting in enhanced axonal regeneration following SCI and functional recovery.

To address this hypothesis, we first needed to establish the optimal stimulation parameters for inducing S6 phosphorylation. Stimulating the motor cortex of uninjured rats for different amounts of time (10 or 20 minutes) and waiting different amounts of time between stimulation and perfusion (in order to establish the duration over which S6 phosphorylation is maintained following stimulation), we found that 20 minutes of high frequency unilateral stimulation resulted in bilateral pS6 induction up to 2 hours post-stimulation. We then tested our stimulation protocol in rats following a contusion

spinal cord injury. Cervical contusion injuries are the most similar to the compressive or contusive injuries seen in the majority of patients with SCI, further contributing to the clinical relevance of this study (Nobunaga et al., 1999). Rats were first given cortical stimulation implants and intracortical injections of AAV-GFP to anterogradely trace the CST. Rats were then given moderate C5 contusion injuries (~156 kdynes). One week after SCI, awake, behaving rats underwent unilateral high frequency stimulation of the motor cortex for 20 minutes, twice a day, 5 days/week, for 6 weeks. Behavioral testing on the grip strength meter (GSM) was done once a week for 8 weeks. After completion of stimulation and behavior, the rats were perfused and the brains and spinal cords collected for histology. Brain sections were immunostained using two phospho-specific antibodies for pS6 (pS6 Ser 235.236, pS6 Ser 240/244) and stained for hematoxylin and eosin (H&E). Spinal cord transverse and horizontal sections were assessed for axonal regeneration based on GFP expression. The relatively minor contusion injury and poor labeling of corticospinal tract (CST) fibers by AAV-GFP precluded us from being able to assess meaningful functional gains or axonal regeneration in stimulated rats. In future experiments, a more severe injury, more sensitive behavioral task, and a more prolific tracer will need to be used in order to more fully understand the impact of cortical stimulation on axonal regeneration and functional recovery after SCI.

METHODS

Cranial implants for stimulation optimization

The Institutional Animal Care and Use Committee (IACUC) at the University of California, Irvine approved all experimental procedures. 12 female Long Evans rats were

implanted with unilateral stimulating electrodes in the forelimb region of the left motor cortex. The rats were anesthetized with a xylazine (10 mg/kg) ketamine (100 mg/kg) cocktail, placed in a small animal stereotaxic apparatus, and the scalp incised. Two craniotomies were performed at to allow for placement of the stimulating electrodes directly on the cortical surface (first craniotomy: -1.0 mm anterior/posterior and -1.0 mm lateral relative to bregma second craniotomy: -1.0 mm anterior/posterior and -4.0 mm lateral relative to bregma). Small burr holes were drilled posterior to the craniotomies and 1.0 mm lateral to midline for the placement of small screws used to anchor the implant. Once the screws were in place, the electrodes were placed on the skull and dental cement was used to secure the implant. After the dental cement fully dried the scalp was sutured with 5-0 silk and the rat was given subcutaneous injections of Lactated Ringer's and Baytril. The rats were then returned to the home cage on water circulating heating pads at 37°C. Once the rat had recovered fully from the anesthetic, liquid Tylenol was administered PO (200 mg/100 mL).

Cortical stimulation in uninjured awake, behaving adult rats

Two days after the implant surgery, implanted animals underwent cortical stimulation. Awake, behaving rats were delivered 400hz trains at 20msec in duration, repeated at 1/10 second intervals for either 10 or 20 minutes. Following electrical stimulation, the rats were perfused at different post-stimulation times (10 minutes, 20 minutes, or 1, 2, 4, or 6 hours). See Figure 5.1 for the stimulation parameters that were tested in each rat.

Tissue collection and histology

Prior to perfusion the rats were given intraperitoneal injections of Euthasol (100 mg/kg) and transcardially perfused with 4% paraformaldehyde. Brain and spinal cord tissue was dissected and allowed to post-fix for 48 hours in 4% PFA before being placed overnight in 30% sucrose phosphate buffered saline (PBS) for cryoprotection. The brain was embedded in OCT compound (Tissue-Tek) and submerged in a container of methyl butane surrounded by crushed dry ice/ethanol slurry. Frozen tissue was sectioned into 20 μm coronal sections on the cryostat and collected in wells containing PBS with 0.1% NaN_3.

Sections were stained for H&E to assess the presence of any surgical damage or infection. Sections were immunostained following antigen retrieval, which involved placing sections in 1.7 ml Eppendorf tubes with 1 mL 10 mM citrate buffer, pH 8.80 and immersing them in boiling water for 5 minutes. Tubes were then placed on ice for 5 minutes, and left at room temperature for 10 minutes before the blocking step. Two phospho-specific antibodies for ribosomal protein S6 (1:250 for both, Ser 235/236-RRID:AB_916156, Ser240/244:RRID:AB_331682) were diluted in Blocking Reagent (PerkinElmer).

Sections were incubated in primary antibody dilutions overnight at room temperature. The secondary antibody, a biotinylated IgG antibody (1:250, RRID:AB_2313606) was also diluted in Blocking Solution and applied for two hours at room temperature. Following secondary incubation, sections were washed 3 times,

incubated for 1 hour with avidin and biotinylated horseradish peroxidase (1:100, RRID:AB_2336819) and reacted with DAB (RRID:AB_2336382).

pS6 Quantification

To quantify pS6 induction following cortical stimulation, pS6 immunostained sections in the forelimb region of the motor cortex were imaged and imported into ImageJ. Using a strip of 20 μm x 20 μm boxes than spanned the 6 cortical layers, the optical density within each box was measured. The strip of boxes was measured every 100 μm across 1000 μm of the cortex (10 total strips/side). This analysis was done for once section/rat, and both cortices were quantified. The changes in optical density were plotted and used to determine optimal stimulation parameters.

Cranial implants and corticospinal tract tracing

An additional 12 female Long Evans rats were used to determine the possible relationship between HFS, S6 induction, and axonal regeneration. A random number generator was used to assign rats to experimental vs. control groups (n=6 for each) and to determine surgical order. All rats received unilateral intracortical injections of AAV-GFP immediately prior to receiving stimulating electrode implants in the forelimb region of the motor cortex. The vectors were AAV serotype 2, and were obtained from Vector Bio Labs (1×10^{13} genome copies/mL). The vector was diluted with sterile-filtered PBS and 5% glycerol for a final concentration of 1×10^{12} genome copies/mL. For intracranial injections, the rats were anesthetized with Isoflurane (2-3%) and placed in a stereotaxic apparatus. Their eyes were swabbed with Vaseline, the scalp was shaved and cleaned with Betadine, and a midline scalp incision was made. A small craniotomy was

performed to expose the surface of the brain. All rats received 5 unilateral intracortical injections of AAV-GFP into the forelimb region of the left motor cortex using a Hamilton syringe with a pulled glass micropipette (2.5 mm lateral and 0.8 mm depth at +2.0 mm, +1.0 mm, +0.0 mm anterior/posterior, and 3.2 mm lateral and 0.8 mm depth at +1.0 mm and +0.0 mm anterior/posterior relative to bregma). Each injection was 1.0 μl in volume, for a total injection volume of 5.0 μl. Injections were performed over one minute and the Hamilton was left in place for three minutes.

Following completion of the injections, the rats were given unilateral cortical stimulating electrode implants using the same procedure described above. The implant was placed above the left forelimb region of the motor cortex, and once the implant procedure was competed, the scalp was sutured with 5.0 silk and rats were given subcutaneous injections of buprenorphine, Baytril, and lactated Ringer's solution. Rat were returned to their home cages on 37°C water circulating heating pads until they recovered from the anesthetic.

Cervical contusion injury and post-operative care

3 days after the injection and implant surgeries, the rats received bilateral C5 contusion spinal cord injuries. Rats were anesthetized with isoflurane (2-3%) and an incision along the dorsal cervical region was made. A C5 laminectomy was performed, and the spinal cord exposed. The C4 and C6 vertebra were clamped for stability, and a force of approximately 200 kdynes was applied to the midline of the exposed C5 region. The muscle was then closed with 5-0 chromic gut and the skin closed with stapes. Rats were given subcutaneous injections of buprenorphine, Baytril, and lactated Ringers

solution. Rat were returned to their home cages on 37°C water circulating heating pads until they recovered from the anesthetic. Rats were given subcutaneous Lactated Ringers solution for 7 days after surgery to provide additional fluid support and treated prophylactically for urinary tract infections (UTI) for 7 days using Baytril. Pain was managed with subcutaneous buprenorphine for 7 days post-operatively and the skin staples were removed after 2 weeks. 2 rats died post-operatively, 1 control and 1 experimental.

Cortical Stimulation of C5 contusion rats

After recovery from the injury, 5 rats began receiving high-frequency stimulation of 400hz at 20msec durations delivered at 1/10second intervals, twice a day for 20 minutes/session. Animals were awake and behaving during the stimulation, and were in no acute distress or pain due to the stimulation. The stimulation was carried out 5 days/week for 6 weeks (a total of 30 days). The 5 control rats were placed in the same box used for stimulation, and were connected to the stimulation commutator but no stimulation was delivered. See Figure 5.2 for descriptions of each rat's stimulation parameters.

Grip strength meter testing

Rats were trained in the grip strength mete (GSM)r task prior to any surgical procedures. To perform the GSM task, the rats were allowed to grasp a bar on the grip strength apparatus and were pulled away until their grip was broken. The apparatus measured the animal's grip strength for each trial. This behavioral test was performed to test for a change in motor ability before the injury, after the injury, and throughout the

stimulation period. Following injury, the same individual who trained the rats also tested them. This individual was blind to whether the rats were receiving stimulation or not. Testing was performed weekly at 8:00am to control for variability in the time of day and activity of the animals.

Tissue collection and histology

8 weeks after the SCI surgery, the rats were given intraperitoneal injections of Euthasol (100 mg/kg) and transcardially perfused with 4% paraformaldehyde. Brain and spinal cord tissue was dissected and allowed to post-fix for 48 hours in 4% PFA before being placed overnight in 30% sucrose phosphate buffered saline (PBS) for cryoprotection. The tissue was processed and quantified using the same protocols described above.

RESULTS

Unilateral motor cortex stimulation in awake, behaving rats results in bilateral pS6 induction

Quantification of the optical density of pS6 in immunostained sections after 10 or 20 minutes of high frequency stimulation (HFS) revealed enhanced pS6 induction 1-2 hours following stimulation (Figure 5.3). Quantification of cases with post-stimulation times shorter than 1 hour or longer than 2 hours revealed negligible differences in pS6 optical density compared to unstimulated implanted controls, indicating that onset of detectable pS6 increases may take longer than 20 minutes and decay after 2 hours (Figure 5.4 and 5.5). Increased S6 phosphorylation was observed bilaterally, despite

unilateral stimulation of the motor cortex, and was seen in both Ser 235/235 and Ser 240/244 immunostains. In most sections, pS6 enhancement was seen predominantly in layer V neurons, which are the cortical motoneurons that give rise to the corticospinal tract (Lassek et al., 1957).

HFS following C5 contusion also triggers S6 phosphorylation

12 adult female Long Evans rats were given intracortical injections of AAV-GFP and cortical stimulating electrode implants roughly one week prior to SCI. Following recovery from a C5 contusion injury, awake behaving rats underwent cortical stimulation for 20 minutes, twice a day, five days a week for 6 weeks. Once a week rats were tested on the GSM (Figure 5.6). Two control rats (received cortical implants but not stimulated) were stimulated the day of perfusion in order to examine the effect of HFS on S6 phosphorylation dynamics without affecting axonal regeneration. Following perfusion brain sections were immunostained for pS6 using phospho-specific antibodies for phosphorylation at Serine 235/236 and Serine 240/244. Quantification of the optical density of pS6 from unstimulated control rats revealed increased pS6 induction likely due to a gliosis reaction due to either the AAV-GFP injections, the implant procedure, or both (Fig 5.7). This increase in pS6 optical density was most apparent in the Ser 235/236 immunostain, and not detectable in the Ser 240/244 immunostain. Regulation of phosphorylation at Ser 235/235 is regulated by several convergent pathways, including mTOR, MAPK/ERK, and cAMP/PKA, while phosphorylation at Ser 240/244 is regulated exclusively by mTOR. This finding indicates that mTOR may play a limited role in the cortical response to injury, which is further supported by evidence that mTOR expression is lowered following axonal injury (Park et al., 2008)

In rats that received all 60 bouts of HFS we observed marked pS6 induction at 30 but not 60 minutes following the last stimulation (Figs 5.8 and 5.9), possibly reflecting a rapid return to baseline pS6. Even in cases perfused one hour after 60 bouts of stimulation had appreciable increases in pS6 optical density compared to the unstimulated controls, indicating that the pS6 "baseline" may become elevated following repeated HFS. Interestingly, the increase in pS6 optical density was more apparent at Ser 235/236 than at Ser 240/244, implicating multiple signaling pathways underlying the effects of HFS or possibly a similar response to surgical damage that was seen in unstimulated controls.

Two control rats were given HFS on the day of perfusion to examine short-term S6 phosphorylation dynamics in an injury setting. One rat received a single bout of 20 minute HFS and was perfused two hours after (Fig 5.10), and the second rat was given two bouts of 20 minute HFS and perfused one hour after the last stimulation (Fig 5.11). Two hours after 20 minutes of HFS, we found increased pS6 induction though not to the degree that is seen 30 minutes after 60 bouts of HFS. The level of pS6 induction at both serine residues appeared comparable. In the rat that was give two bouts of HFS and perfused one hour later, we observed a larger magnitude of pS6 induction in the Ser 235/236 immunostain but not Ser 240/244. Assessment of the cortical area revealed significant surgical damage which precluded the reliable interpretation of these results.

Grip strength meter and axonal regeneration

To examine functional performance following C5 contusion, all rats were trained in the GSM and tested weekly following injury. Briefly, rats were trained to grab a metal handle connected to a force transducer and were pulled backwards by the experimenter until their grip on the handle was lost. The force exerted by the animal at the time it loses its grip was recorded. Because HFS was administered unilaterally to the left motor cortex, we hypothesized that functional gains would be observed in the contralateral right forelimb. Analyzing the data from training and testing we found no significant effect of stimulation on GSM performance for either forelimb, though performance of the stimulated, right forelimb was approaching significance (Fig 5.12, two-way ANOVA for right forelimb: for stimulation $p= 0.0549$, day relative to injury $p< 0.0001$, interaction $p= 0.8549$, two-way ANOVA for left forelimb: for stimulation $p= 0.7675$, day relative to injury $p< 0.0001$, interaction $p= 0.7221$).

Labeling of CST axons by GFP was not detectable even with amplification via immunostaining. It is possible that the time between injection and perfusion resulted in loss of GFP expression, though we have observed low levels of maintained GFP expression one year after injection in mice (Gutilla et al., 2016). Complications with performing intracortical injections after the implant procedure precluded us from using a more conventional tracer, such as biotinylated dextran amine (BDA), which is injected a few days prior to perfusion. The lack of CST tracing prevented us from being able to determine what, if any, effect HFS stimulation had on axonal regeneration or sprouting following a contusion SCI.

DISCUSSION

Mounting evidence supports the use of stimulation to promote neuronal regeneration. While the utility of various stimulation paradigms has been demonstrated, few have examined the potential efficacy of high frequency stimulation following spinal cord injury. Regardless of the type of stimulation that is used, the mechanism underlying the regenerative effect of stimulation has the not been elucidated. Here we show that induction of S6 activation via a regulatory phosphorylation event, a biomarker for the mTOR pathway, may provide a useful assay for stimulation-driven mTOR activity. The usefulness of this assay lays in the well-established role of mTOR in promoting neuronal growth and repair, and identifying the stimulation parameters that optimally drive mTOR would have great translational potential.

Here we have shown that 10 or 20 minutes of unilateral HFS in the forelimb region of the motor cortex in uninjured rats results in enhanced S6 phosphorylation, and that phosphorylation occurs at both the Ser 235/236 and Ser 240/244 residues. The phosphorylation at both serine residues supports the interpretation that multiple signaling pathways are responsive to HFS, including mTOR, MAPK/ERK, and cAMP/PKA. Increased pS6 induction at Ser 240/244, the only residue believed to be exclusively regulated by mTOR, supports our hypothesis that the regenerative effect of neuronal stimulation may at least in part be due to increased mTOR activation.

Examination of pS6 levels at different times post-stimulation allowed us to determine the onset and longevity of HFS-induced pS6 induction. At 20 minutes post-

stimulation we did not observe an appreciable increase in pS6 optical density for either Ser 235/236 or Ser 240/244. The highest levels of pS6 induction were observed at 1 and 2 hours post-stimulation, by 4 hours pS6 optical density for both serine residues began to diminish and was almost returned to baseline (unstimulated) values by 6 hours post-stimulation.

Following a C5 contusion SCI, we observed similar trends in S6 phosphorylation following chronic unilateral stimulation over 6 weeks. The interpretation of pS6 induction was somewhat complicated by the presence of surgical damage from AAV injections or the stimulation implant in a handful of control cases. Rats that had undergone 60 bouts of HFS had the most elevated pS6 optical density, for both residues, at 30 minutes following the last stimulation. One hour after the last stimulation, rats that had received 60 rounds of HFS also had noticeable increases in pS6 optical density, though these values tended to be slightly lower than what was seen in at 30 minutes post-stimulation, indicating that by 1 hour pS6 levels are beginning to return to baseline. Regardless of the number of HFS rounds or time post-stimulation, all cases had higher optical density levels for pS6 Ser 235/236 than pS6 Ser 240/244. This is likely due to the convergence of multiple signaling pathways responsible for regulating phosphorylation of S6 at Ser 235/236 and the presence of mild cortical damage that could reasonably be activating some of these pathways.

The relatively mild contusion injury that we used and the grip strength meter's low sensitivity to mild functional impairment prevented us from being able to detect any meaningful functional changes following HFS administration. It's likely that the mild

contusion resulted in significant numbers of spared fibers, thereby preventing appreciable losses in gross forelimb function. To determine the relationship between HFS and functional recovery after SCI, we will either need to increase the severity of our injury model or assess forelimb function with more sensitive tasks, such as pellet reaching or pasta eating/handling (Allred et al., 2008; Hurd et al., 2013).

Going forward it will be important to clearly demonstrate mTOR's role in mediating the effects of HFS. We could do this by ablating mTOR activity through rapamycin administration, a known mTOR inhibitor, or by quantifying mTOR protein levels in the stimulated region of the motor cortex. Following hypoxic neuronal and acute axonal injury, mTOR activity is suppressed and protein translation is dysregulated (Brugarolas et al., 2004; Reiling and Hafen, 2004; Corradetti et al., 2005; Park et al., 2008). By upregulating mTOR and concomitant protein synthesis, HFS may hold great therapeutic promise for ameliorating the functional deficits associated with neuronal injury and disease.

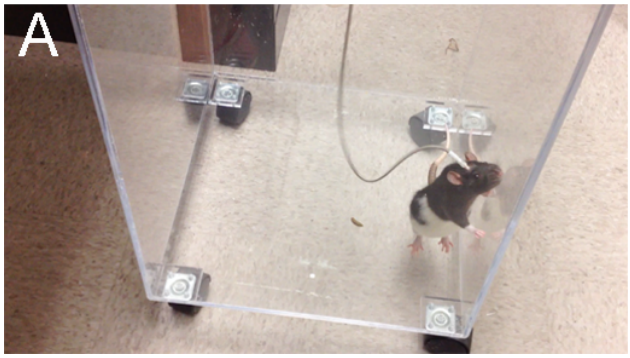

B

	Stimulation duration	Post-stimulation Time	Number of rats
1	10 minutes	20 minutes	2
2	10 minutes	1 hour	1
3	10 minutes	2 hours	2
4	10 minutes	6 hours	1
5	20 minutes	20 minutes	1
6	20 minutes	1 hour	2
7	20 minutes	2 hours	1
8	20 minutes	4 hours	1
9	20 minutes	6 hours	1

Figure 5.1- Long-term cortical stimulation implants and HFS parameters. A. Unilateral stimulating electrodes were implant above the left motor cortex and were well-tolerated in the rats. Stimulation was done in awake, behaving rats. **B.** Stimulation duration and post-stimulation time of perfusion for 12 rats used to determine the dynamics of S6 phosphorylation following HFS.

Animal #	# of Stimulation Bouts	Time between last stimulation and perfusion
1	Control	NA
2	Control	NA
3	1 (Control)†	2 hours
4*	18	25 minutes
5	60	1 hour
6	60	1 hour
7*	24	20 hours
9	60	30 minutes
10	2 (Control)†	1 hour*
12*	17	45 minutes

#s 8 & 11 died post-operatively

*: Cortical implant fell out prematurely, perfused ASAP
†: Two control mice were stimulated on the day of perfusion to examine short-term S6 phosphorylation dynamics within the experiment without affecting regeneration

Figure 5.2- Breakdown of rats in C5 contusion study. 12 female Long Evans rats were randomly assigned to control (no stimulation) and experimental (with HFS) groups. 2 rats died post-operatively after the contusion procedure. During the experiment 2 rats has their cortical implants fall off prematurely, requiring immediate perfusion. On the final day of the experiment, two control rats were given one or two bouts of HFS in order to examine S6 phosphorylation dynamics following SCI. We decided to do this on the final day of the experiment to avoid any interaction between HFS and regeneration.

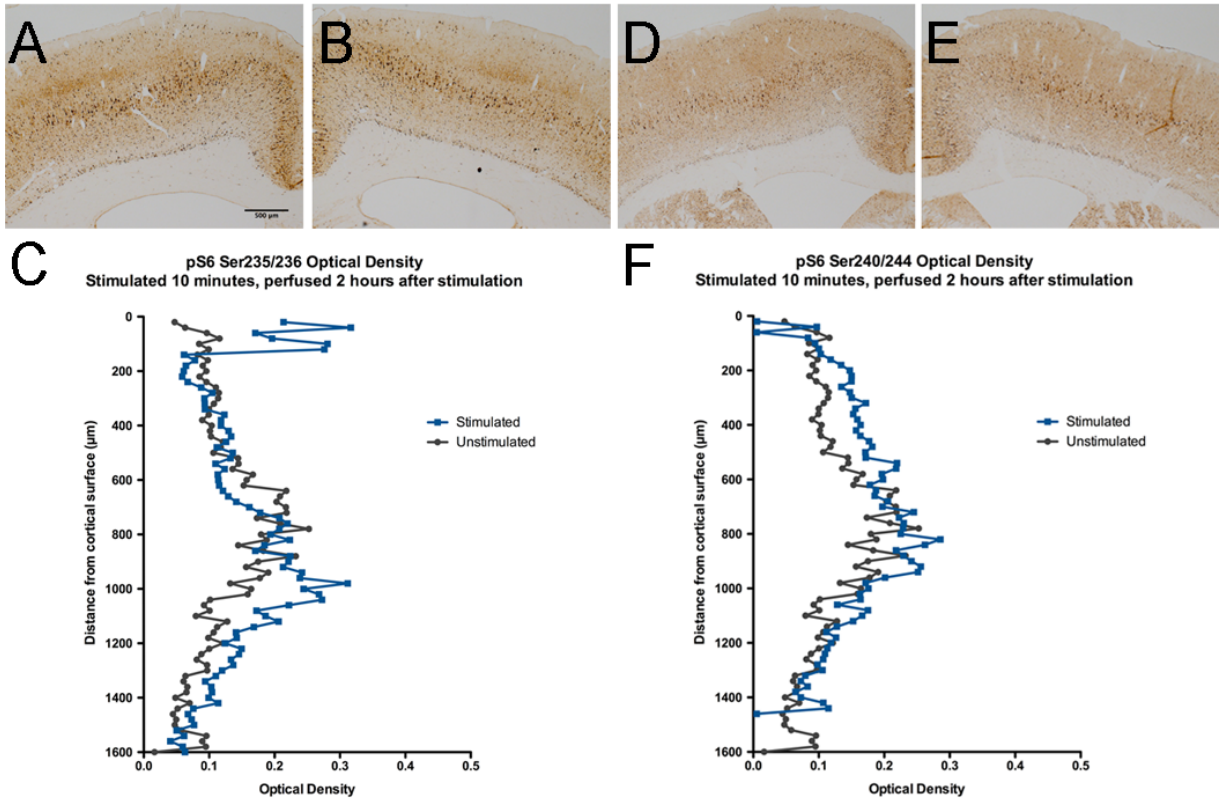

Figure 5.3- 10 minutes of HFS results in increased S6 phosphorylation at Ser 235/236 and Ser 240/244 2 hours following stimulation. A. The motor cortex ipsilateral to HFS, immunostained for pS6 235/236. The largest increases in pS6 induction were seen ipsilateral to stimulation, and pS6 optical density appeared highest in layer V neurons. **B.** The contralateral motor cortex from the same section in **A.**, also immunostained for pS6 Ser 235/236. Despite receiving unilateral HFS, both motor cortices had increased levels of pS6 induction compared to unstimulated controls and areas outside of the motor cortex (where HFS occurred). **C.** Quantification of pS6 optical density in **A.** and **B.** reveals increased levels of pS6 235/236 in both motor cortices, especially in layer V (corresponds to ~1000 µm away from cortical surface). **D.** A nearby section to **A.** and **B.**, immunostained for pS6 240/244 ipsilateral to HFS shows increased pS6 immunolabeling in the area of stimulation. **E.** The contralateral motor cortex from the same section in **D.** also shows elevated pS6 240/244 immunolabeling. **F.** Quantification of pS6 240/244 optical density in **D.** and **E.** shows a similar pattern of pS6 induction to pS6 Ser 235/235 in **C.**, with marked bilateral pS6 240/244 induction especially in layer V.

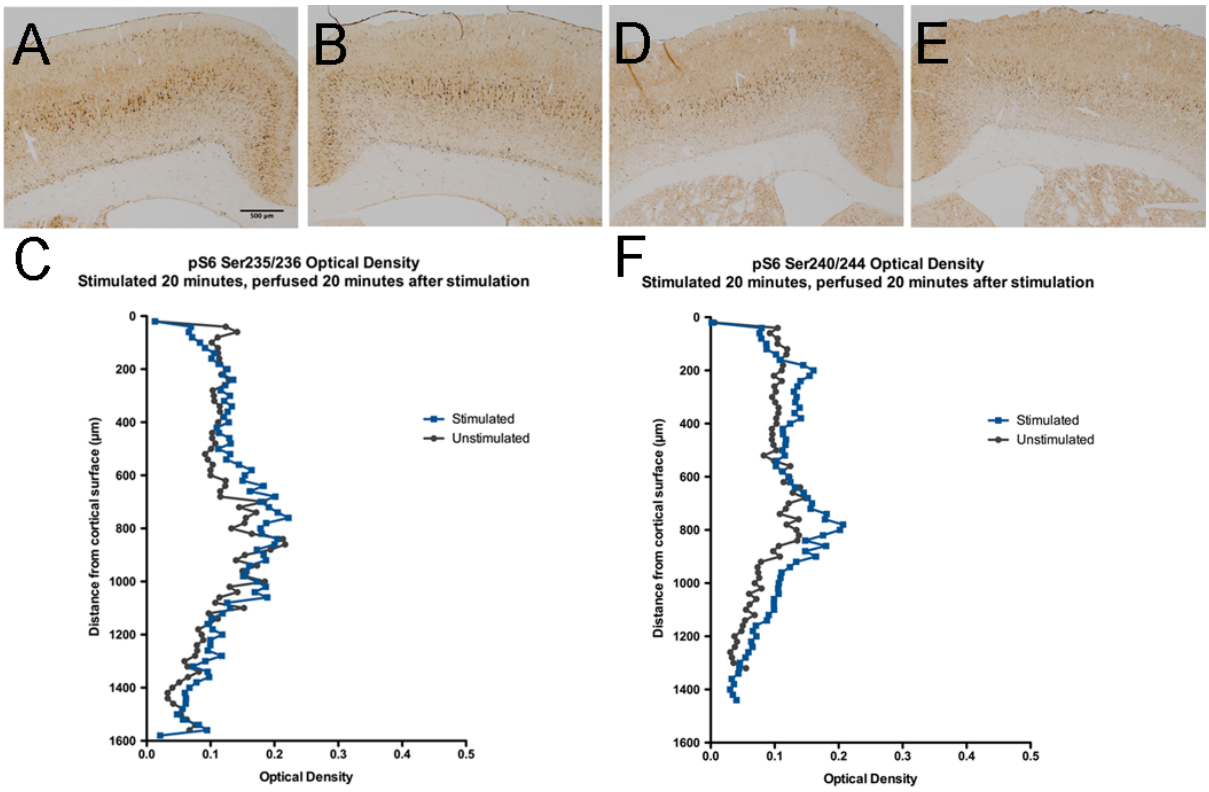

Figure 5.4- 20 minutes of HFS results in less pS6 induction 20 minutes after stimulation. A. The motor cortex ipsilateral to HFS, immunostained for pS6 235/236. The magnitude of pS6 immunolabeling increases were not as noticeable as at 1-2 hours following 10 or 20 minutes of HFS, indicating that more than 20 minutes post-stimulation is required to see maximal pS6 induction. Despite the relatively low level of pS6 235/236 induction, layer V cells are appreciably labeled. **B.** The contralateral motor cortex from the same section in **A.**, also immunostained for pS6 Ser 235/236. pS6 235/236 immunolabeling was similar to **A.** in the motor cortex 20 minutes after HFS 20. **C.** Quantification of pS6 optical density in **A.** and **B.** reveals only minor increases in pS6 235/236 optical density in both motor cortices, though layer V neurons again appear to have higher pS6 induction. **D.** A nearby section to **A.** and **B.**, immunostained for pS6 240/244 ipsilateral to HFS shows a low level of pS6 induction in the region of stimulation. **E.** The contralateral motor cortex from the same section in **D.** shows even less pS6 240/244 immunolabeling than **D**. **F.** Quantification of pS6 240/244 optical density in **D.** and **E.** shows very little pS6 240/244 induction at 20 minutes post-stimulation.

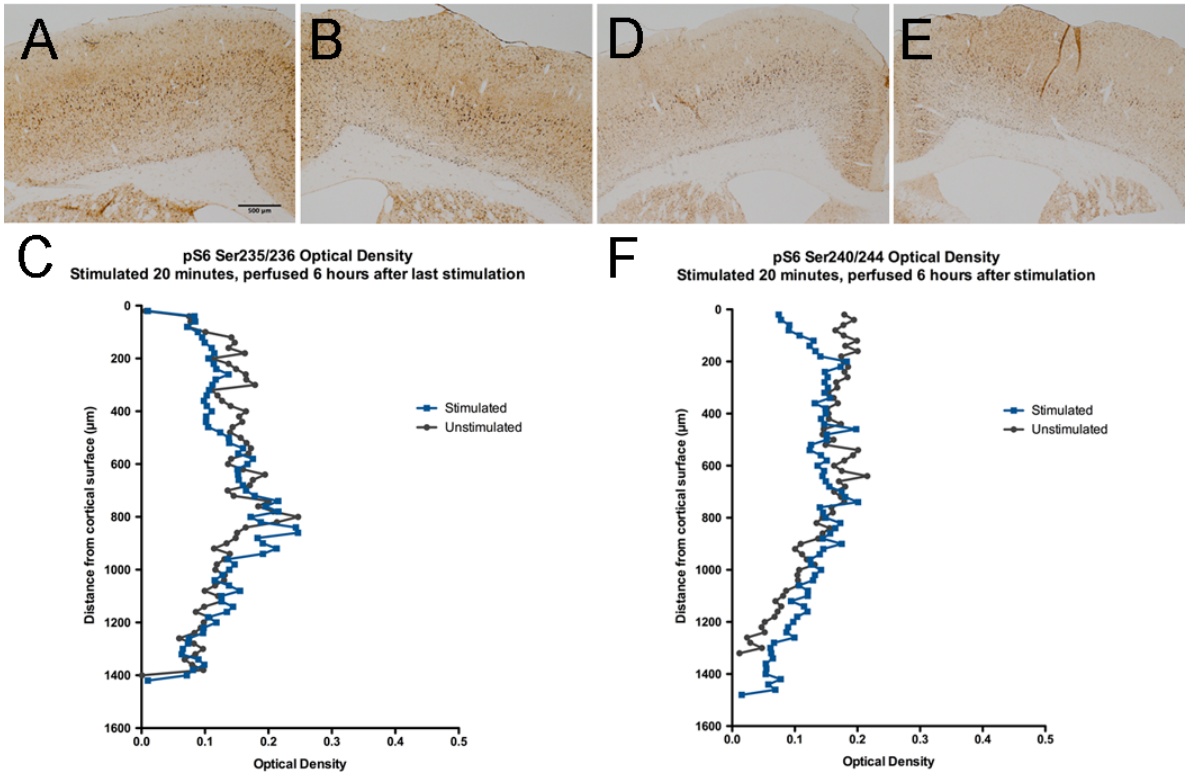

Figure 5.5- pS6 induction is diminished 6 hours after 20 minutes of HFS. A. The motor cortex ipsilateral to HFS, immunostained for pS6 235/236. Increases in pS6 immunolabeling increases were comparable to what we saw 20 minutes after HFS, but not as elevated as what we found 1-2 hours after HFS. It's likely that S6 phosphorylation levels begin to return to baseline beyond 2 hours after stimulation. **B.** The contralateral motor cortex from the same section in **A.**, also immunostained for pS6 Ser 235/236. pS6 235/236 immunolabeling was similarly decreased in the motor cortex contralateral to HFS 20 minutes after stimulation. **C.** Quantification of pS6 optical density in **A.** and **B.** reveals only minor increases in pS6 235/236 optical density in both motor cortices, and the layer V increase is less prominent. **D.** A nearby section to **A.** and **B.**, immunostained for pS6 240/244 ipsilateral to HFS shows a low level of pS6 immunolabeling in the region of stimulation. **E.** The contralateral motor cortex from the same section in **D.** shows even less pS6 240/244 immunolabeling than **D.**, with the exception of the cortical defect caused by the stabilization screw used to anchor the electrode implant. **F.** Quantification of pS6 240/244 optical density in **D.** and **E.** shows very little pS6 240/244 induction at 20 minutes post-stimulation, and no layer V-specific increase.

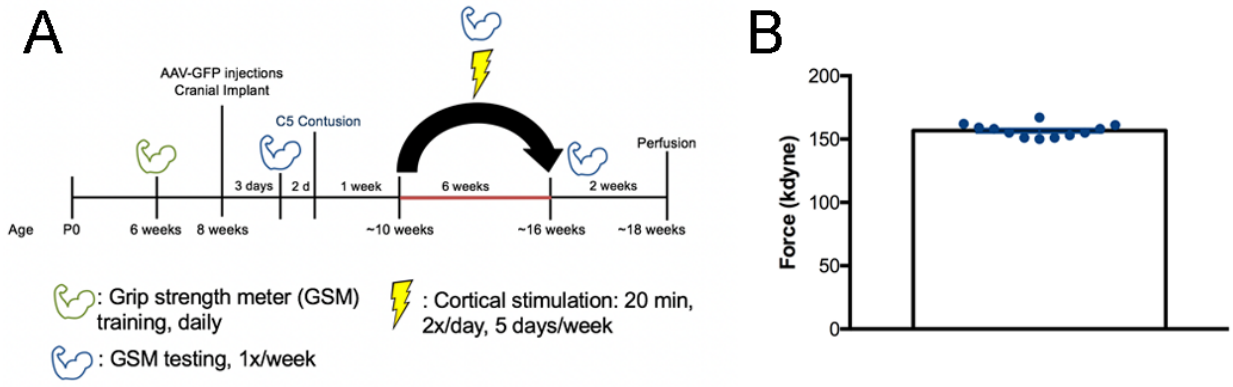

Figure 5.6- Timeline of C5 contusion with HFS experiment and contusion forces. A. The C5 contusion experiment was conducted over roughly 18 weeks, with 6 weeks of stimulation and 8 weeks of grip strength meter (GSM) testing. Rats were trained in the GSM task prior to any surgical procedures. **B.** The average force of C5 contusion with the Infinite Horizons device was 156 kdynes.

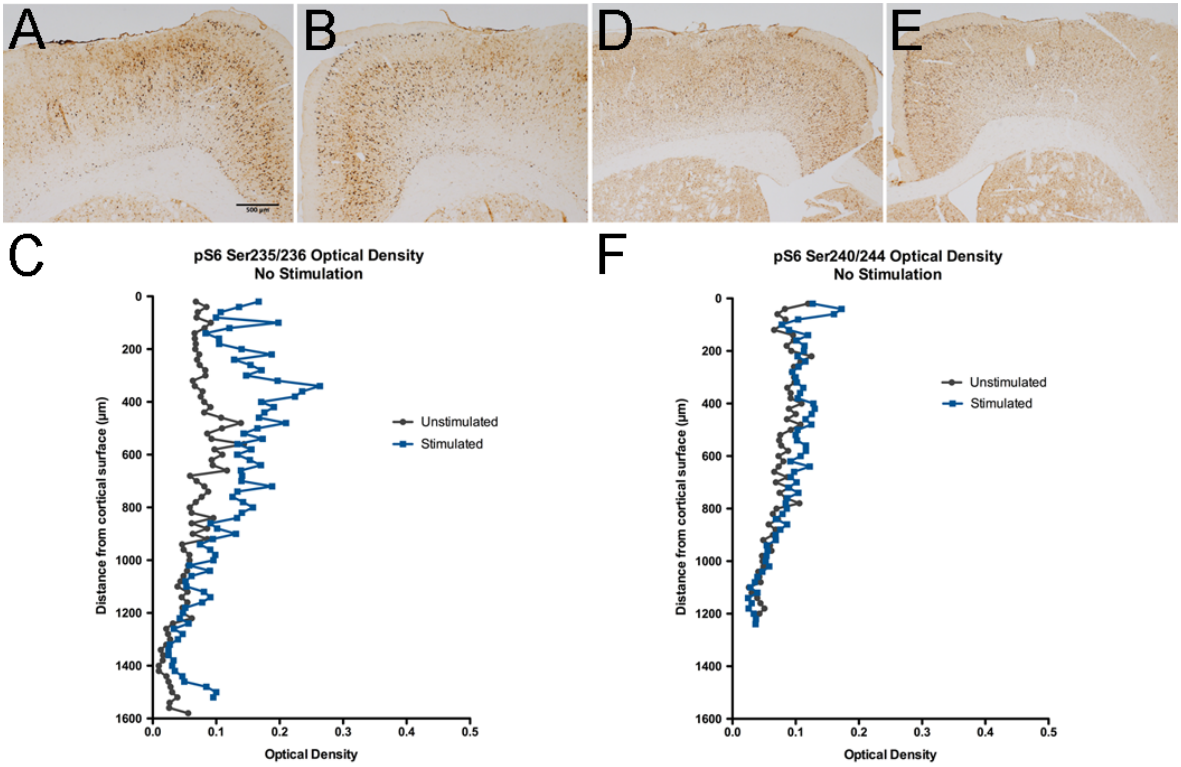

Figure 5.7- pS6 immunostaining of control rat with C5 contusion and no HFS. A. The motor cortex implanted with cortical stimulating electrodes, immunostained for pS6 235/236. Control rats were implanted with electrodes and connected to the stimulation commutator, but not HFS was delivered. pS6 immunolabeling appeared typical of unstimulated controls, with the exception of the cortical region that appears to have been injured during either the AAV-GFP injections or the electrode implant procedure. **B.** The contralateral motor cortex from the same section in **A.**, also immunostained for pS6 Ser 235/236. pS6 235/236 immunolabeling was not elevated in the contralateral cortex of unstimulated rats, unless there was cortical damage due to anchoring screws. **C.** Quantification of pS6 optical density in **A.** and **B.** reveals only pS6 235/236 optical density characteristic of unstimulated rats. **D.** A nearby section to **A.** and **B.**, immunostained for pS6 240/244 ipsilateral to HFS shows even less pS6 240/244 immunolabeling than pS6 235/236. **E.** The contralateral motor cortex from the same section in **D.** shows comparable pS6 240/244 immunolabeling to **D**. **F.** Quantification of pS6 240/244 optical density in **D.** and **E.** shows normal pS6 240/244 immunolabeling in unstimulated rats.

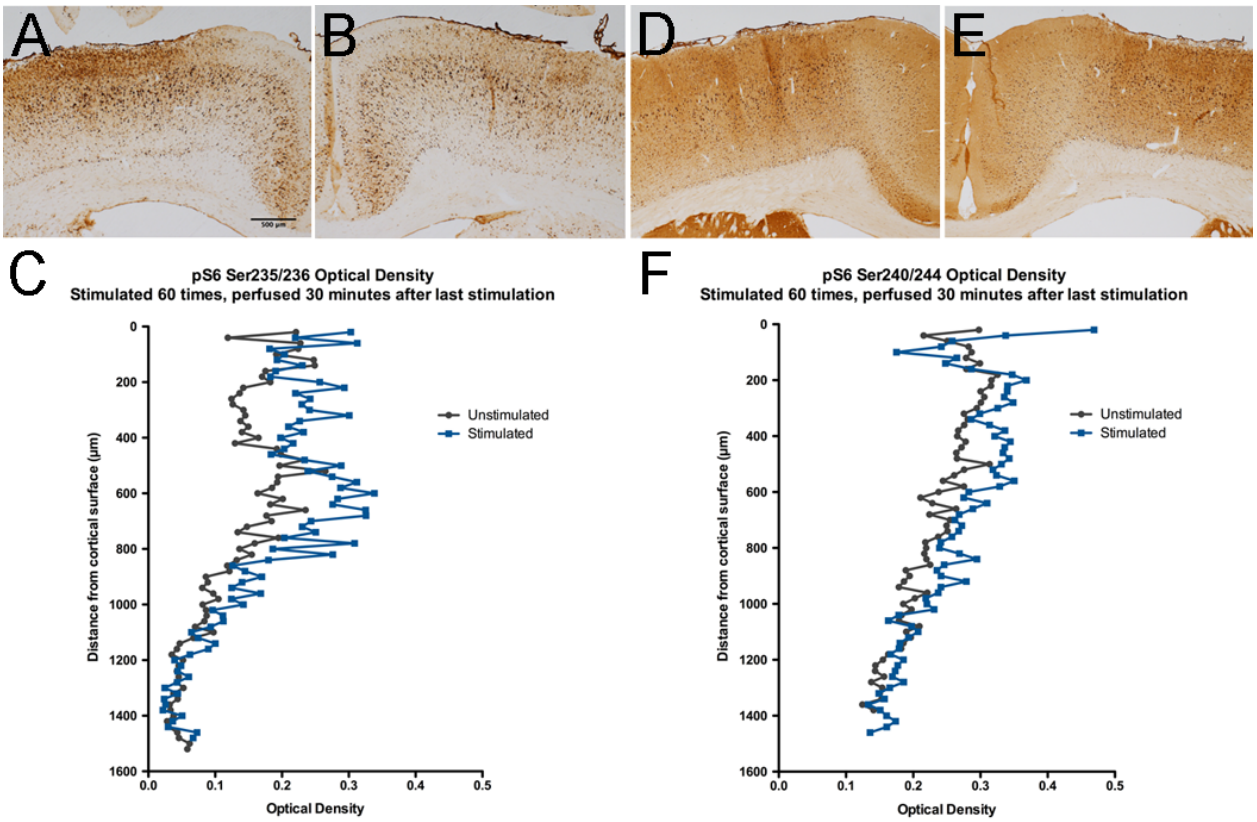

Figure 5.8- Marked pS6 induction following chronic HFS. A. The motor cortex ipsilateral to HFS, immunostained for pS6 235/236. Increases in pS6 immunolabeling were striking 30 minutes after the final bout of HFS, especially in cortical layers I-V. **B.** The contralateral motor cortex from the same section in **A.**, also immunostained for pS6 Ser 235/236. pS6 235/236 immunolabeling was similarly increased in the upper cortical layers of the motor cortex contralateral to HFS 30 minutes after the last stimulation. **C.** Quantification of pS6 optical density in **A.** and **B.** reflects these trends in pS6 235/236 optical density in both motor cortices. **D.** A nearby section to **A.** and **B.**, immunostained for pS6 240/244 ipsilateral to HFS shows elevated pS6 immunolabeling in the region of stimulation. **E.** The contralateral motor cortex from the same section in **D.** also shows elevated pS6 240/244 immunolabeling. **F.** Quantification of pS6 240/244 optical density in **D.** and **E.** shows bilateral pS6 240/244 induction 30 minutes post-stimulation, with no discernible layer-specific increases.

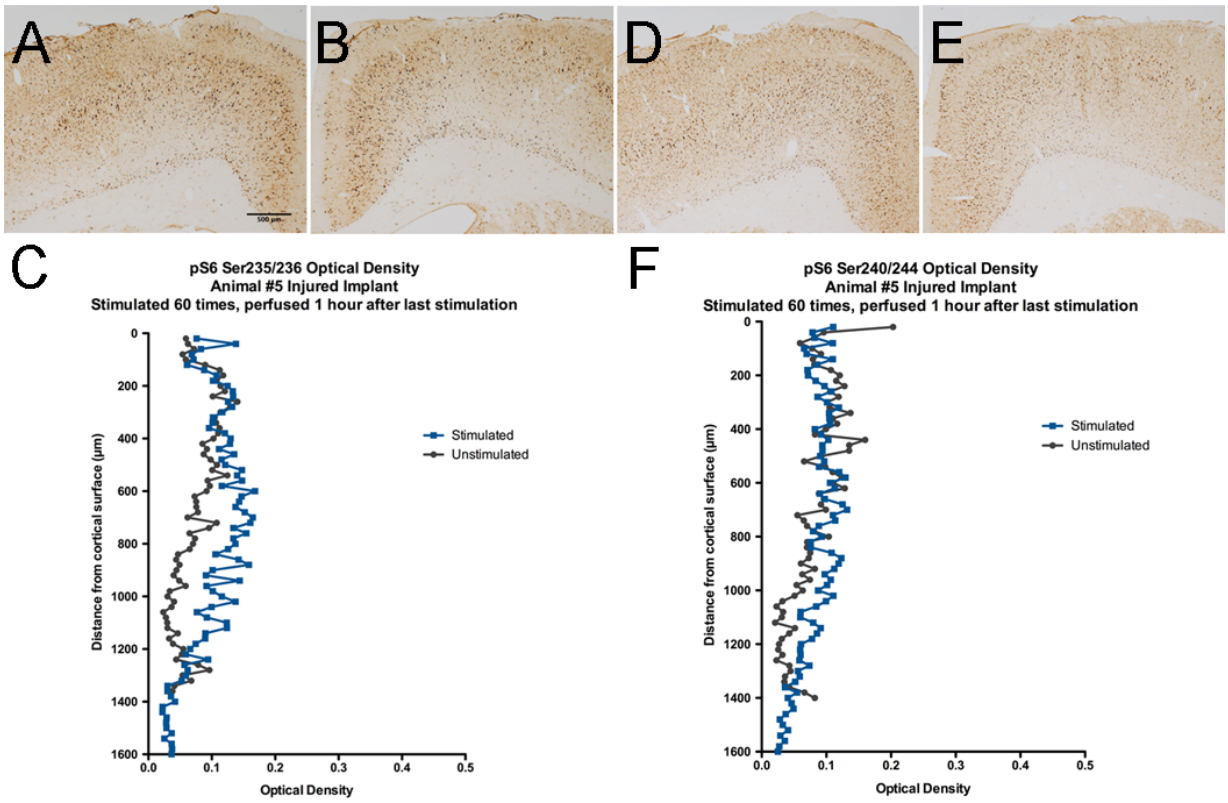

Figure 5.9- pS6 induction following chronic HFS begins to diminish 1 hour after stimulation. **A.** The motor cortex ipsilateral to HFS, immunostained for pS6 235/236. Increases in pS6 immunolabeling were diminished 1 hour after the final bout of HFS, and layer-specific increases were absent (compared to 30 minutes after the last bout of HFS). **B.** The contralateral motor cortex from the same section in **A.**, also immunostained for pS6 Ser 235/236. pS6 235/236 immunolabeling was similarly decreased in all cortical layers of the motor cortex contralateral to HFS 1 hour after the last round of stimulation. **C.** Quantification of pS6 optical density in **A.** and **B.** reflects these trends in pS6 235/236 optical density in both motor cortices. **D.** A nearby section to **A.** and **B.**, immunostained for pS6 240/244 ipsilateral to HFS shows near-control levels of pS6 immunolabeling in the region of stimulation. **E.** The contralateral motor cortex from the same section in **D.** has even less pS6 240/244 immunolabeling than the ipsilateral motor cortex in **E**. **F.** Quantification of pS6 240/244 optical density in **D.** and **E.** shows bilateral pS6 240/244 induction at near-control levels, indicating that S6 phosphorylation more quickly returns to baseline following chronic stimulation than after a single round of HFS.

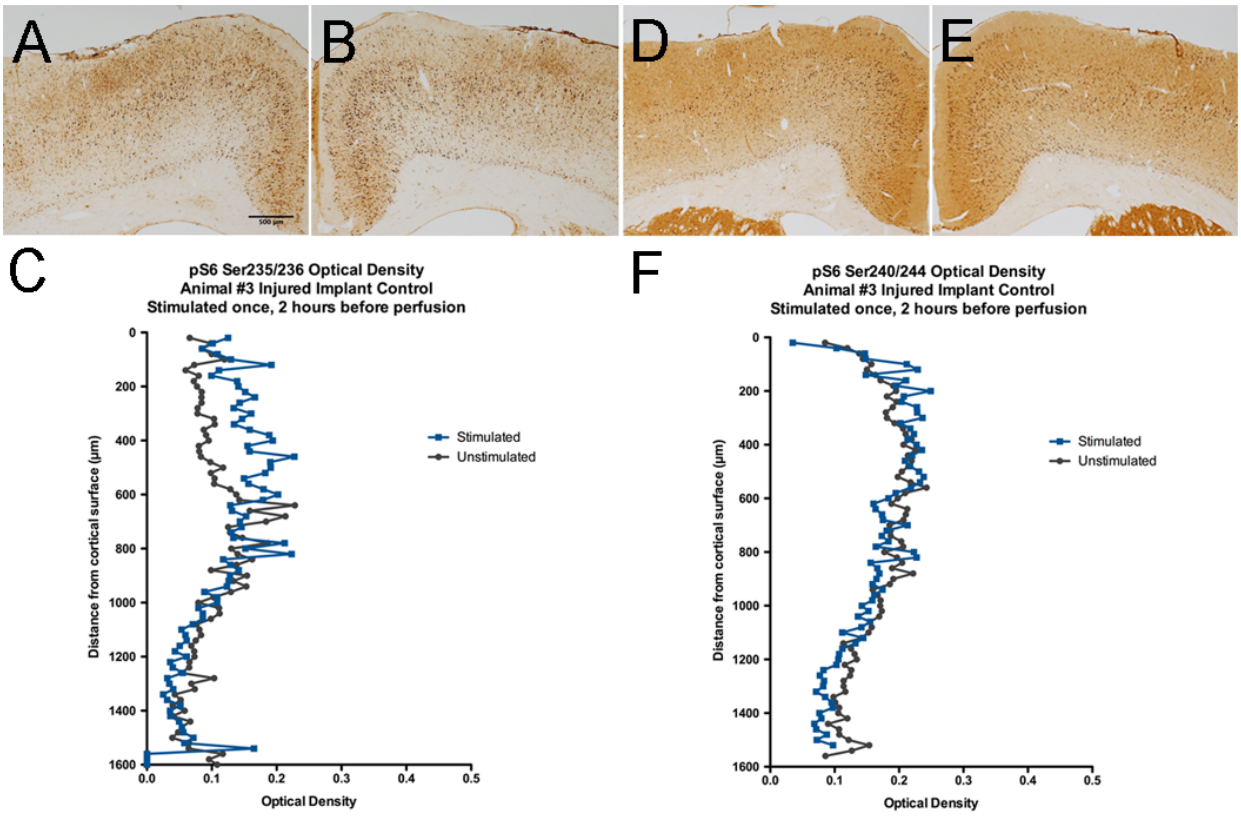

Figure 5.10- Control rat given a single round of HFS for 20 minutes has marked pS6 induction 2 hours after stimulation. A. The motor cortex ipsilateral to HFS, immunostained for pS6 235/236. Increases in pS6 immunolabeling were elevated 2 hours after a single bout of HFS, though the increase was not as large as what is seen 30 minutes after chronic HFS. pS6 labeling appeared highest in cortical layers 1-V. **B.** The contralateral motor cortex from the same section in **A.**, also immunostained for pS6 Ser 235/236. pS6 235/236 immunolabeling was similarly increased in the motor cortex contralateral to HFS 2 hours after 20 minutes of HFS. **C.** Quantification of pS6 optical density in **A.** and **B.** reveals pS6 235/236 induction primarily in the motor cortex ipsilateral to HFS, and predominantly in layers I-V. **D.** A nearby section to **A.** and **B.**, immunostained for pS6 240/244 ipsilateral to HFS shows elevated pS6 immunolabeling in all cortical layers in the region of stimulation. **E.** The contralateral motor cortex from the same section in **D.** has similar pS6 240/244 immunolabeling to the ipsilateral (stimulated) motor cortex in **E**. **F.** Quantification of pS6 240/244 optical density in **D.** and **E.** shows elevated bilateral pS6 240/244, with no layer-specific differences.

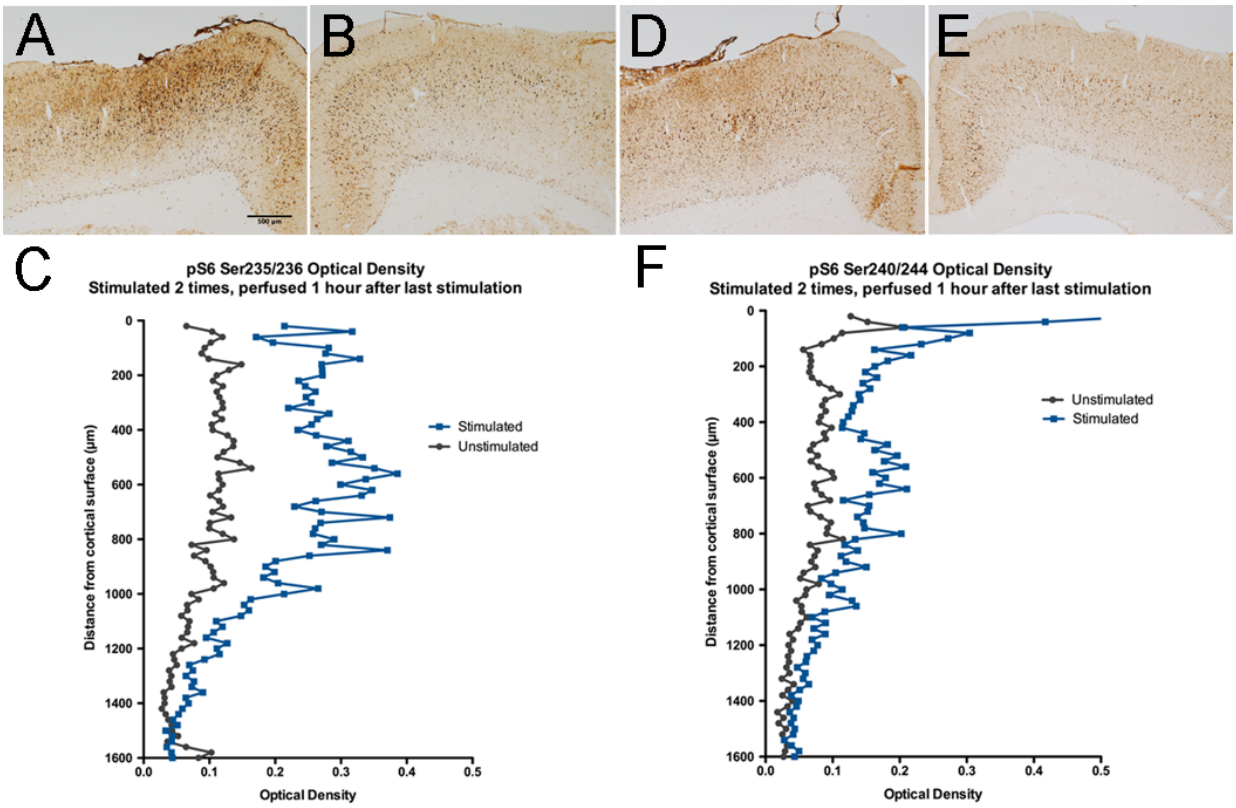

Figure 5.11- Bilateral induction of pS6 requires more than 1 hour in rats with C5 contusions. **A.** The motor cortex ipsilateral to HFS, immunostained for pS6 235/236. Increases in pS6 immunolabeling were elevated 1 hour after HFS. **B.** The contralateral motor cortex from the same section in **A.**, also immunostained for pS6 Ser 235/236. pS6 235/236 immunolabeling was not elevated in the cortex contralateral to HFS after 1 hour. **C.** Quantification of pS6 optical density in **A.** and **B.** reveals pS6 235/236 induction primarily in the motor cortex ipsilateral to HFS, with the contralateral cortex expressing near-control levels of pS6 235/236. **D.** A nearby section to **A.** and **B.**, immunostained for pS6 240/244 ipsilateral to HFS shows elevated pS6 immunolabeling in all cortical layers in the region of stimulation. **E.** The contralateral motor cortex from the same section in **D.** has near-control levels of pS6 240/244 immunolabeling. **F.** Quantification of pS6 240/244 optical density in **D.** and **E.** shows elevated pS6 240/244 ipsilateral to HFS, but not in the contralateral cortex.

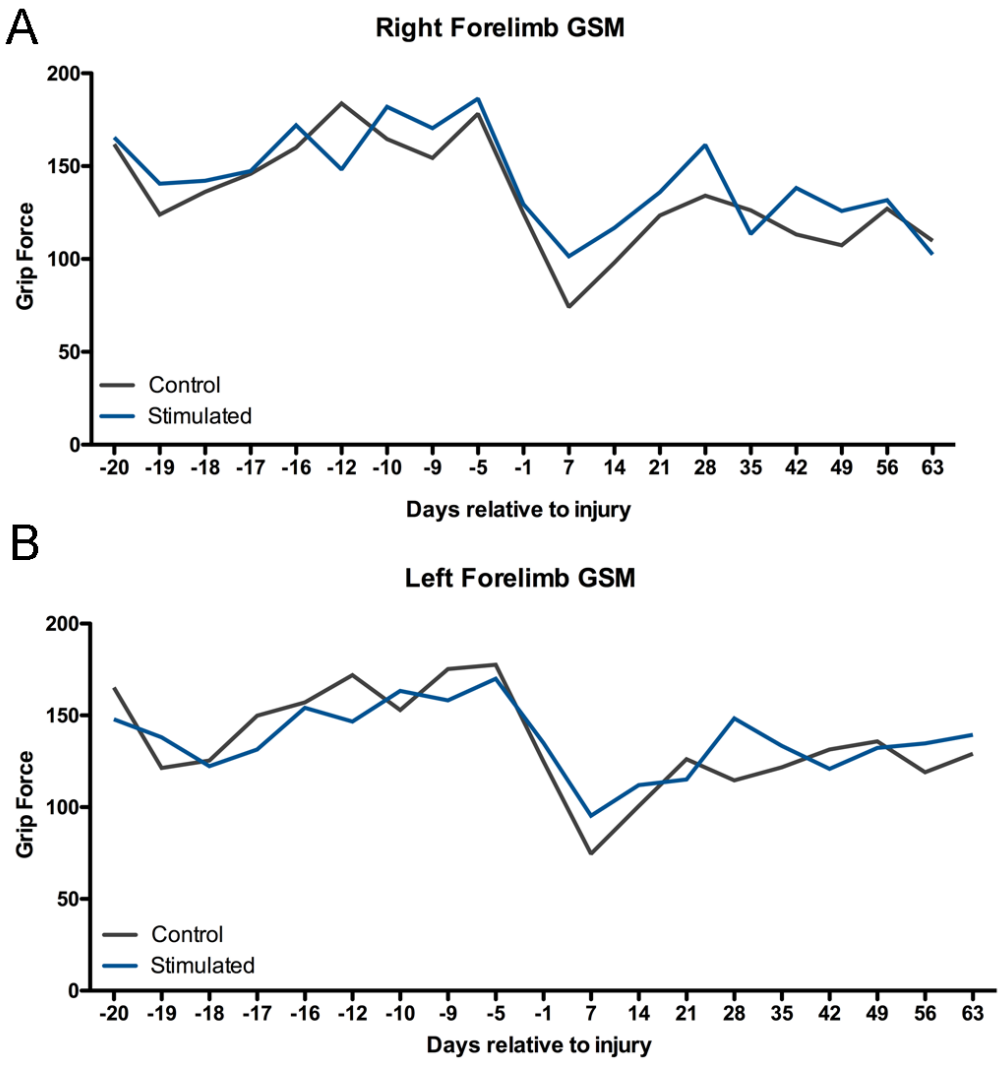

Figure 5.12- Grip strength meter assessment of forelimb function after mild C5 contusion did not reveal significant improvement with chronic unilateral HFS. A. Unilateral HFS of the left motor cortex did not result in improved forelimb function after C5 contusion as measured by GSM (two-way ANOVA, for stimulation p= 0.0549, day relative to injury p< 0.0001, interaction p= 0.8549). **B.** Left forelimb function in the GSM was also not significantly improved following chronic HFS (two-way ANOVA for left forelimb, for stimulation p= 0.7675, day relative to injury p< 0.0001, interaction p= 0.7221).

Chapter 6: Summary & conclusions

It has long been thought that fully mature adult neurons are, at best, capable of only modest levels of growth or regeneration (Bernstein, 1964; Argiro et al., 1984; Dusart et al., 1997; Verdu et al., 2000). Here we show compelling evidence in support of a robust growth program in young and older adult neurons, arguing against the notion that the efficacy of growth-promoting pathways such as mTOR is restricted to development. Following deletion of *PTEN* in young adult neurons, we observed somatic and axonal enlargement, as well as increased dendritic density. We found that older adult neurons undergo similar somatic enlargement, and though we did not examine axonal size or the dendritic arbor in these neurons we would expect to see similar patterns of growth as after *PTEN* deletion in young adult neurons.

This expectation gets to the heart of our findings- that regardless of the timing of *PTEN* deletion, neurons will ultimately express a similar morphological outcome. Previous work already supports the notion that the time of onset for *PTEN* deletion-induced morphological changes varies depending on when the deletion occurs. With increasing age at time of deletion, it takes increasingly long for the onset of significant somatic hypertrophy, dendritic spine increases, and electrophysiological changes (Luikart et al., 2011). Here we have added to our understanding of the manifestation of *PTEN* deletion-induced structural changes in adult neurons by showing that this principle of age-dependent onset applies even to older adult neurons, to dendrites themselves, and that advancing neuronal age seems to interact with *PTEN* deletion to promote further somatic size increases.

One year after we deleted *PTEN* in the motor cortex of adult mice, axons in the medullary pyramid had increased cross-sectional area and increased G-ratio. The G-ratio is the proportion of the axoplasm diameter divided by the axoplasm plus myelin diameter. A G-ratio value of 1.0 corresponds to an unmyelinated axon, and a value less than 1.0 is indicative of a myelinated axon (the smaller the G-ratio, the more myelinated the axon). The significant increase in axon cross-sectional area paired with the increased G-ratio in *PTEN* deleted axons suggest that neuronal *PTEN* deletion has a growth-promoting effect on the axon but not on the oligodendrocyte-derived myelination. This is in contrast to the findings by Goebbels et al., who showed that following neuronal loss of *PTEN* in cerebellar granule cells, normally unmyelinated parallel fibers demonstrated significant gains in myelination and therefore decreased G-ratio (Goebbels et al., 2017). This discrepancy may be explained by a lesser-emphasized finding of white matter tract atrophy also by Goebbels et al., possibly signifying a differential effect of neuronal *PTEN* deletion on myelination depending on whether the axon in question is normally myelinated or not. Another possibility is that using expression of the $GABA_{\alpha}$ subunit promoter to regulate Cre expression in $Pten^{LoxP/LoxP}$ mice may have resulted in unintentional *PTEN* deletion in oligodendrocytes at some point during fetal or neonatal development, leading to changes in myelination that we did not observe following AAV-Cre injection.

In addition to the significant level of adult neuronal growth that we observed, we found that in the early stages of structural change, when differences between *PTEN* deletion neurons from control neurons were modest, that *PTEN* deletion did not alter

behavioral function. Importantly, this result was only uncovered after performing bilateral *PTEN* deletion in both motor cortices. Unilateral *PTEN* deletion appeared to cause behavioral impairment on the rotarod (measured by decreased latency to fall/maximum speed attained) and in lowered baseline motor coordination. Prior to performing the long-term bilateral deletion behavioral study, we could not be certain whether *PTEN* deletion itself or the unilateral nature of the deletion was causing the functional impairment. Since the two motor cortices are well-connected by commissural projections and bilateral deletion is benign and eventually even beneficial to rotarod performance, the evidence supports the interpretation that the imbalanced, unilateral loss of *PTEN* resulted in the previously seen functional impairments.

In the long-term bilateral *PTEN* deletion behavioral study, we found no significant effect on rotarod performance or baseline coordination until 8 months after deletion in adult mice. At 8 and 10 months after adult *PTEN* deletion, there was significant improvement in rotarod performance and baseline coordination, signifying a beneficial effect of *PTEN* loss on motor learning. While this finding is promising when considering PTEN interference as a possible therapy for neurological injury or disease, the long duration required for the onset of meaningful functional changes may alter our expectations when quantifying treatment-induced regeneration and recovery in both the clinic and the laboratory. To date, *PTEN* deletion is still one of the most efficacious ways to promote regeneration after spinal cord injury in mice. Keeping this fact in mind, we did not observe maximal somatic size following adult *PTEN* deletion until 15 months post-deletion. Thus, it is reasonable to think that other interventions may take as long or even longer to exert their maximal effects on regeneration and functional recovery. The

commonly held belief that recovery from spinal cord injury plateaus by 6-8 weeks after injury is well-before we'd expect to observe greatest histological or functional efficacy following *PTEN* deletion (Kjell and Olson, 2016).

The long time to onset for structural and functional changes following *PTEN* deletion also has important consequences when considering pro-regenerative therapies in clinical trial. Since PTEN targeting therapies will likely not result in expression loss as complete as what is seen following *PTEN* deletion, further emphasizing the importance of approaching meaningful regeneration with combinatorial therapies. While PTEN inhibition would address the low intrinsic regenerative potential of adult neurons and provide some protection of vulnerable injured neurons, it would not ameliorate many of the other problematic aspects of spinal cord injury. McDonald and Sadowsky have suggested that optimal treatment of spinal cord injury will only be achieved with a multi-pronged approach, involving (i) minimization of secondary damage,(ii) remyelination of injured axons, (iii) removal of inhibitory components of the injury environment, (iv) promotion of neuronal growth and axonal regeneration, (v) delivery of guidance cues to direct regenerating axons to proper targets, (vi) bridging the injury site, and (vii) removal of injury site debris (McDonald and Sadowsky, 2002). Combinatorial therapies will likely expedite the onset of regeneration and functional recovery, as well as increase the overall efficaciousness of PTEN hypofunction as a treatment.

Several groups have demonstrated the neuroprotective effect of *PTEN* deletion (Yue et al., 2005; Park et al., 2008; Diaz-Ruiz et al., 2009; Domanskyi et al., 2011),

supporting the potential for using PTEN targeting therapies in the context of neurodegenerative diseases. Examination of *PTEN* deletion in Parkinson's disease mouse models has showed increased survival of dopaminergic neurons and improved behavioral outcomes, though it remains to be seen if a more clinically relevant approach to inhibit PTEN would be as efficacious (Diaz-Ruiz et al., 2009; Domanskyi et al., 2011). It will also be interesting to see if PTEN inhibition or silencing could be used to halt the progression of neurodegenerative diseases such as Parkinson's disease, and if coupling with cell-based therapies could possibly reverse disease-related damage.

In Chapter 2 we examined the long-term histological and functional consequences of deleting *PTEN* in early postnatal neurons of the motor cortex. The necessity for this study stemmed from the multitudinous number of previous studies that reported significant neuropathology associated with neuronal *PTEN* deletion (See Table 1.1 for review). In our model, we observed no histopathology or significant behavioral impairments, which is likely attributable to the relatively low number of affected neurons and the use of a neuron-specific vector to deliver Cre recombinase. It is undeniable, however, that *PTEN* loss in certain areas of the brain during development leads to severe disorders including autism, epilepsy, and macrocephaly (Zhou et al., 2003; Butler et al., 2005; Zhou and Parada, 2012; Meng et al., 2013). Based on our findings and others, it seems reasonable that *PTEN*-deletion induced structural changes will have different functional effects depending on where the deletion occurs and which cell types are affected. It is worth noting that despite PTEN's function as a tumor suppressor, we did not observe tumor formation in any mice following postnatal or adult *PTEN* deletion.

Much of *PTEN* deletion's effect on neuronal growth and regeneration is known to be due to mTOR activation (Kwon et al., 2003; Park et al., 2008; Ljungberg et al., 2009; Zhou et al., 2009). mTOR is down-regulated following injury and hypoxia, indicating that neurons respond to various insults by becoming more metabolically conservative, minimizing their use of resources by turning off nutrient-utilizing pathways. While this response may be useful in preventing cell death soon after injury, it is likely deleterious to the processes of growth and regeneration which require a more anabolic state. In our studies, there was sustained mTOR activity following *PTEN* deletion in postnatal and adult neurons, as indicated by increased phosphorylation of ribosomal protein S6 (pS6, a biomarker for mTOR). We observed visible increases in pS6 even at 15 months post-deletion, suggesting that no regulatory mechanism compensates for the loss of PTEN-mediated inhibition of mTOR.

In the lab, *PTEN* deletion and PTEN hypofunction have shown great promise for promoting regeneration after injury and preventing the progression of neurodegenerative diseases. Despite the seemingly benign or even beneficial effects that we have found following *PTEN* deletion, application of these genetic approaches to regeneration in human patient populations will prove much more difficult. Being that PTEN is a tumor suppressor, the risks associated with PTEN hypofunction in off-target cells would be great. A more clinically relevant approach to promoting neuronal growth and regeneration that results in comparable mTOR activation or regulation of targets downstream of mTOR would be of great therapeutic import. We have explored one such possibility in Chapter 6, wherein we studied the effect of high frequency stimulation on

mTOR activation (via induction of pS6) and the potential role of stimulation in mediating regeneration after injury.

Another way that we might be able to elicit *PTEN* deletion-like effects without actually interfering with *PTEN* expression is by targeting the specific downstream effectors of mTOR that underlie regeneration. To elucidate which specific targets are responsible for promoting growth, we have begun a study in collaboration with the Carmichael Lab (specifically Dr. Mary Teena Joy) at UCLA, wherein we are characterizing the transcriptomic profile of neurons with *PTEN* deletion in the motor cortex. Our goal is to identify specific transcripts that are up- or down-regulated in *PTEN* deleted neurons, and then examine the role of each of these putative targets in promoting growth after deletion (either by using double knockout mice or gene silencing with shRNA).

Due to mTOR's well-known regulation of protein synthesis, it will also be important to characterize the proteomic profile of *PTEN* deleted neurons. While PTEN has been shown to directly regulate the transcription of some genes, it is likely that PTEN has a greater effect on transcription via downstream mediators and that mTOR-dependent changes in the translation of specific mRNA transcripts will not be reflected in a transcriptomic profile of *PTEN* deleted neurons (Chung and Eng, 2005; Chung et al., 2006). By generating a proteomic profile of *PTEN* deleted neurons, and assessing the phosphorylation state of proteins within this profile, we could compare and contrast the transcriptomic and proteomic results allowing us to identify the most likely effectors of mTOR-mediated growth and regeneration.

Going forward it will be important to characterize the electrophysiological consequences of *PTEN* deletion in adult neurons, determine the consistency of our findings in other neuronal subpopulations (such as dopaminergic cells of the substantia nigra for application to Parkinson's disease), and further elucidate the mechanisms by which *PTEN* loss and mTOR activation result in neuroprotective and pro-regenerative effects.

To summarize, our major findings were:

- *PTEN* deletion in cortical motoneurons, regardless of age, results in substantial growth of the soma and axon
- Neuronal *PTEN* loss does not proportionally increase size of axon: myelination
- Pyramidal neurons have progressive increases in basal dendritic density following *PTEN* deletion in adulthood
- Localized loss of *PTEN* does not result in tumorigenesis, even during postnatal development
- Unilateral *PTEN* deletion in the motor cortex causes impairment in motor coordination, not function
- Bilateral *PTEN* deletion eventually triggers improved motor learning and coordination
- *PTEN* deletion in postnatal and adult neurons results in persistent mTOR activation
- High frequency stimulation of the motor cortex results in marked induction of pS6, a biomarker for mTOR

REFERENCES

Akache B, Grimm D, Pandey K, Yant SR, Xu H, Kay MA (2006) The 37/67-kilodalton laminin receptor is a receptor for adeno-associated virus serotypes 8, 2, 3, and 9. Journal of virology 80:9831-9836.

Ali IU, Schriml LM, Dean M (1999) Mutational spectra of PTEN/MMAC1 gene: a tumor suppressor with lipid phosphatase activity. Journal of the National Cancer Institute 91:1922-1932.

Allred RP, Adkins DL, Woodlee MT, Husbands LC, Maldonado MA, Kane JR, Schallert T, Jones TA (2008) The vermicelli handling test: a simple quantitative measure of dexterous forepaw function in rats. Journal of neuroscience methods 170:229-244.

Argiro V, Bunge MB, Johnson MI (1984) Correlation between growth form and movement and their dependence on neuronal age. The Journal of neuroscience : the official journal of the Society for Neuroscience 4:3051-3062.

Aschauer DF, Kreuz S, Rumpel S (2013) Analysis of transduction efficiency, tropism and axonal transport of AAV serotypes 1, 2, 5, 6, 8 and 9 in the mouse brain. PloS one 8:e76310.

Backman SA, Stambolic V, Suzuki A, Haight J, Elia A, Pretorius J, Tsao MS, Shannon P, Bolon B, Ivy GO, Mak TW (2001) Deletion of Pten in mouse brain causes seizures, ataxia and defects in soma size resembling Lhermitte-Duclos disease. Nature genetics 29:396-403.

Barron KD, Dentinger MP, Popp AJ, Mankes R (1988) Neurons of layer Vb of rat sensorimotor cortex atrophy but do not die after thoracic cord transection. J Neuropathol Exp Neurol 47:62-74.

Barron KD, Banerjee M, Dentinger MP, Scheibly ME, Mankes R (1989) Cytological and cytochemical (RNA) studies on rubral neurons after unilateral rubrospinal tractotomy: the impact of GM1 ganglioside administration. J Neurosci Res 22:331-337.

Bartlett JS, Samulski RJ, McCown TJ (1998) Selective and rapid uptake of adeno-associated virus type 2 in brain. Hum Gene Ther 9:1181-1186.

Bernstein JJ (1964) Relation of Spinal Cord Regeneration to Age in Adult Goldfish. Experimental neurology 9:161-174.

Biever A, Valjent E, Puighermanal E (2015) Ribosomal Protein S6 Phosphorylation in the Nervous System: From Regulation to Function. Frontiers in molecular neuroscience 8:75.

Bregman BS, Diener PS, McAtee M, Dai HN, James C (1997) Intervention strategies to enhance anatomical plasticity and recovery of function after spinal cord injury. Adv Neurol 72:257-275.

Brenner M, Kisseberth WC, Su Y, Besnard F, Messing A (1994) GFAP promoter directs astrocyte-specific expression in transgenic mice. The Journal of neuroscience : the official journal of the Society for Neuroscience 14:1030-1037.

Bronfman FC, Moechars D, Van Leuven F (2000) Acetylcholinesterase-positive fiber deafferentation and cell shrinkage in the septohippocampal pathway of aged amyloid precursor protein london mutant transgenic mice. Neurobiol Dis 7:152-168.

Brugarolas J, Lei K, Hurley RL, Manning BD, Reiling JH, Hafen E, Witters LA, Ellisen LW, Kaelin WG, Jr. (2004) Regulation of mTOR function in response to hypoxia by REDD1 and the TSC1/TSC2 tumor suppressor complex. Genes Dev 18:2893-2904.

Brus-Ramer M, Carmel JB, Chakrabarty S, Martin JH (2007) Electrical stimulation of spared corticospinal axons augments connections with ipsilateral spinal motor circuits after injury. The Journal of neuroscience : the official journal of the Society for Neuroscience 27:13793-13801.

Burger C, Gorbatyuk OS, Velardo MJ, Peden CS, Williams P, Zolotukhin S, Reier PJ, Mandel RJ, Muzyczka N (2004) Recombinant AAV viral vectors pseudotyped with viral capsids from serotypes 1, 2, and 5 display differential efficiency and cell tropism after delivery to different regions of the central nervous system. Mol Ther 10:302-317.

Burgin KE, Waxham MN, Rickling S, Westgate SA, Mobley WC, Kelly PT (1990) In situ hybridization histochemistry of Ca2+/calmodulin-dependent protein kinase in developing rat brain. The Journal of neuroscience : the official journal of the Society for Neuroscience 10:1788-1798.

Butler MG, Dasouki MJ, Zhou XP, Talebizadeh Z, Brown M, Takahashi TN, Miles JH, Wang CH, Stratton R, Pilarski R, Eng C (2005) Subset of individuals with autism spectrum disorders and extreme macrocephaly associated with germline PTEN tumour suppressor gene mutations. J Med Genet 42:318-321.

Carmel JB, Martin JH (2014) Motor cortex electrical stimulation augments sprouting of the corticospinal tract and promotes recovery of motor function. Frontiers in integrative neuroscience 8:51.

Carmel JB, Kimura H, Martin JH (2014) Electrical stimulation of motor cortex in the uninjured hemisphere after chronic unilateral injury promotes recovery of skilled locomotion through ipsilateral control. The Journal of neuroscience : the official journal of the Society for Neuroscience 34:462-466.
Carmel JB, Berrol LJ, Brus-Ramer M, Martin JH (2010) Chronic electrical stimulation of the intact corticospinal system after unilateral injury restores skilled locomotor control and promotes spinal axon outgrowth. The Journal of neuroscience : the official journal of the Society for Neuroscience 30:10918-10926.
Carmel JB, Kimura H, Berrol LJ, Martin JH (2013) Motor cortex electrical stimulation promotes axon outgrowth to brain stem and spinal targets that control the forelimb impaired by unilateral corticospinal injury. The European journal of neuroscience 37:1090-1102.
Chamberlin NL, Du B, de Lacalle S, Saper CB (1998) Recombinant adeno-associated virus vector: use for transgene expression and anterograde tract tracing in the CNS. Brain research 793:169-175.
Chung JH, Eng C (2005) Nuclear-cytoplasmic partitioning of phosphatase and tensin homologue deleted on chromosome 10 (PTEN) differentially regulates the cell cycle and apoptosis. Cancer research 65:8096-8100.
Chung JH, Ostrowski MC, Romigh T, Minaguchi T, Waite KA, Eng C (2006) The ERK1/2 pathway modulates nuclear PTEN-mediated cell cycle arrest by cyclin D1 transcriptional regulation. Hum Mol Genet 15:2553-2559.
Chung K, Deisseroth K (2013) CLARITY for mapping the nervous system. Nature methods 10:508-513.
Corradetti MN, Inoki K, Guan KL (2005) The stress-inducted proteins RTP801 and RTP801L are negative regulators of the mammalian target of rapamycin pathway. The Journal of biological chemistry 280:9769-9772.
Danilov CA, Steward O (2015) Conditional genetic deletion of PTEN after a spinal cord injury enhances regenerative growth of CST axons and motor function recovery in mice. Experimental neurology.
Diaz-Ruiz O, Zapata A, Shan L, Zhang Y, Tomac AC, Malik N, de la Cruz F, Backman CM (2009) Selective deletion of PTEN in dopamine neurons leads to trophic effects and adaptation of striatal medium spiny projecting neurons. PloS one 4:e7027.
Domanskyi A, Geissler C, Vinnikov IA, Alter H, Schober A, Vogt MA, Gass P, Parlato R, Schutz G (2011) Pten ablation in adult dopaminergic neurons is neuroprotective in Parkinson's disease models. FASEB journal : official publication of the Federation of American Societies for Experimental Biology 25:2898-2910.
Don AS, Tsang CK, Kazdoba TM, D'Arcangelo G, Young W, Zheng XF (2012) Targeting mTOR as a novel therapeutic strategy for traumatic CNS injuries. Drug discovery today 17:861-868.
Du K, Zheng S, Zhang Q, Li S, Gao X, Wang J, Jiang L, Liu K (2015) Pten Deletion Promotes Regrowth of Corticospinal Tract Axons 1 Year after Spinal Cord Injury. The Journal of neuroscience : the official journal of the Society for Neuroscience 35:9754-9763.
Dusart I, Airaksinen MS, Sotelo C (1997) Purkinje cell survival and axonal regeneration are age dependent: an in vitro study. The Journal of neuroscience : the official journal of the Society for Neuroscience 17:3710-3726.
Ferreira TA, Blackman AV, Oyrer J, Jayabal S, Chung AJ, Watt AJ, Sjostrom PJ, van Meyel DJ (2014) Neuronal morphometry directly from bitmap images. Nature methods 11:982-984.
Filbin MT (2006) Recapitulate development to promote axonal regeneration: good or bad approach? Philosophical transactions of the Royal Society of London Series B, Biological sciences 361:1565-1574.
Finch CE (1993) Neuron atrophy during aging: programmed or sporadic? Trends Neurosci 16:104-110.
Fitch MT, Silver J (2008) CNS injury, glial scars, and inflammation: Inhibitory extracellular matrices and regeneration failure. Experimental neurology 209:294-301.
Forss-Petter S, Danielson PE, Catsicas S, Battenberg E, Price J, Nerenberg M, Sutcliffe JG (1990) Transgenic mice expressing beta-galactosidase in mature neurons under neuron-specific enolase promoter control. Neuron 5:187-197.
Fraser MM, Bayazitov IT, Zakharenko SS, Baker SJ (2008) Phosphatase and tensin homolog, deleted on chromosome 10 deficiency in brain causes defects in synaptic structure, transmission and plasticity, and myelination abnormalities. Neuroscience 151:476-488.
Fraser MM, Zhu X, Kwon CH, Uhlmann EJ, Gutmann DH, Baker SJ (2004) Pten loss causes hypertrophy and increased proliferation of astrocytes in vivo. Cancer research 64:7773-7779.
Funfschilling U, Reichardt LF (2002) Cre-mediated recombination in rhombic lip derivatives. Genesis 33:160-169.
Georgescu MM (2010) PTEN Tumor Suppressor Network in PI3K-Akt Pathway Control. Genes & cancer 1:1170-1177.

Goebbels S, Wieser GL, Pieper A, Spitzer S, Weege B, Yan K, Edgar JM, Yagensky O, Wichert SP, Agarwal A, Karram K, Renier N, Tessier-Lavigne M, Rossner MJ, Karadottir RT, Nave KA (2017) A neuronal PI(3,4,5)P3-dependent program of oligodendrocyte precursor recruitment and myelination. Nature neuroscience 20:10-15.
Goffin A, Hoefsloot LH, Bosgoed E, Swillen A, Fryns JP (2001) PTEN mutation in a family with Cowden syndrome and autism. American journal of medical genetics 105:521-524.
Greenough WT, Juraska JM, Volkmar FR (1979) Maze training effects on dendritic branching in occipital cortex of adult rats. Behav Neural Biol 26:287-297.
Gutilla EA, Buyukozturk MM, Steward O (2016) Long-term consequences of conditional genetic deletion of PTEN in the sensorimotor cortex of neonatal mice. Experimental neurology 279:27-39.
Haws ME, Jaramillo TC, Espinosa F, Widman AJ, Stuber GD, Sparta DR, Tye KM, Russo SJ, Parada LF, Stavarache M, Kaplitt M, Bonci A, Powell CM (2014) PTEN knockdown alters dendritic spine/protrusion morphology, not density. The Journal of comparative neurology 522:1171-1190.
Hoeffer CA, Klann E (2010) mTOR signaling: at the crossroads of plasticity, memory and disease. Trends Neurosci 33:67-75.
Hollander MC, Blumenthal GM, Dennis PA (2011) PTEN loss in the continuum of common cancers, rare syndromes and mouse models. Nature reviews Cancer 11:289-301.
Hurd C, Weishaupt N, Fouad K (2013) Anatomical correlates of recovery in single pellet reaching in spinal cord injured rats. Experimental neurology 247:605-614.
Jaworski J, Sheng M (2006) The growing role of mTOR in neuronal development and plasticity. Mol Neurobiol 34:205-219.
Jaworski J, Spangler S, Seeburg DP, Hoogenraad CC, Sheng M (2005) Control of dendritic arborization by the phosphoinositide-3'-kinase-Akt-mammalian target of rapamycin pathway. The Journal of neuroscience : the official journal of the Society for Neuroscience 25:11300-11312.
Jefferies HB, Fumagalli S, Dennis PB, Reinhard C, Pearson RB, Thomas G (1997) Rapamycin suppresses 5'TOP mRNA translation through inhibition of p70s6k. EMBO J 16:3693-3704.
Kjell J, Olson L (2016) Rat models of spinal cord injury: from pathology to potential therapies. Dis Model Mech 9:1125-1137.
Kobayashi NR, Fan DP, Giehl KM, Bedard AM, Wiegand SJ, Tetzlaff W (1997) BDNF and NT-4/5 prevent atrophy of rat rubrospinal neurons after cervical axotomy, stimulate GAP-43 and Talpha1-tubulin mRNA expression, and promote axonal regeneration. The Journal of neuroscience : the official journal of the Society for Neuroscience 17:9583-9595.
Kumar V, Zhang MX, Swank MW, Kunz J, Wu GY (2005) Regulation of dendritic morphogenesis by Ras-PI3K-Akt-mTOR and Ras-MAPK signaling pathways. The Journal of neuroscience : the official journal of the Society for Neuroscience 25:11288-11299.
Kwon CH, Zhu X, Zhang J, Baker SJ (2003) mTor is required for hypertrophy of Pten-deficient neuronal soma in vivo. Proceedings of the National Academy of Sciences of the United States of America 100:12923-12928.
Kwon CH, Zhu X, Zhang J, Knoop LL, Tharp R, Smeyne RJ, Eberhart CG, Burger PC, Baker SJ (2001) Pten regulates neuronal soma size: a mouse model of Lhermitte-Duclos disease. Nature genetics 29:404-411.
Kwon CH, Luikart BW, Powell CM, Zhou J, Matheny SA, Zhang W, Li Y, Baker SJ, Parada LF (2006) Pten regulates neuronal arborization and social interaction in mice. Neuron 50:377-388.
Laplante M, Sabatini DM (2012) mTOR signaling in growth control and disease. Cell 149:274-293.
Lassek AM, Woolsey CN, Walker AE, Boshes B (1957) The pyramidal tract. Neurology 7:496-509.
Lewandowski G, Steward O (2014) AAVshRNA-mediated suppression of PTEN in adult rats in combination with salmon fibrin administration enables regenerative growth of corticospinal axons and enhances recovery of voluntary motor function after cervical spinal cord injury. The Journal of neuroscience : the official journal of the Society for Neuroscience 34:9951-9962.
Liu K, Lu Y, Lee JK, Samara R, Willenberg R, Sears-Kraxberger I, Tedeschi A, Park KK, Jin D, Cai B, Xu B, Connolly L, Steward O, Zheng B, He Z (2010) PTEN deletion enhances the regenerative ability of adult corticospinal neurons. Nature neuroscience 13:1075-1081.
Ljungberg MC, Sunnen CN, Lugo JN, Anderson AE, D'Arcangelo G (2009) Rapamycin suppresses seizures and neuronal hypertrophy in a mouse model of cortical dysplasia. Dis Model Mech 2:389-398.
Lugo JN, Smith GD, Arbuckle EP, White J, Holley AJ, Floruta CM, Ahmed N, Gomez MC, Okonkwo O (2014) Deletion of PTEN produces autism-like behavioral deficits and alterations in synaptic proteins. Frontiers in molecular neuroscience 7:27.

Luikart BW, Schnell E, Washburn EK, Bensen AL, Tovar KR, Westbrook GL (2011) Pten knockdown in vivo increases excitatory drive onto dentate granule cells. The Journal of neuroscience : the official journal of the Society for Neuroscience 31:4345-4354.
Ma XM, Blenis J (2009) Molecular mechanisms of mTOR-mediated translational control. Nature reviews Molecular cell biology 10:307-318.
Marino S, Krimpenfort P, Leung C, van der Korput HA, Trapman J, Camenisch I, Berns A, Brandner S (2002) PTEN is essential for cell migration but not for fate determination and tumourigenesis in the cerebellum. Development 129:3513-3522.
McBride RL, Feringa ER, Garver MK, Williams JK, Jr. (1989) Prelabeled red nucleus and sensorimotor cortex neurons of the rat survive 10 and 20 weeks after spinal cord transection. J Neuropathol Exp Neurol 48:568-576.
McDonald JW, Sadowsky C (2002) Spinal-cord injury. Lancet 359:417-425.
Meng XF, Yu JT, Song JH, Chi S, Tan L (2013) Role of the mTOR signaling pathway in epilepsy. J Neurol Sci 332:4-15.
Nobunaga AI, Go BK, Karunas RB (1999) Recent demographic and injury trends in people served by the Model Spinal Cord Injury Care Systems. Archives of physical medicine and rehabilitation 80:1372-1382.
Nygard O, Nilsson L (1990) Translational dynamics. Interactions between the translational factors, tRNA and ribosomes during eukaryotic protein synthesis. Eur J Biochem 191:1-17.
Ogawa S, Kwon CH, Zhou J, Koovakkattu D, Parada LF, Sinton CM (2007) A seizure-prone phenotype is associated with altered free-running rhythm in Pten mutant mice. Brain research 1168:112-123.
Park KK, Liu K, Hu Y, Kanter JL, He Z (2010) PTEN/mTOR and axon regeneration. Experimental neurology 223:45-50.
Park KK, Liu K, Hu Y, Smith PD, Wang C, Cai B, Xu B, Connolly L, Kramvis I, Sahin M, He Z (2008) Promoting axon regeneration in the adult CNS by modulation of the PTEN/mTOR pathway. Science 322:963-966.
Perlmutter JS, Mink JW (2006) Deep brain stimulation. Annu Rev Neurosci 29:229-257.
Pirbhoy PS, Farris S, Steward O (2016) Synaptic activation of ribosomal protein S6 phosphorylation occurs locally in activated dendritic domains. Learn Mem 23:255-269.
Pun RY, Rolle IJ, Lasarge CL, Hosford BE, Rosen JM, Uhl JD, Schmeltzer SN, Faulkner C, Bronson SL, Murphy BL, Richards DA, Holland KD, Danzer SC (2012) Excessive activation of mTOR in postnatally generated granule cells is sufficient to cause epilepsy. Neuron 75:1022-1034.
Ramon-Cueto A, Cordero MI, Santos-Benito FF, Avila J (2000) Functional recovery of paraplegic rats and motor axon regeneration in their spinal cords by olfactory ensheathing glia. Neuron 25:425-435.
Reiling JH, Hafen E (2004) The hypoxia-induced paralogs Scylla and Charybdis inhibit growth by down-regulating S6K activity upstream of TSC in Drosophila. Genes Dev 18:2879-2892.
Rothwell PE, Fuccillo MV, Maxeiner S, Hayton SJ, Gokce O, Lim BK, Fowler SC, Malenka RC, Sudhof TC (2014) Autism-associated neuroligin-3 mutations commonly impair striatal circuits to boost repetitive behaviors. Cell 158:198-212.
Ruvinsky I, Meyuhas O (2006) Ribosomal protein S6 phosphorylation: from protein synthesis to cell size. Trends Biochem Sci 31:342-348.
Sadowsky CL (2001) Electrical stimulation in spinal cord injury. NeuroRehabilitation 16:165-169.
Sawyers CL (2008) The cancer biomarker problem. Nature 452:548-552.
Schwab ME, Bartholdi D (1996) Degeneration and regeneration of axons in the lesioned spinal cord. Physiological reviews 76:319-370.
Shi Y, Paluch BE, Wang X, Jiang X (2012) PTEN at a glance. Journal of cell science 125:4687-4692.
Sholl DA (1953) Dendritic organization in the neurons of the visual and motor cortices of the cat. Journal of anatomy 87:387-406.
Silva NA, Sousa N, Reis RL, Salgado AJ (2014) From basics to clinical: a comprehensive review on spinal cord injury. Progress in neurobiology 114:25-57.
Simon P, Dupuis R, Costentin J (1994) Thigmotaxis as an index of anxiety in mice. Influence of dopaminergic transmissions. Behavioural brain research 61:59-64.
Smits SM, Smidt MP (2006) The role of Pitx3 in survival of midbrain dopaminergic neurons. Journal of neural transmission Supplementum:57-60.
Sperow M, Berry RB, Bayazitov IT, Zhu G, Baker SJ, Zakharenko SS (2012) Phosphatase and tensin homologue (PTEN) regulates synaptic plasticity independently of its effect on neuronal morphology and migration. The Journal of physiology 590:777-792.

Summerford C, Samulski RJ (1998) Membrane-associated heparan sulfate proteoglycan is a receptor for adeno-associated virus type 2 virions. Journal of virology 72:1438-1445.
Summerford C, Bartlett JS, Samulski RJ (1999) AlphaVbeta5 integrin: a co-receptor for adeno-associated virus type 2 infection. Nature medicine 5:78-82.
Sunnen CN, Brewster AL, Lugo JN, Vanegas F, Turcios E, Mukhi S, Parghi D, D'Arcangelo G, Anderson AE (2011) Inhibition of the mammalian target of rapamycin blocks epilepsy progression in NS-Pten conditional knockout mice. Epilepsia 52:2065-2075.
Takeuchi K, Gertner MJ, Zhou J, Parada LF, Bennett MV, Zukin RS (2013) Dysregulation of synaptic plasticity precedes appearance of morphological defects in a Pten conditional knockout mouse model of autism. Proceedings of the National Academy of Sciences of the United States of America 110:4738-4743.
Taymans JM, Vandenberghe LH, Haute CV, Thiry I, Deroose CM, Mortelmans L, Wilson JM, Debyser Z, Baekelandt V (2007) Comparative analysis of adeno-associated viral vector serotypes 1, 2, 5, 7, and 8 in mouse brain. Hum Gene Ther 18:195-206.
Teskey GC, Flynn C, Goertzen CD, Monfils MH, Young NA (2003) Cortical stimulation improves skilled forelimb use following a focal ischemic infarct in the rat. Neurol Res 25:794-800.
Thoreen CC, Chantranupong L, Keys HR, Wang T, Gray NS, Sabatini DM (2012) A unifying model for mTORC1-mediated regulation of mRNA translation. Nature 485:109-113.
Tsokas P, Grace EA, Chan P, Ma T, Sealfon SC, Iyengar R, Landau EM, Blitzer RD (2005) Local protein synthesis mediates a rapid increase in dendritic elongation factor 1A after induction of late long-term potentiation. The Journal of neuroscience : the official journal of the Society for Neuroscience 25:5833-5843.
Urbanska M, Gozdz A, Swiech LJ, Jaworski J (2012) Mammalian target of rapamycin complex 1 (mTORC1) and 2 (mTORC2) control the dendritic arbor morphology of hippocampal neurons. The Journal of biological chemistry 287:30240-30256.
van Diepen MT, Eickholt BJ (2008) Function of PTEN during the formation and maintenance of neuronal circuits in the brain. Developmental neuroscience 30:59-64.
Varga EA, Pastore M, Prior T, Herman GE, McBride KL (2009) The prevalence of PTEN mutations in a clinical pediatric cohort with autism spectrum disorders, developmental delay, and macrocephaly. Genet Med 11:111-117.
Verdu E, Ceballos D, Vilches JJ, Navarro X (2000) Influence of aging on peripheral nerve function and regeneration. J Peripher Nerv Syst 5:191-208.
Waite KA, Eng C (2002) Protean PTEN: form and function. American journal of human genetics 70:829-844.
Wen Y, Li W, Choudhury GR, He R, Yang T, Liu R, Jin K, Yang SH (2013) Astroglial PTEN Loss Disrupts Neuronal Lamination by Dysregulating Radial Glia-guided Neuronal Migration. Aging and disease 4:113-126.
Wettenhall RE, Erikson E, Maller JL (1992) Ordered multisite phosphorylation of Xenopus ribosomal protein S6 by S6 kinase II. The Journal of biological chemistry 267:9021-9027.
Williams MR, DeSpenza T, Jr., Li M, Gulledge AT, Luikart BW (2015) Hyperactivity of newborn Pten knock-out neurons results from increased excitatory synaptic drive. The Journal of neuroscience : the official journal of the Society for Neuroscience 35:943-959.
Yue Q, Groszer M, Gil JS, Berk AJ, Messing A, Wu H, Liu X (2005) PTEN deletion in Bergmann glia leads to premature differentiation and affects laminar organization. Development 132:3281-3291.
Zhou J, Parada LF (2012) PTEN signaling in autism spectrum disorders. Current opinion in neurobiology 22:873-879.
Zhou J, Blundell J, Ogawa S, Kwon CH, Zhang W, Sinton C, Powell CM, Parada LF (2009) Pharmacological inhibition of mTORC1 suppresses anatomical, cellular, and behavioral abnormalities in neural-specific Pten knock-out mice. The Journal of neuroscience : the official journal of the Society for Neuroscience 29:1773-1783.
Zhou XP, Marsh DJ, Morrison CD, Chaudhury AR, Maxwell M, Reifenberger G, Eng C (2003) Germline inactivation of PTEN and dysregulation of the phosphoinositol-3-kinase/Akt pathway cause human Lhermitte-Duclos disease in adults. American journal of human genetics 73:1191-1198.
Zukor K, Belin S, Wang C, Keelan N, Wang X, He Z (2013) Short hairpin RNA against PTEN enhances regenerative growth of corticospinal tract axons after spinal cord injury. The Journal of neuroscience : the official journal of the Society for Neuroscience 33:15350-15361.